The Effect of Anisotropy Field on Dispersion Relation and Thermodynamic Properties of Antiferromagnetic Materials : Employing Quantum Field Theory

Desalegne Tefera

ADDIS ABABA UNIVERSITY

College of Natural and Computational Sciences
Physics Department

Advisor: Dr. Chernet Amente

Co-advisor: Prof. P. Singh

Submitted in accordance with the requirements for the degree of

Doctor of Philosophy in Physic (Condensed matter Physics)

August, 2024

Approvals

Addis Ababa University
Graduate Programs

Thesis Title: **The Effect of Anisotropy Field on the Dispersion Relation and Thermodynamic Properties of Antiferromagnetic Materials : Employing the Quantum Field Theory**

By: Desalegne Tefera Yimer

Department: Physics

A dissertation submitted to in fulfillment of the requirements for the degree of Doctor of Philosophy in Physics (Condensed Matter Physics)

The dissertation was reviewed and approved by the following:

Dr. Cherninet Amentie	_____
Advisor	signiture
Professor P. Singh	_____-
Co-advisor	signiture
Dr. Habtie Dulla	_____
External Examiner	signiture
Professor Teshome Senbeta	_____-
Internal Examiner	signiture
Dr. Newayemedhin Abera	_____-
Chairman	signiture

Intellectual Property Statement

The candidate confirms that the work submitted is his own and that appropriate credit has been given where reference has been made to the work of others.

Acknowledgements

I am grateful to my supervisors, Prof. P. Singh and Dr. Chernet Amente, for their guidance, support, and the valuable lessons on punctuality, work, and respect. I especially thank Dr. Chernet Amente for his ongoing guidance, warmth, and wisdom, and for tolerating my unconventional problem-solving approach, which has greatly contributed to my professional growth

Furthermore, I am grateful to the Department of Physics, College of Natural and Computational Sciences, Addis Abeba University, and Debre Birhan University for their encouragement and financial support.

I also want to thank my colleagues in the Department of Physics at Addis Abeba University for creating a good and supportive atmosphere, especially during difficult times.

While it is difficult to thank everyone personally, I would want to offer my heartfelt gratitude to all members of the Condensed Matter Physics group. Without their friendship and encouragement, our journey would not have been nearly as rewarding.

I am grateful to thank Dr. Ephreme Tesfaye for assisting me in writing python scripts and providing suitable soft ware for drawing and plotting graphs. I'd like to express my gratitude to my former friend, Dr. Getachew Worku, for his great assistance, which cannot be expressed in words.

I extend my gratitude to Dr. Kebede Yimer for carefully reviewing this manuscript and providing invaluable assistance in organizing its structure. I would also like to express my appreciation to Dr. Kibebe Tshayu and Mr. Wassu Belayneh for their contributions.

Lastly, I wish to express my deep gratitude to my wife, Mrs. Ayslnesh Fekadu, and my son, Nahom Desalegne. Their unwavering support and understanding have been indispensable, making all of this possible even in the face of challenges.

Desalegne Tefera

Abstract

In this thesis, we look at the complex dynamics of spin waves in a two-sublattice antiferromagnetic (AFM) system, with an emphasis on spin interactions and the magnon dispersion relation. The main purpose of this study was to examine spin wave interaction and how anisotropy field influence on dispersion relation and characteristics of (AMF) systems. The theoretical framework is based on the Heisenberg Hamiltonian model, which was specifically built to manage a uniaxial anisotropy field within an antiferromagnetic system. To overcome the problem, we employ quantum field theory, namely the double-time temperature-dependent Green function technique to achieve magnon dispersion. A random phase approximation is used to decouple and diagonalize higher order components. The discovery of a relationship between the anisotropy field and the dispersion relation for the wave vector k at low temperatures is particularly interesting. The findings indicate that as the anisotropic field becomes stronger, the magnon dispersion progressively shifts from a curved trajectory to linearity, finally adopting a sinusoidal form with further expansion into the first Brillouin zone. Furthermore, we investigate the thermodynamic parameters of magnetization and heat capacity within the uniaxial symmetric AFM crystal lattice, concentrating on excitation temperature at low temperatures and utilizing the long-wavelength approximation. The results show that AFM magnetization and heat capacities are sensitive to anisotropic fields, with magnetization trending upward and the greatest peak of heat capacity dropping as anisotropy increased. The findings provide understanding of the complicated relationship between anisotropy and exchange fields in antiferromagnetic systems, indicating their significant impact on magnetization, heat capacity, and other thermodynamic parameters. Furthermore, this model gives information on the variations in susceptibility and heat capacity between transition metal antiferromagnetic fluorides. Further investigation may be necessary in this situation.

Abbreviations

AFM	$\rightarrow$	Antiferromagnet
FM	$\rightarrow$	Ferromagnet
J	$\rightarrow$	Exchange Integral
H_0	$\rightarrow$	External magnetic field
H_A	$\rightarrow$	Anisotropy field
γ	=	$\frac{g\mu_B}{\hbar}$
ω_A	=	γH_A
ω_0	=	γH_0
ω_e	=	$2\lvert J\rvert zS$
α	=	$\frac{\omega_A}{\omega_e}$ (anisotropy factor)
θ	=	$\frac{k_B T}{\hbar\omega_e}$ (excitation temperature)
Θ	=	$\frac{k_B T}{c}$ (temperature parameter)
m_k	=	$\langle a_k^\dagger a_k \rangle$
n_k	=	$\langle b_k^\dagger b_k \rangle$
R	=	$\omega_e + h_A - \frac{2Jz}{N}\Upsilon_k m_k$
R'	=	$\omega_e + h_B - \frac{2Jz}{N}\Upsilon_k n_k$
B	=	$\omega_e\Upsilon_k - \frac{Jz}{N}\Upsilon_k(n_k + m_k)$
Υ_k	$\rightarrow$	geometric structure facot

Contents

List of Figures

List of Tables

Chapter 1

Introduction

Magnetic materials' effect on science and technology may be traced back to prehistoric times, when lodestone was used for navigation. Fast forward to now, and magnetic materials continue to play an important role in cutting-edge applications like spintronics, which revolutionizes data storage, transmission, and processing technologies. The development of magnetic materials has played a critical role in influencing advances in a variety of scientific and technological fields demonstrating their long-term importance and effect on contemporary society [26, 20].

Magnetic materials currently inspire the cutting-edge spirit in condensed matter physics [63]. They also encourage creativity and innovation by giving us with data storage, sensors, motors, and transformers, etc. Magnetism and magnetic materials are also used in a variety of modern technologies, including power generators and transformers, electric motors, radios, televisions, telephones, computers, and sound and video reproduction systems, as well as antiferromagnetic systems.

The idea of antiferromagnetic ordering was proposed independently by Landau and Néel as a hypothesis used to explain the unusual properties of some paramagnetic crystals. Landau suggested the model of layers of magnetic moments directed in opposite sides. Néel also proposed the 'staggered' order, in which the nearest neighbors of each moment are oriented opposite to it. The magnetic neutronography proved the reality of antiferromagnetic ordering and allowed the determination of magnetic structures of many substances. It became clear that both types of antiferromagnetic order, the layered and the staggered, as well as many more complicated

types of magnetic order, do exist.

Materials that exhibit antiferromagnetism, the magnetic moments of atoms or molecules, usually related to the spins of electrons, align in a regular pattern with neighbouring spins (on different sublattices) pointing in opposite directions. Antiferromagnetism, like ferromagnetism, is a manifestation of ordered magnetism.

The energy required to magnetize a crystal is governed by the orientation of the applied field relative to the crystal axes. Magnetic anisotropy is one of magnetic materials' most essential technical properties. Depending on the application, materials with high, medium, or low magnetic anisotropy will be required, such as permanent magnets, magnetic cores in transformers, information storage media, and magnetic recording heads.

Furthermore, information science and technology depend extensively on data transport between multiple carriers. This transmission is enabled thanks to the high coupling of information carriers. Photons are closely associated with condensed matter excitations such as electrons, phonons, plasmons, superconductor qubits, excitons in quantum wells, and magnons. Magnons, which are excitations of magnetic moments, are attractive information carriers in spintronics due to their low energy consumption, long coherent distance/time, nanometer-scale wavelength, and suitable information processing frequency spanning from gigahertz (GHz) to terahertz (THz) [116].
In terms of scientific inquiry, our research aims to probe extensively into the complex interaction between anisotropy and antiferromagnetic physical properties. This investigation is driven by a strong desire to understand the subtle ways in which anisotropy may dramatically influence the properties of antiferromagnetic materials.

1.1 Background

Louis Néel said in his 1970 Nobel lecture that although antiferromagnetic materials are very fascinating in theory, they don't seem to have any practical uses. A few decades later, this unfavourable attitude toward antiferromagnets would be completely altered. Because these materials now have a few real-world applications, with the potential for many more. The debut of antiferromagnets in

technology was made possible with the discovery of the giant magnetoresistance effect (GMR) in 1988, by him Albert Fert and Peter Grúnberg [86]. Since ferromagnetic materials play the active role in spintronic devices whereas antiferromagnetic materials have played a passive role earlier time. However, new experimental and theoretical findings have begun to change this picture and clearly demonstrating that antiferromagnets have several advantages over ferromagnets in spintronics phenomena.

When most people think about technological devices in today's society, they think about devices based on electronics. Electronics is a technology that relies on information processing through the controlled transport of the fundamental electrical charge of electrons. Although significant progress has been achieved in the field of electronic device technology, there are intrinsic constraints, such as joule heating, that may impede future developments. Joule heating happens when charged particles interaction and produce heat as a consequence of current flow. Recognizing these electrical constraints, an important transformation toward a more technological approach is essential to maintain the rising trend of advancement. The developing science of spintronics, which focuses on electrons' inherent angular momentum or spin, has promise for overcoming these issues. Since, spintronics is based on the electron's charge and spin [33, 107, 66].

The electron possesses a negative charge in addition to having an intrinsic angular momentum, or spin, which is another internal degree of freedom. This is the foundation of the spintronics field. The name spintronics is the short for "spin transport electronics", and it refers to the use of the electron's spin rather than its charge in information processing, storage, and control [38, 16]. Information transfer using electron spins does not suffer from the same issues that electrons do in electronics, such as Joule heating. Insulator spintronics, in particular, offer significant promise as a possibility for solving some of the most fundamental challenges in electronics. If the insulator has magnetic ordering, information can be transported via spins, which pair to nearby spins. Spin transport involves the passage of a spin wave from the source to a detector..

Hypothetically, one area of research is the features of spin-wave spectra in magnonic devices, which provide functionality not found in photonic or electrical devices.

Magnonic devices, for example, may be easily controlled by magnetic fields. Furthermore, magnetic nanostructures serve as non-volatile memory components, paving the path for programmable electronics with reprogramming periods as short as nanoseconds. Magnetic devices may now communicate with microwave electronics and photonic devices at the same time because of this integration. Spin waves have far shorter wavelengths than electromagnetic waves in the visible spectrum. In practically relevant situations (between GHz and THz), magnonic devices provide an intriguing possibility for downsizing at these frequencies.

Naturally, magnetic ordering is classified into two types: ferromagnetic and antiferromagnetic. Ferromagnets and antiferromagnets are more common in nature. In ferromagnetic ordering, all spins are aligned in the same direction, i.e. parallel; in antiferromagnetic ordering, each spin points in the opposite direction as its surrounding spins, i.e. antiparallel. In practical use, the shortcomings of FM materials have been gradually revealed as information storage memory devices develop toward ultrafast speed, higher density capacity, and lower power consumption. As a result, this is a promisable contribution in recent time, antiferromagnetic (AFM) spintronics has become a hot research field, focusing on the utilization of antiferromagnetic materials as a key element.

Magnonics is concerned with the excitation, propagation, control, and detection of spin waves (quanta of which are referred to as magnons) through periodic magnetic media that are modulated passively (patterned structures, modulated magnetic properties) or actively (spin texture, electric field, magnetic field). It is analogous to photonics or phononics, but it offers significant benefits over those technologies. These advantages include, to name a few, lower energy consumption, easier integrability and compatibility with complementary metal-oxide semiconductor (CMOS) structures, programmability, shorter wavelength, smaller device features, anisotropic properties, negative group velocity, non-reciprocity, and efficient tunability by various external stimuli. As a result, despite being a relatively new scientific topic, magnonics has gone a long way since its start.

Moreover, magnon spintronics is an emerging field concentrating on the generation, detection and manipulation of magnons, the quanta of spin-wave, in ferromagnetic or antiferromagnetic metals and insulators [30, 15, 11]. As spin waves in magnetic

insulators exhibit both low energy dissipation and long coherence length, these constitute a competitive alternative to electronic devices and are deemed to be a promising candidate as a high-quality information carrier [120, 119, 11].

To exploit antiferromagnetic systems in spintronics and data processing applications, a full understanding of the dispersion relationship inside the antiferromagnetic spin system is necessary. This knowledge should cover a wide range of subjects, including free energy densities, staggered magnetization, and other observables in Heisenberg quantum antiferromagnets.

1.2 Perspectives of Antiferromagnetics

Antiferromagnetism research is critical in current and future technologies, particularly in terms of extending the lifespan of data storage in spintronics, enhancing transmission over long distances, and making decoding methods more efficient. Data storage and process are highly dependent on electron spin interactions and magnetic moments. This breakthrough not only enhances spintronics, but it also has the potential to increase the efficiency and endurance of data storage systems, changing technology's long-term trajectory.

The magnetic moment of ferromagnetic (FM) materials is used for data storage and manipulation. Intensive research has been conducted on antiferromagnetic (AFM) materials with desirable physical properties, high Néel temperature, spin-orbit coupling, magnetic anisotropy, conductive or non-conductive semiconducting. Efforts have been made to use antiferromagnets (AFMs) materials as active components in devices over the last 5-10 years [118, 73, 45, 91]. As a result, the first thing to inquire is, "Why are AFMs being studied at all?" Antiferromagnetic data storage and transmission, a potentially useful application scenario, involves identifying specific characteristics and parameters that enhance and simplify the presentation of AFM advantages. Antiferromagnetic materials show potential for future high-density and fast-speed spintronic devices, comparable to the reasoning underlying present ferromagnet (FM)-based spintronic applications such magnetic random-access memory and hard disk drives. Antiferromagnets (AFMs) have no stray field, hence they are resistant to magnetic interactions with other unit cells. This feature might aid in the reduction of spintronic device sizes to sub-nanometers. Furthermore, the exchange

mode of AFMs operates in the Tera Herz (THz) range, causing a shift in spintronic device speed from nanoseconds to picoseconds [110].

Information is encoded using both antiferromagnetics (AFMs) and ferromagnets. Figures 1.1(a and b) demonstrate how magnetic bits in FMs and AFMs store data.

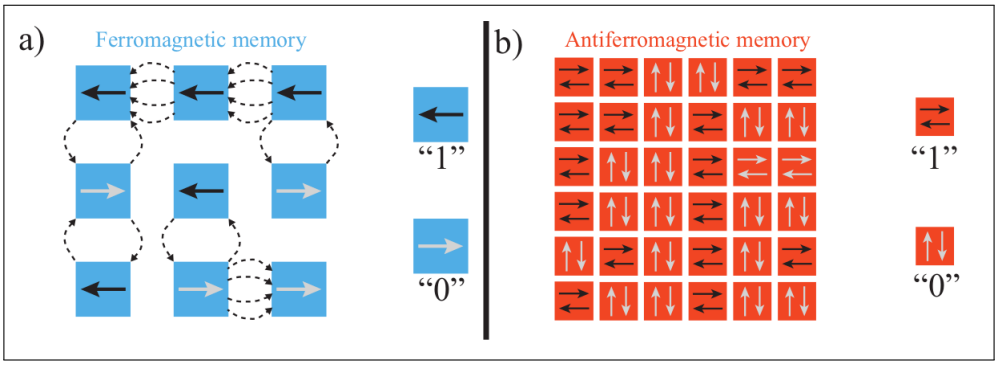

Figure 1.1: Schematic representation of (a) ferromagnetic, (b) antiferromagnetic memory Image; adapted from [55].

Fig. (1.1a) shows how the magnetization direction affects the logical "1" and "0" in FMs, represented by a single arrow. The same magnetization, however, causes a problem for FM memory devices in the form of stray fields, as seen by the dotted lines in the figure. When bit sizes and spacing are too small, inter-bit interference from stray fields degrade memory stability and limiting bit packing density. On the other hand, Fig.(1.1b) demonstrates the benefits of AFM-based memory. The antiparallel magnetic ordering and lack of stray fields allow for increased packing density, perhaps leading to denser memory. Furthermore, the absence of net magnetization makes the system less vulnerable to external magnetic field variations, which improves the longevity of stored data. Antiferromagnetic coupling in AFMs causes spin dynamics in the THz regime, which differs from the GHz dynamics reported in FMs [79, 92, 103]. This difference shows the potential for quicker magnetic state switching [17, 50].

Antiferromagnets (AFMs) clearly offer advantages over ferromagnetic materials, such as enhanced stability against external field perturbations and less cross-interaction with surrounding AFM elements due to the absence of stray fields. AFM dynamics frequently operate in the THz range, which is far faster than the GHz dynamics observed in ferromagnets. These remarkable properties have prompted interest in many aspects of antiferromagnetic spintronics, including domain wall motion,

skyrmions, magnetoresistance, magnetic switching, spin pumping, and spin current transmission. Mn-based alloys, such as CuMnAs and Mn_2Au [105, 106, 13, 59], have been extensively studied as AFM materials.

Another notable progress lies in the spin transport of these materials, where spin currents are typically carried by spin-polarized electrons. The potential transfer of spin currents without an electrical current can significantly reduce losses associated with Joule heating. Collective excitations of antiferromagnetic spins in antiferromagnetic insulators (AFMIs), known as spin waves or magnons, can achieve this. Spin information can be transported using these spin waves without the need for moving electrons. Furthermore, with good control over these spin waves, logic operations can be performed by leveraging the wave character of these excitations [24].

The study of collective spin excitation in magnetically structured materials, known as spin waves and their related quasi-particles termed magnons, has resulted in an entirely novel field known as "Magnonics". Spin waves are gaining popularity due to technological advancements, new experimental techniques for studying high-frequency magnetization dynamics, and the potential for functional devices controlled by magnetic fields that use spin waves (magnons) to carry and process information [57, 108].

These fascinating inherent features of antiferromagnetic materials (AFMs) greatly contribute to the impetus for current study in this material class. AFMs provide material flexibility, as antiferromagnetism is more frequent than ferromagnetism [45]. This is a strong incentive for the researcher to study them.

The benefits of AFM-based memory, as demonstrated in the examination of magnetic fields and spins during the magnetism lecture, were not only educational but also fascinating, acting as an excellent source of inspiration. The stunning environment aroused my interest in learning more about this profession. The motivations for this study are frequently centred in the practical applications and use of magnetic materials and antiferromagnetics. Furthermore, the study of current magnetism and magnetic materials is a captivating aspect that motivates people to learn more.

A substantial motivation for this work arises from the undiscovered domain of higher-order antiferromagnetic boson interactions, which has not received attention in decades of research[86, 48, 49, 83]. The complexity of mathematical computations, along with a historical focus on quadratic products, has impeded research into higher-order spin wave phenomena. Recent discoveries in spintronic utilization of antiferromagnetic materials, as documented in [108], have generated a fresh interest in investigating spin waves for data transmission, storage, and spintronic devices, as well as the newly emerging field of magnonics. Despite the promising prospects for the practical use of antiferromagnetic spin waves and spintronic devices, certain basic questions remain unresolved. The effect of anisotropic variables, exchange field, and crystal structure are all significant topics that require more investigation.

This work was inspired by the researcher's teaching experience and interest in magnetism, namely ferromagnetism and antiferromagnetism, in low-dimensional quantum physics. Antiferromagnetism, a fascinating phenomenon, motivated this research even further.

1.3 Statement of Problem

We know antiferromagnetic materials exhibit unique magnetic properties, and understanding their behavior is crucial for various technological applications. This study focuses on investigating the effects of uniaxial anisotropy on key aspects such as the dispersion relation, temperature-dependent sublattice magnetization, and heat capacity in antiferromagnetic compounds characterized by nearest-neighbor exchange interactions.

Magnons or basic spin excitations, are important concepts in condensed matter physics. They have an effect on phenomena such as magnetic ordering, electrical and thermal transport properties, rapid magnetisation processes, and, most importantly, electron and spin dynamics have potential applications in information processing, especially spintronics [117]. However, several studies oversimplified spin-magnon interaction concepts by disregarding higher-order interactions amongst boson operators. This oversimplification is caused by both kinematic and dynamic interactions among ions in the system. It is important to note that this simplification

may become ineffective when the number of spin-wave quanta increases.

Previous studies have frequently neglected higher-order antiferromagnetic (AFM) boson interactions. These interactions have been largely overlooked in research on ion kinematics, dynamics, and Hamiltonian products. As a result, the AFM gaps caused by these previously ignored physical influences remain undiscovered.

Low working temperatures and small consequences restrict the practical application of anisotropy field effects in antiferromagnetic systems, despite their elegant nature. This emphasizes the need for more research to fully realize its promise in real-world applications.
The study begins by looking at the interaction of antiferromagnetic spin waves in the presence of a uniaxial anisotropy field. This study produced initial information demonstrating the possible influence of the anisotropy field on several thermodynamic variables.

Given this omission, it is evident that more research is required to determine the impacts of the anisotropic field, exchange field, and crystal structure on higher-order spin magnon interactions. Knowing these gaps and influential factors, we can now clarify the study's primary research question and specific aims as follows:

The Statement problems are:

- What will the dispersion relation be for the AFM spin interaction of a higher order combination of bosonic operators?
- How can anisotropy fields affect the dispersion relation and thermodynamic parameters of antiferromagnets?

1.4 General Objective

The general objectives of this research is: to investigate the effects of anisotropy fields on the dispersion relation and thermodynamic parameters of antiferromagnetic materials using Quantum Field Theory.

Specifice Objectives

This study intends to investigate the properties of antiferromagnetic spin waves, with an emphasis on anisotropy fields. The purpose of researching their behavior is to acquire insights for practical applications and a better knowledge of the materials. The objectives are to examine spin wave interactions and the effect of anisotropic fields on antiferromagnetic systems, ultimately connecting theoretical understanding with practical application.

- To find out the dispersion relations of antiferromagnets spin interactions with higher-order bosonic operators.
- To looking into the effects of anisotropy fields on the physical properties of antiferromagnet materials..

1.5 Significance

The investigation into the interaction of spin waves, specifically the examination of their dispersion relation, and the influence of anisotropy fields on the thermodynamic parameters of antiferromagnetic materials holds profound significance for researchers in the fields of spintronics, materials engineering, and magnonics. Understanding the intricate dynamics of spin waves and their behavior in the presence of anisotropy fields is crucial for advancing our knowledge in these domains.

Understanding the influence of anisotropy on antiferromagnetic materials is crucial for both fundamental research and practical applications. This knowledge could pave the way for the development of novel materials with tailored magnetic properties, leading to advancements in fields such as data storage, magnetic sensors, and quantum computing.

This research holds significant implications for various stakeholders:

1. This study provides valuable insights for teachers and advisors within the field, offering them a deeper understanding of the subject matter to better educate and guide their students.
2. The research may be relevant for researchers involved in the design and development of antiferromagnetic materials.

3. This work acts as a driving force and a springboard for future research endeavors and stimulating greater study and invention.

4. It is hoped that this work will serve as a useful reference.

Overall, this research not only contributes to the existing body of knowledge but also has practical implications across various disciplines, making it a significant and impactful contribution to the scientific community.

1.6 Scope

- The focus and emphasis of the study's themes are :- anisotropy field, dispersion, thermodynamic properties, and AFM materials.

- The method for analysis used "A Quantum Field Theory Approach",i.e Heisenberg Hamiltonian and Green Function technique.

1.7 Relevance of Study

The result of the research has importance in Spintronics:

- **Data Storage**: Insights into AFM spin waves aid in the development of spintronic devices, where magnetic properties are used for data storage and manipulation.

- **Quantum Computing**: Understanding spin dynamics is essential for developing quantum computing elements that rely on spin states for information processing.

Chapter 2

Literature Review on the Fundamental Theory of Antiferromagnetism

Magnetism, the phenomenon in which materials exhibit an attractive or repulsive force, has been known for millennia. Despite their ancient understanding, scientists have been unable to understand the complicated principles and mechanisms behind the magnetic phenomena until recently. These intricate and complex ideas have just lately begun to be understood. Magnetism and magnetic materials play an important role in many modern technological products. These include a wide range of technologies, namely electrical power generators and transformers, electric motors, radio and television sets, telephones, computers, and components for sound and video reproduction systems. The intricate interplay of magnetic forces in various applications demonstrates magnetism's deep effect and essential role in molding our technologically evolved environment.

This section will begin with an introduction to antiferromagnetism. It will cover the general concept (2.1), fundamental spin physics principles (2.2), antiferromagnetic ordering and exchange using the Heisenberg exchange Hamiltonian (2.3) and Molecular Field theory (2.4).

2.1 Physical Properties of Magnetism

A thorough understanding of magnetism and the physical properties of magnetic materials is required to appreciate the fundamental science behind this occurrence.

Many physical processes in magnetic materials are inextricably linked to fundamental quantum mechanics challenges, such as highly correlated systems, quantum phase transitions, and fluctuations. Beyond theoretical physics, magnetic materials have a substantial influence on materials engineering and our daily life.

2.1.1 Basic Concepts of Magnetism

The origin of magnetism can be traced back to electron spin. In ferromagnetic materials, the electron spins of neighboring atoms align parallel to the direction of the applied magnetic field; whereas, in antiferromagnetism, electron spins are antiparallel, causing the energy difference between nearest neighbor spins to drop and resulting in materials with no net magnetic moment. In most compounds, magnetic atoms or ions are contained in a crystalline lattice and surrounded by other ions. The crystal structure dictates the symmetry of nearest neighbor coordination. Metal ions are frequently surrounded by diamagnetic ions that have a negative charge. After contributing their valence electrons to the conduction band, the component atoms in metallic systems retain an effective electric charge. Conduction electrons partly screen positive ions, reducing their effective charge in contrast to equal ionic charges. The crystal field or ligand field is the electrostatic force that affects a magnetic ion's unpaired electrons, and the surrounding ions are referred to as ligands [65].

2.1.2 Magnetic Materials

Magnetism and quantum mechanics are closely related in physics because a completely classical system in thermal equilibrium lacks a magnetic moment, even in the presence of a magnetic field. Magnetic materials are frequently classified into two types based on their magnetic properties. The first kind consists of diamagnets and Pauli paramagnets, which are distinguished by atoms with fully occupied electron shells. In the absence of an external magnetic field, these materials have no visible magnetization. The second category contains compounds with spontaneous magnetic order, which commonly contain transition metal atoms with partially filled d- and f-electron shells. Strong chemical bonding, or delocalization of valence electrons in solids, promotes the formation of non-magnetic structures with doubly occupied lower electronic states. While almost all free atoms with partially complete d-shells have nonzero spin and orbital moments, only transition metals toward

the end of the third row (Mn, Fe, Co, Ni) exhibit significant magnetic characteristics [68, 69]. The magnetization of d-orbital metals is essentially defined by spin moments.

2.1.3 Antiferromagnetically Ordered State

Strong magnetic interactions occur when the magnetic moments of adjacent atomic sites interact, resulting in magnetic ordering inside the crystal. Antiferromagnetism, like ferromagnetism, appears as a collective phenomena with an ordered state appearing below a well-defined critical temperature. Antiferromagnets have negative exchange energy, which favors antiparallel alignment of neighboring spins.

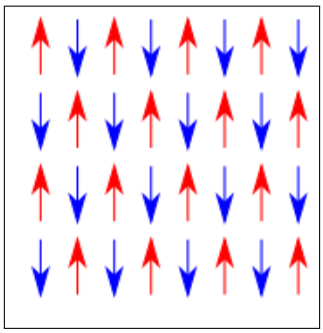

Figure 2.1: Array of antiferromagnetic ordering [43]

The two-sublattice model remains the most often used framework for understanding antiferromagnetism. Within this concept, the array of magnetic atoms is divided into two symmetrical and interpenetrating sublattice. In antiferromagnetic material ordering, nearby spins tend to point in opposing directions [43]. When outlining antiferromagnetic materials, it is useful to divide the material into two sublattices, as seen in Fig.2.1. Within each sublattice, all spins align in the same direction for a spatially uniform antiferromagnet.

When only nearest-neighbor interactions are examined, spins on one sublattice interact with their closest counterparts on the next sublattice. The negative exchange interaction energy allows the two sublattices to magnetize spontaneously in opposing directions. This model, initially developed by Néel, serves as the foundation for subsequent theoretical studies of antiferromagnetism. At extremely low temperatures, the spins of each sublattice are perfectly antiparallel. As temperature rises, each sublattice's spontaneous magnetization reduces and eventually disappears in

the absence of an applied field, reaching a critical temperature known as the Néel point. The net magnetization is zero since the two sublattices are the same. The two-sublattice concept applies solely to basic hypercubic crystal formations [109].

Antiferromagnetic ordering is common in transition metal compounds, which include metal oxides and other compounds [82]. All $3d$ transition metal elements with non-ferromagnetic behavior are predicted to have antiferromagnetic behavior below their critical temperatures.

The proportionality constant is positive for ferromagnetic materials but negative for antiferromagnetic ones. The lowest state of antiferromagnetism occurs when neighboring magnetic moments are always antiparallel, whereas the highest state occurs when all magnetic moments are parallel. This condition may be useful to view as a ground level ordering of the antiferromagnetic state. In an ordered antiferromagnet, magnetic moments form interpenetrating sublattices.

2.1.4 Basics of Antiferromagnetism

A basic antiferromagnet is represented by two magnetic sublattices (A and B). In the magnetically ordered condition, the atomic moments are parallel or ferromagnetically coupled inside the two sublattices. Any two atomic magnetic moments from different sublattices have an antiparallel orientation. This connection creates an antiparallel alignment in such a group; antiferromagnetism occurs when the spin moments of nearby atoms or ions align in completely opposite directions.

To describe the magnetic properties of antiferromagnets, we can use an electron's inherent electronic properties in a crystal. In addition to its negative charge, the electron possesses an inherent degree of freedom known as intrinsic angular momentum, or spin. Antiferromagnetism arises when nearby atoms or ions' spin moments align in completely opposing orientations [43], comparable to how the electron spins about its own axis like the Earth (Fig.2.2).

A spin flipped distributed over a group of sites corresponds to a quasi-particle called a magnon, the operators $a_j^\dagger$ and a_j can also be viewed as magnon (or spin deviation) creation and annihilation operators, respectively. More than one flipped spin can exist on a site (depending on the total spin), it is possible for multiple magnons

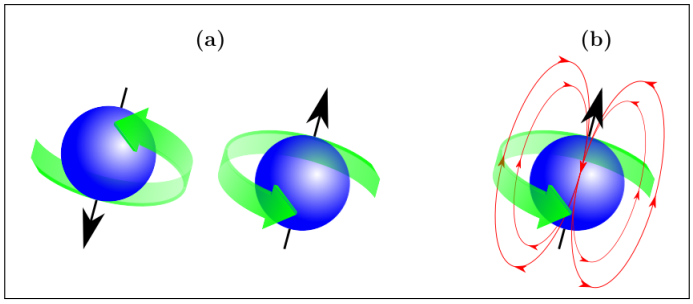

Figure 2.2: Two electrons with spin down and spin up(a), The electron spin results in a magnetic moment (b), adapted from [43]

to exist at the same location, and we conclude that the quasi-particles do not obey the Pauli exclusion principle. This means that magnons behave as bosons. Antiferromagnets have been used as the active component in spintronic devices has been surging [43, 46, 87].

This is interesting because antiferromagnets have several advantages over ferro-

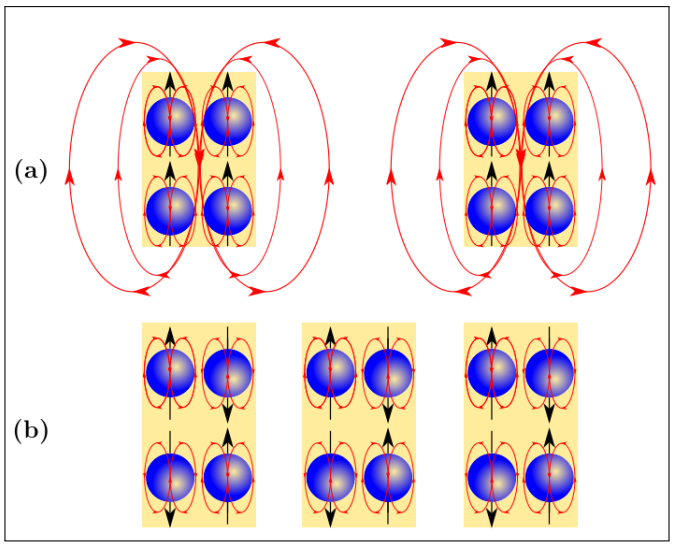

Figure 2.3: Ferromagnetic components require adequate separation to avoid unwanted crossing induced by the external magnetic fields they create (see red field lines). (b) Antiferromagnetic components have a strong internal magnetic field, while the external magnetic field cancels due to antiparallel ordering. As a result, antiferromagnetic components may be packed more densely than ferromagnetic components, adapted from [43]

magnets. Antiferromagnets produce no external/stray magnetic fields, which allows for a denser packing of antiferromagnetic components, as shown in Fig.2.3. Antiferromagnetic components have a strong internal magnetic fields, but the external magnetic fields is cancelled due to the antiparallel ordering. They can therefore

be more densely packed than ferromagnetic components. Further more, antiferromagnets are insensitive to magnetic noise and have very high resonance frequency compared to ferromagnets.

Antiferromagnetism, like ferromagnetism, is a cooperative phenomenon with an ordered state below a well-defined critical temperature. For the antiferromagnet, the exchange integral is negative, and neighboring spins tend to align antiparallel. The interaction between spins originates mainly in the exchange interaction, with magnitude represented by an exchange parameter(J). The intra-sublattice exchange interaction (J) is considered to be positive because it is due to direct exchange, while the inter-sublattice exchange parameter (J) is negative because it arises from the super-exchange that is mediated by ligand ions between the magnetic ions [72].

2.2 Electronic States of Free Magnetic Ions

We begin by describing the ground states of free magnetic ions which have incomplete shells. There are three series of magnetic ions, iron-group series, rare-earth series and actinide series. They have 3d-, 4f- and 5f-incomplete shells, respectively. These magnetic ions play an important role in the field of magnetism [69].

2.2.1 Magnetic Moments of Electron

Magnetism is intimately connected with angular momentum of elementary particles, so the quantum theory of magnetism is closely linked to the quantization of angular momentum. Electrons possess an intrinsic angular momentum $\frac{1}{2}\hbar$ known as spin , where $\hbar$ is Planck's constant.

The magnetic moments in solids are associated with electrons. The microscopic theory of magnetism is based on the quantum mechanics of electronic angular momentum, which has two distinct sources, orbital motion and spin. They are coupled by the spin-orbit interaction.

The magnetic moment of a free atom is essentially determined by three sources: electron spin, electron orbital angular momentum about the nucleus, and the change in orbital momentum generated by an external magnetic field. The first two acts

provide paramagnetic contributions to magnetization, whereas the third causes diamagnetism. Atoms with fully populated electron shells have no spin or orbital moment. Atomic magnetic moments relate to partially filled electron shells.

Magnetic moments originate from the macroscopic magnetic properties of materials, which are created by electron spins associated with single electrons. These concepts are difficult to understand and need exact quantum-mechanical laws; nonetheless, simplifications have been developed to achieve mental embodiment. Each electron in an atom has magnetic moments that come from two sources. (2.4).

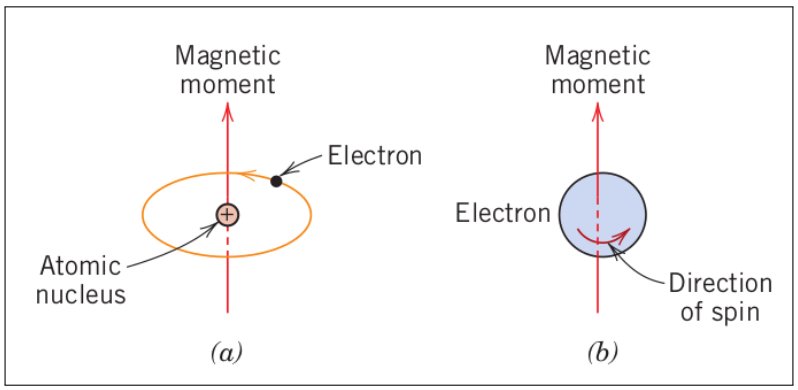

Figure 2.4: Magnetic moment associated with (a) an orbiting electron and (b) a spinning electron.

An electron's orbital motion around the nucleus is analogous to a tiny current loop, producing a small magnetic field and possessing a magnetic moment along its axis of rotation, as seen in Fig.2.4. The production of current is directly associated with the movement of charged particles. In the context of atomic structures, this phenomenon appears as a very small current loop. Electrons in an atomic orbital move around the atomic nucleus, causing a dynamic interaction between electric charge and magnetic field, as seen in Fig.2.4.

When an electron rotates with an average orbital velocity ω, it produces a current of $\frac{e\omega}{2\pi c}$ where e (electrin charge), ω (angular frequency), and c (speed of light). Of course, such a current will create a magnetic field perpendicular to the plane of the rotation, with the magnetic moment provided by the product of the current and the area of the orbit.

$$\mu = \frac{e\omega}{2\pi c}\pi r^2 \tag{2.1}$$

where r is the mean radius of the orbit.

The magnetic moment of an orbital electron is a critical metric in this situation. It describes the magnetic characteristics of an electron's orbital motion. It describes the complicated movement of charged particles surrounding the atomic nucleus, which generates a subtle but considerable magnetic field. The interaction between electron motion and the resulting magnetic moment has important consequences for understanding the fundamentals of atomic and quantum physics. It is expressed as:

$$\vec{\mu} = IA\hat{n} \tag{2.2}$$

where μ is magnetic moment, I is current, and A is the loop area. The vector $\hat{n}$ is a unit vector normal to the loop surface accordiγng to the right-hand rule. The torque on the loop is

$$\vec{\tau} = \mu_0 \vec{\mu} \times \vec{H} \tag{2.3}$$

The loop will also have angular momentum in the direction parallel (or antiparallel) to $\hat{n}$. Electrons with charge e spin on their axis and have a magnetic dipole $\vec{\mu}$. When exposed to an external magnetic field $\vec{H}$, a free electron acquires potential energy as follows:

$$E = -\vec{\mu} \cdot \vec{H} \tag{2.4}$$

The relationship between magnetic moment $\vec{\mu}$ and spin angular momentum $\vec{S}$ may be expressed as:

$$\vec{\mu} = \gamma \vec{S} \tag{2.5}$$

where γ refehim in accordance with the Copyright, Designs and Patents Act 1988.rs to the gyromagnetic ratio. For an electron in a uniform sphere with uniform charge distribution, $\gamma = e/2m$. However, real electrons have a greater magnetic moment than this basic model predicts, and the discrepancy can usually be corrected by expressing in terms of the Landé-g factor; $\mathrm{g} = \dfrac{\gamma}{\mathrm{e}/2\mathrm{m}} > 1$. If we consider a magnetic field $\vec{H}$ to be along the z-direction, the potential energy is:

$$E = \mu_z H_z = \gamma S_z H_z \tag{2.6}$$

We know from quantum mechanics that S_z can only have two values: $S_z = \pm\dfrac{1}{2}\hbar$.
The difference in the two energies is then:

$$\Delta E = \gamma \hbar H_z \tag{2.7}$$

If a photon incident on an electron has an energy corresponding to this energy difference and the electron is in the lower energy state, the photon may be absorbed, inducing the electron to 'flip' its orientation: this phenomenon is electron spin resonance. Since the photon energy is just $h\nu$, we can re-write Eq.(2.7) in terms of the frequency of the incident radiation:

$$\omega = \gamma H_z \tag{2.8}$$

The magnetism of materials originates from the magnetic moment of electrons, which are either itinerant or localized. The electron has a unique angular momentum $\hbar s$ due to its spin degree of freedom, and the spin magnetic moment is proportional to **S**:

$$\mu_s = -\mathrm{g}\mu_\mathrm{B}\mathrm{S} \tag{2.9}$$

where μ_B is called the Bohr magneton; its magnitude is in cgs-Gauss units $\mu_B = \frac{e\hbar}{2mc} = 0.927 \times 10^{-20} emu$, here e is the magnitude of the charge of electron, m its mass, c the speed of light, and $\hbar$ the Plancks constant. The minus sign in Eq.(2.9) is due to the negative charge of the electron, g is usually called the g-value; the magnitude for free electrons is $\mathrm{g} = 2.003$. The spin magnetic moment in Eq.(2.9) can be derived from Dirac's relativistic theory of the electron [115], approximately, it comes from the rotation of the electron. In addition to the spin magnetic moment, the electron has the orbital magnetic moment

$$\mu_{or} = -\frac{e}{2c}(\vec{r} \times \vec{v}) \tag{2.10}$$

which arises from the orbital motion of the electron. Here r is the position vector of the electron and v the velocity. This quantity can be written as

$$\mu_{or} = -\frac{e}{2mc}(\vec{r} \times \vec{p}) = -\mu_B \mathbf{l} \tag{2.11}$$

As previously stated, electrons are responsible for the dominant angular momentum that results in macroscopic magnetism. Spin and orbital angular momentum will have an equivalent connection to magnetic moment. Electrons in atoms can have two forms of angular momentum: orbital ($\vec{L}$) and spin ($\vec{S}$). The total angular momentum is just the vector sum.

$$\vec{J} = \vec{L} + \vec{S} \tag{2.12}$$

Orbital angular momentum is due to the motion of the electron about the atom. In the presence of both spin and orbital angular momenta, we can rewrite the equation for magnetic moment

$$\vec{\mu} = \gamma(\vec{L} + 2\vec{S}) \tag{2.13}$$

then, $\vec{\mu}$ and $\vec{J}$ are no longer parallel or antiparallel when both $\vec{L}$ and $\vec{S}$ contribute to $\vec{J}$. The constant of proportionality between the magnetic moment and the angular momentum is called the gyromagnetic ratio as already defined;

$$\vec{\mu} = \gamma\vec{J} \tag{2.14}$$

If the charge is negative, the conventional current and particle velocity will have opposing directions, $\vec{\mu}$ and $\vec{J}$ will be antiparallel, and γ will be negative.

The macroscopic magnetic properties of a material are the consequence of interactions between an external magnetic field and the magnetic dipole moments of its constituent atoms. Each electron contains both orbital and spin magnetic moments. The net magnetic moment of an atom is just the sum of its electrons' contributions, with spin and orbital moment cancelling out between electron pairs. The distinction between B and H is trivial in free space. They are simply related by the magnetic constant μ_0:

$$B = \mu_0 H \tag{2.15}$$

Permeability, μ, is a quality of the medium through which the H field passes and **B** is measured. The fundamental field **B**, the auxiliary field **H** and the magnetization **M** of the medium is normally rearranged as

$$B = \mu_0(H + M) \tag{2.16}$$

In the presence of a H field, the magnetic moments inside a material attempt to align with and enhance the field using their magnetic fields, provided by $M = \chi_m H$. The above expression describes another field quantity, M, also called the solid's magnetization. and χ_m is called the magnetic susceptibility, which is a unitless. The magnetic susceptibility and the relative permeability are related as follows:

$$\mu = \chi_m + 1 \tag{2.17}$$

This is a dielectric analogue for magnetic field parameters.

2.2.2 Localized Magnetic Model in Solid

The magnetic nature of of an ions in the solid are characterized by an incomplete electron shell whose structure is determined by the Russel-Saunders coupling [14, 80]. The orbital angular momenta of the electrons are coupled into **L** and the spin angular momenta into **S** by the electrostatic interaction. Then **L** and **S** couple into the total angular momentum **J**. For a free ion, J_z and J^2 are constants of motion of the system. In the presence of magnetic field **H**, the interaction between the electrons in the incomplete shell of an ion and the field is given by (in units $\hbar = 1$)

$$\mathcal{H} = \sum_j \frac{e}{2mc}\vec{H}\cdot(\vec{r}_j \times \vec{p}_j) - \sum_j \frac{e}{mc}\vec{H}\cdot\vec{S}_j \tag{2.18}$$

where e is the charge of an electron, $\vec{r}_j$, $\vec{p}_j$ and $\vec{S}_j$ are the position, momentum, and spin vectors of the j-th electron, and the summation is taken over all electrons in the shell. By definition of the $\vec{L}$ and $\vec{S}$ operators, $\mathcal{H}$ can be written as

$$\mathcal{H} = \frac{e}{2mc}\vec{H}\cdot(\vec{L}+2\vec{S}) \tag{2.19}$$

Taking $\vec{H}$ in the z-direction, one obtains

$$\begin{aligned}\mathcal{H} &= \frac{e}{2mc}H(L_z+2S_z)\\ &= \frac{e}{2mc}H(J_z+S_z)\end{aligned} \tag{2.20}$$

The matrix element of the interaction is, to first order,

$$\langle JJ_z^{'}|\mathcal{H}|JJ_z\rangle = \frac{e}{2mc}H\langle JJ_z^{'}|J_z+S_z|JJ_z\rangle \tag{2.21}$$

By the projection theorem for angular momentum, this is equal to

$$\begin{aligned}\langle JJ_z^{'}|\mathcal{H}|JJ_z\rangle &= \frac{e}{2mc}H\langle JJ_z^{'}|1+\frac{\vec{S}\cdot\vec{J}}{2j(j+1)}J_z|JJ_z\rangle\\ &= \Big[1+\frac{j(j+1)-l(l+1)+S(S+1)}{2j(j+1)}\Big]\frac{e}{2mc}HJ_z\delta_{J_zJ_z^{'}}\\ &= \mathrm{g}\frac{\mathrm{e}}{2\mathrm{mc}}\mathrm{HJ_z}\delta_{\mathrm{J_zJ_z'}}\end{aligned} \tag{2.22}$$

The quantity in the square bracket is called the Landé g-factor and is denoted by g and we recall that ($\frac{|e|}{2mc}$) is the Bohr magneton μ_B. Therefore the degeneracy in J_z is completely splitted and the energy levels are equally spaced

$$E_z = \mathrm{g}\mu_\mathrm{B}\mathrm{HJ_z} \tag{2.23}$$

The magnetic moment operator is $\vec{\mu}_z$ defined by

$$\mathcal{H}_z = -\mu \vec{H} \cdot \vec{J}_z \tag{2.24}$$

Therefore, with $\vec{H}$ in the z-direction

$$\begin{aligned} \mu_z &= -(\frac{|e|}{2mc})(L_z + 2S_z) \\ &= -(\frac{|e|}{2mc})(J_z + S_z) \end{aligned} \tag{2.25}$$

The expectation value of μ_z in the state $|JJ_z\rangle$ is therefore

$$\begin{aligned} \langle \mu_z \rangle &= -(\frac{|e|}{2mc})\langle JJ_z|J_z + S_z|JJ_z\rangle \\ &= -g\mu_B J_z \end{aligned} \tag{2.26}$$

For a system of N free ions per unit volume in thermal equilibrium, the energy levels of different are occupied according to the Boltzmann distribution. The total magnetic moment of the system is therefore

$$\begin{aligned} M &= N\frac{\left[\sum_{J_z}\langle \mu_z \rangle e^{-\frac{xJ_z}{J}}\right]}{\sum_{J_z} e^{-\frac{xJ_z}{J}}} \\ &= Ng\mu_B J \mathbf{B_J}(\mathbf{x}) \end{aligned} \tag{2.27}$$

where $x = \frac{g\mu_B J}{k_B T}H$, and

$$\mathbf{B_J}(\mathbf{x}) = \frac{\mathbf{2j+1}}{\mathbf{2j}}\coth\left(\frac{\mathbf{2j+1}}{\mathbf{2j}}\mathbf{x}\right) - \frac{\mathbf{1}}{\mathbf{2j}}\coth\left(\frac{\mathbf{1}}{\mathbf{2j}}\mathbf{x}\right) \tag{2.28}$$

Where $\mathbf{B_J}(\mathbf{x})$ is the Brillouin function. This expression gives the magnetic moment of a collection of free ions as a function of temperature and applied field.

For transition metal ions in solids, the orbital angular momentum of the electrons in the incomplete shell is often quenched by the crystalline electric field [29]. In this picture, each ion is regarded as being in a state with total orbital quantum number $L = 0$ and total spin quantum number $\mathbf{S}$. Then, for a system of N free ions, the total magnetic moment reduces to

$$M = N\mathrm{g}\mu_\mathrm{B}\mathrm{S}\mathbf{B_S}(\mathbf{x}) \tag{2.29}$$

by the substitutions of $J = S$ and $L = 0$ from Eq. (22) and (23). Actually, the Lande g-factor should be 2, since the absence of any orbital angular momentum is assumed. Nevertheless, small amounts of residual orbital angular momentum may be taken into account by allowing g to take on values slightly different from 2.

2.2.3 Exchange Interaction

The fundamental problem of coupled spin systems is the origin of the exchange interaction. The exchange interaction and antiferromagnetism both originate from quantum mechanics. In order to understand antiferromagnetism, which varies from ferromagnetism in that it has a negative exchange integral, one must return to the theory of the chemical bond. The challenge of defining an antiferromagnets quantum state is analogous to that of explaining the state of a complex chemical molecule. As the number of spins rises, the number of bond configurations with which the molecule is in resonance rises very quickly.

There is only one state, and it has a brief description. This is the state that a ferromagnet would be in at its lowest point, and an antiferromagnet would be in at its maximum point. The explanation for the chemical bond was provided by the newly developed quantum theory. If the spin state of the resulting molecule is one in which the electrons of the two atoms have antiparallel spins, an atom with an unpaired spin can form a bond with another atom of a similar kind. This was explained using a negative exchange integral [34].

The exchange field is defined as the interaction between magnetic moments. The resulting exchange force is the cause of the magnetic moment's tendency to align parallel to one another, and it is dependent on the relative orientation of the spins of the two electrons. The exchange force is quantum mechanical and has no classical counterpart [21]. The energy of the exchange interaction between a pair of electrons, i and j, is given by

$$E_{ex} = -2\mathbf{J}_{ij}\mathbf{S}_i \cdot \mathbf{S}_j = -2J_{ij}S_iS_j\cos\phi \tag{2.30}$$

where $\mathbf{S_i}$ and $\mathbf{S}_j$ are the spins of the electrons, and $\mathbf{J_{ij}}$ is the exchange integral and is related to the overlap of the charge distributions of atoms i and j. Therefore, the energy will depend on the orientation of spins. Note that for a parallel spin orientation, $\phi = 0$ and $\cos\phi = 1$, so $J_{ij} = J$ must be positive for energy to be minimized. This gives rise to ferromagnetic ordering. Conversely, if $\phi = \pi$, and $\cos\phi = -1$, then J can be negative to minimize energy, giving the antiferromagnetic order.

The most important magnetic interaction in antiferromagnetism is exchange interaction. The presence of of both ligand and magnetic ions suggests that superexchange.

In any event, the Heisenberg Hamiltonian will be assumed to express the exchange interaction between two magnetic ions is

$$\mathsf{H} = -2\sum_{\langle ij\rangle} J_{ij}\vec{S}_i \cdot \vec{S}_j \tag{2.31}$$

The Heisenberg model only includes nearest-neighbor interactions, denoted by $\langle ij\rangle$, but it can be extended to include interactions over several atomic distances. However, the exchange interaction is a short-ranged interaction, and a nearest-neighbor model often captures the essential physics.

2.2.4 Magnetic Anisotropy

Thus, magnetic anisotropy is frequently associated with spin-orbit coupling, which occurs when the electron's velocity interacts with its spin, as the name suggests. The spin-orbit interaction is a relativistic phenomenon. Its creation may be explained systematically as follows: from the electron's reference frame, the positively charged nuclei of the crystal move, resulting in a dynamical electric potential. This produces a magnetic field that interacts with the electron's magnetic moment, also known as its spin.

The orientation of spins, and consequently magnetization of a material, will have some favored orientations in the crystalline lattice known as easy axes. They are separated by energy barriers. Magneto-crystalline anisotropy energy is also required to push magnetisation over such a barrier.

The energy required to change the orientation of a single spin is referred to as the single ion anisotropy energy k_a. The anisotropy energy density K is related to single ion anisotropy by the equation $K = nk_a s^2$, where n is the density of magnetic ions and S is their spin. An anisotropy field B_A [2] can be described as:

$$B_A = \frac{|K|}{M_s} = \frac{2k_a S}{\mathrm{g}\mu_\mathrm{B}} \tag{2.32}$$

where M_s is the sublattice magnetisation given by $M_s = \frac{1}{2}\mathrm{g}\mu_\mathrm{B}\mathrm{nS}$.

The magnetic dipolar interactions among the ions, as well as the crystal field contribution from the surrounding ions, are essential factors contributing to the anisotropy of materials with transition metal magnetic ions in unfilled 3d shells. In oxide

samples, incomplete electron orbitals of a magnetic ion interact with electrons in neighboring oxygen anions [115]. This causes the orbital moments to be coupled to the lattice, resulting in anisotropy owing to the lattice's asymmetry. If the lattice is stressed, the coupling changes, resulting in strain anisotropy.

2.2.5 Zeeman Effect

The Zeeman effect describes the interaction energy, called Zeeman energy, between a material's magnetization M and an external magnetic field H. It causes the magnetic moment to align with the field, resulting in spin-dependent splitting of electron energy levels. This interaction makes it energetically favourable for the magnetization to align with the magnetic field, whether the field is static or varying. The free energy's contribution from the Zeeman interaction can be expressed as

$$\mathcal{H}_Z = \frac{g\mu_B \tilde{H}}{\hbar} \cdot \sum_i \vec{S}_i \tag{2.33}$$

While antiferromagnets are famous for being exceedingly resistant to magnetic fields, there is still interaction with external magnetic fields even when the material has vanishing net magnetization. We'll see later that an easy-axis antiferromagnet in resonance has a modest net magnetization that can interact with external magnetic fields.

2.3 Molecular Field Theory of Antiferromagnetism

NÃ©el (1971) first proposed the molecular field theory for an antiferromagnetic material with two sublattices, A and B. This theory is especially useful for a body-centered cubic lattice, in which the A sublattice occupies the corner positions and the B sublattice fills the body-centered positions [72, 61]. In this arrangement, an atom at an A site has nearest neighbors on B sites and next nearest neighbors on A sites. The same holds true for an atom on a B site. The physical situation is described using molecular fields H_A and H_B, dependent on the magnetization M_A and M_B for each sublattice. Therefore, the molecular field H_A^m acting on an atom at an A site can be expressed as follows:

$$H_A^m = -\alpha_{aa} M_A - \beta_{ab} M_B \tag{2.34}$$

where M_A and M_B are the magnetizations of the A and B sublattices, respectively, β_{ab} is a molecular field constant for the nearest neighbor interaction, and α_{aa} is a molecular field constant for the next nearest neighbor interaction.
Similarly, the molecular field H_B^m acting on an atom at a B site may be written

$$H_B^m = -\beta_{ab} M_A - \alpha_{bb} M_B \tag{2.35}$$

Since the same type of atoms occupy the A and B lattice sites, the intrasublattice-molecular-field constant $\alpha_{aa} = \beta_{bb} = \alpha_{ii}$ is different in magnitude and sign from the intersublattice-molecular-field constant $\alpha_{ab} = \beta_{ab} = \beta$. Here we note that λ_{ii} is intrasublattice molecular constant, and β is intersublattice molecular constant.
Then, suppose the field is applied parallel to the easy magnetization axis in an antiferromagnetic single crystal, with H parallel to the A-sublattice magnetization and antiparallel to the B-sublattice magnetization. The fields H_A and H_B of an atom on the A and B lattices, respectively, are given by

$$\begin{aligned} H_A^m &= H - \alpha_{ii} M_A - \beta M_B \\ H_B^m &= H - \beta M_A - \alpha_{ii} M_B \end{aligned} \tag{2.36}$$

The interaction between nearest neighbors is antiferromagnetic and therefore the molecular field constant β must be positive. On the other hand, it is conceivable that α_{ii} may be positive, negative, or even zero, depending on the particular material.

The expression for the spontaneously magnetizations M_A and M_B as function of temperature T and those for the susceptibilities above and below the Néel temperature can now be derived. At thermal equilibrium the magnetizations of the sublattices from thermodynamical analysis yields [61]; Eq.(2.27) and Eq.(2.28) can be rewrite for spin system as

$$M = \frac{1}{2} N \mathrm{g} \mu_{\mathrm{B}} \mathrm{S} \mathbf{B_s}(\mathbf{x}), \qquad \mathbf{x} = \frac{\mathbf{S} \mathrm{g} \mu_{\mathrm{B}}}{\mathbf{k_B T}} \mathbf{H} \tag{2.37}$$

where $\mathbf{B_s}(\mathbf{x})$ is the Brillouin function defined by

$$\mathbf{B_s}(\mathbf{x}) = \frac{\mathbf{2S+1}}{\mathbf{2S}} \coth\left(\frac{\mathbf{2S+1}}{\mathbf{2S}}\right)\mathbf{x} - \frac{\mathbf{1}}{\mathbf{2S}} \coth\left(\frac{\mathbf{x}}{\mathbf{2S}}\right) \tag{2.38}$$

Thus the magnetization of each sublattice can be written as

$$\begin{aligned} M_A &= \frac{1}{2} N \mathrm{g} \mu_{\mathrm{B}} \mathrm{S} \mathbf{B_s}(\mathbf{x_A}) \\ M_B &= \frac{1}{2} N \mathrm{g} \mu_{\mathrm{B}} \mathrm{S} \mathbf{B_s}(\mathbf{x_B}) \end{aligned} \tag{2.39}$$

Here N is the total number of atoms (or ions) with a permanent dipole moment per unit volume, and has been set equal to S.

Expansion of the Brillouin function to the first term of the series in x, (i.e $\mathbf{B_s(x)} = \frac{\mathbf{s+1}}{\mathbf{3s}}\mathbf{x}$). Then the sublattice magnetization becomes

$$\begin{aligned} M_A &= \frac{C'}{T}H_A = \frac{C'}{T}(H - \alpha_{ii}M_A - \beta M_B) \\ M_B &= \frac{C'}{T}H_B = \frac{C'}{T}(H - \beta M_A - \alpha_{ii}M_B) \end{aligned} \tag{2.40}$$

where $C' = \frac{N\mathrm{g}^2\mu_\mathrm{B}^2\mathrm{S}(\mathrm{S}+1)}{6k_B}$. Since H, M_A and M_B are parallel in the paramagnetic region. Addition of these magnetization (M_A and M_B) equation yields

$$M = M_A + M_B = \frac{C'}{T}[2H - (\alpha_{ii} + \beta)M] \tag{2.41}$$

Hence the susceptibility of magnetization ($\chi = \frac{M}{H}$) is given by

$$\chi = \frac{2C'}{T + C'(\alpha_{ii} + \beta)} = \frac{2C'}{T + \theta} \tag{2.42}$$

Where $\theta = C'(\alpha_{ii} + \beta)$ and generally the magnitude of $\beta > \alpha_{ii}$ and θ is positive. We recall that, below the Néel temperature both sublattices possess a spontaneous magnetization (at external field H = 0) of equal magnitude. The critical temperature at which the spontaneous magnetization of one of these sublattices vanishes can be found by approaching from the high temperature side ($T > T_N$). The equations of sublattice magnetizations M_A and M_B in the vicinity of T_N with H=0 becomes

$$\begin{aligned} M_A &= \frac{C'}{T}(-\alpha_{ii}M_A - \beta M_B) \\ M_B &= \frac{C'}{T}(-\beta M_A - \alpha_{ii}M_B) \end{aligned} \tag{2.43}$$

For non-zero values of the magnetizations M_A and M_B the determinant of the coefficients of M_A and M_B must be zero. Application of this condition yields the Néel temperature, namely,

$$\begin{vmatrix} 1 + \frac{C'}{T}\alpha_{ii} & \frac{C'}{T}\beta \\ \frac{C'}{T}\beta & 1 + \frac{C'}{T}\alpha_{ii} \end{vmatrix} = 0 \tag{2.44}$$

Solving we get

$$T_N = C'(\beta - \alpha_{ii}) = \frac{N\mathrm{g}^2\mu_\mathrm{B}^2\mathrm{S}(\mathrm{S}+1)}{6k_B}(\beta - \alpha_{ii}) \tag{2.45}$$

Hence, the Néel temperature is higher, the stronger the AB interaction and the weaker the AA or BB interaction, as is to be expected on physical reason. In particular, if there are nearest neighbor interactions only, α_{ii} vanishes [61] and hence

$$T_N = \frac{N\mathrm{g}^2\mu_\mathrm{B}^2}{6k_B} S(S+1)\beta \tag{2.46}$$

Substitution for C from $\theta = C'(\alpha_{ii}+\beta)$ into Eq.(29) gives the ratio of the "paramagnetic" temperature θ to the Néel temperature.

$$\frac{\theta}{T_N} = \frac{\beta+\alpha_{ii}}{\beta-\alpha_{ii}} \tag{2.47}$$

If $\alpha_{ii} = 0$, $T_N = \theta$, whereas if $\alpha_{ii} > 0$, $\theta > T_N$. Further, there is an upper limit to the ratio $\dfrac{\theta}{T_N}$. If α_{ii} becomes too large in comparison to β, the two sublattice arrangement assumed to be unstable.

The simplest basic situation in molecular field theory consists of two sub-lattices, each with half of the total number of magnetic moments, and the moments on each intra-sublattices are mutually parallel. The sum of the magnetic moments of each sublattice results in two macroscopic mutually antiparallel magnetization vectors $\vec{M}_A$ and $\vec{M}_B$, with magnitudes $\dfrac{N_A}{M}\mathrm{g}\mu_\mathrm{B}\langle \mathrm{S}\rangle$. Here, N_A is Avogadro's number, M is the molecular weight, and $\langle S\rangle$ is the expected value of the spin quantum number. In the ordered state of an antiferromagnet, the lattice of magnetic moments can be divided into a number of interpenetrating sublattices, with magnetic ions from one sublattice having only nearest neighbors from other sublattices.

The coupling of spins is represented by the ions' effective magnetic fields. One half of the effective field is formed by another ion in the same sublattice, while the other part is formed by the contribution of another sublattice. The molecular field constant for sublattices may be estimated using the method used in the analysis of [61], as illustrated below:

$$\begin{aligned} \alpha_{ii} &= \frac{4}{N\mathrm{g}^2\mu_\mathrm{B}^2}\sum_{ii'} J_{ii'} \\ \beta &= \frac{4}{N\mathrm{g}^2\mu_\mathrm{B}^2}\sum_{ij} J_{ij} \end{aligned} \tag{2.48}$$

Since α_{ii} is intra-sublattice molecular field constant of the species of spin, the transition temperature can be approximated as

$$T_N = \frac{4C'}{N\mathrm{g}^2\mu_\mathrm{B}^2}\Big(\sum_{ij} J_{ij} - \sum_{ii} J_{ii}\Big) = \frac{2S(S+1)}{3k_B}\Big(\sum_{ij} J_{ij} - \sum_{ii} J_{ii}\Big) \tag{2.49}$$

2.4 Magnetization in Antiferromagnetism

The magnetic moments of atoms or molecules, which are normally linked to the spins of electrons, align in a predictable way in antiferromagnetic materials with neighboring spins (on different sublattices) pointing in the opposite directions. It resembles ferromagnetism and it is a type of structured magnetism.
At a very low temperature, the net antiferromagnetic magnetization should be zero, however spin canting frequently results in a modest net magnetization developing. The average magnetism at each site of all the sublattices, each properly rotated to align them all in the same direction, is summed to define staggered magnetization in a general sense that is valid for any lattice in any dimension . We may find the staggered magnetization order parameter by using:

$$M_{stag} = \sum_{i}^{A,B} (-1)^i \vec{S}_i^z \tag{2.50}$$

where $(-1)^i = \begin{cases} 1 & \text{for} \quad i = A \\ -1 & \text{for} \quad i = B \end{cases}$
One needs to employ a representation of the relevant rotations for more complex shapes in 2D or 3D. The magnetizations at sites ℓ and m located on the spin-up and spin-down sublattices, respectively, are generally given by

$$\begin{aligned} \langle S_\ell^z \rangle &= S - \langle a_\ell^\dagger a_\ell \rangle \\ \langle S_m^z \rangle &= -S + \langle b_m^\dagger b_m \rangle \end{aligned} \tag{2.51}$$

The basis of this microscopic model is the nearest-neighbor sites ℓ and m on a hypercubic crystal lattice with spacing a. The relevant double-time Green's functions of the spin deviation operators correlation relation may be used to calculate the statistical averages $\langle a_\ell^\dagger a_\ell \rangle$ and $\langle b_m^\dagger b_m \rangle$ as well as the ones that have already been introduced. According to the statistical mechanics rule, the Bose-Einstein distribution function $(e^{\beta\hbar\omega_k} - 1)^{-1}$ gives the mean magnon number $\langle n_k \rangle$ at temperature $T > 0$. Next, we calculate the magnetic system's sublattice magnetization.

$$M(T,H) = \frac{N}{V} g\mu_B \Big(S - \frac{1}{N} \sum_k \langle n_k \rangle \Big) \tag{2.52}$$

In the recap of the fundamental physical theory review, we examine the nature of spin and its interactions, focusing on electron spin, exchange interactions, and the anisotropy field, which includes Zeeman energy. We also consider molecular field

theory and magnetic moments of magnetization. These properties provide the ability and incentive to develop a mathematical basis for exploring antiferromagnetic interactions.

Chapter 3

Mathematical Formalism and Green Function Method

Exploring the lowest quantum state in an antiferromagnetic material model has distinct challenges, especially in a confined spin system with nearest neighbor interactions. To cope with this complexity, we propose introducing a strategy that is particular to this system. Setting aside any further challenges that may arise in real antiferromagnetic crystals for the time being, our major aim is to design an integrated strategy to dealing with the inherent difficulties.
Understanding the underlying basic excitations is critical for completely understanding phenomena such as temperature dependence, superconductivity, phase transitions, and magnetic characteristics, to mention a few. This chapter examines the antiferromagnetic interaction between matter's basic excitations. Spin waves will be characterized using the Hamiltonian of Antiferromagnetic model. Spin waves result from the periodic arrangement of an atom's electron spins. Bloch developed the Heisenberg theory of exchange interaction between magnetic spins in 1930, laying the framework for spin wave theory to emerge. Spin wave theory emerges as a powerful theoretical framework for studying the low-temperature features of magnetic materials containing an ordered arrangement of fundamental magnetic moments. Fundamentally, this method employs spin waves to define low-lying energy levels in a system composed of numerous strongly interacting spin moments. Spin waves, or magnons, interact at low temperatures, and their energies easily integrate into the low-lying energy eigenvalues of the spin moment system within magnetic crystals.

Furthermore, spin wave theory is very helpful for assessing thermodynamic prop-

erties at low temperatures, such as spontaneous magnetization, spin contribution to specific heat, the influence of anisotropy constants on thermodynamic variables, and relaxation or transport coefficients. Understanding different spin wave energies and their interactions is essential for determining these critical properties.

According to spin wave theory, low-lying Heisenberg Hamiltonian eigenstates are wave-like excitations associated with the transverse components of spin (S_x and S_y) that deviate from the ground state and obey the spin commutation laws.

$$[S_{\alpha,i}, S_{\alpha,j}] = i\delta_{\alpha\beta\gamma}S_{\gamma,i}$$

where $\alpha = x, y, z$ and $i, j = 1, 2$

Magnetic excitations is the free motion of magnetic moment vector **m** resembles small harmonic vibrations of a crystal. Like the latter, this motion may propagate as spin waves, each of them possessing a wave vector **k** and frequency ω, related by the dispersion law $\omega = \omega(k)$. In terms of quantum physics, a spin wave transforms into a set of quasi-particles, viz. magnons, with the energy spectrum $\varepsilon_k = \hbar\omega(k)$

A single quantized spin deviation can be dispersed throughout the spins at a cheaper energy cost than if the variation occurred just in one spin. Similar to how quantized lattice vibrations are referred to as "phonons", these quantized spin waves are referred to as "magnons" likewise. The name "Spin Wave" refers to a semiclassical description in which the spins are thought to precess around their z-axes and their x- and y-components are controlled by travelling wave functions with frequency ω and wave vector **k**. The quantum mechanical illustration shows connections between the transverse components of spin at various locations.

The dispersion relation can be derived using a classical analogy that expresses spin wave energy as a function of wave vector. Spin waves are quantized, and the quanta of spin waves are referred to as magnons. In this sense, spin waves are analogous to other quasi-particles such as phonons and plasmons. A magnon has a magnetic moment of $g\mu_B l$ and an angular momentum of $\hbar l$. Due to their integer spin number, bosons can be distinguished from fermions as magnons. The use of classical spin interaction dynamics and thermodynamics to study spin interaction in its large-S limit is inconvenient. In this context, a special quantum Heisenberg model and the

low-order (harmonic) spin wave theory are considered. By utilizing this technique, a physically pleasing treatment can be introduced as (real or artificial) time-dependent oscillations around the classical ground state. We attempt to derive the spin wave modes and dispersion using the linearized double time temperature dependent Green Function equation of motion.
This section discusses the mathematical calculation of physical quantities related to the elementary excitations known as spin waves in antiferromagnetic systems, also known as magnons. We present the formal equipment necessary for the calculations described in the following sections.

In Section 3.1, we present a model of antiferromagnetic systems. Section 3.2 provides a comprehensive study of the Heisenberg Hamiltonian formalism, addressing the difficulties associated with attempting to simulate spin interactions using a bosonic model.

Section 3.3 includes a description of the Green Function equation of motion. Subsequently, in Section 3.4, we use the Green function on the Heisenberg Hamiltonian to decouple the bosonic operators. Finally, Section 3.5 includes computations for establishing the dispersion relation.

3.1 Model Description

Antiferromagnetic systems are generally approached by analogy with ferromagnetic systems, assuming that the system can be divided up into two or more sublattices, i.e. infinite interpenetrating subsets of the lattice whose union is the entire lattice.

To acquire a complete knowledge of the intricacies of interactions between antiferromagnetic spin waves, we shall concentrate on a specific case using an idealized lattice. This lattice has a regular, repeating structure, with spins arranged symmetrically and interpenetrating each other in a preset pattern, as seen in Fig.3.1.

The term ”ideal antiferromagnetic spin wave interaction” refers to a theoretical framework for investigating the behavior of spin waves in an antiferromagnetic medium under ideal conditions. Antiferromagnetism is a magnetic arrangement in which nearby spins align in opposite directions, resulting in distinct properties.

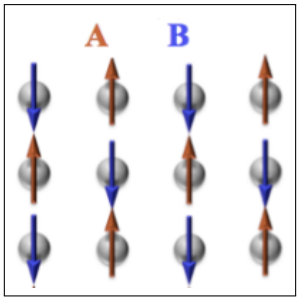

Figure 3.1: An example of an altermagnetic ordering, with the direction of the spins and the spatial orientation of the atoms alternating on the neighbouring sites in the crystal, site A up-arrow and site B down-arrow, adapted from [89]

Investigators can discover basic rules governing magnetic occurrences by studying how spin waves interact inside such a system.

In the A(B) sublattices, the B(A) spins are always the closest neighbors of the A(B) spin. This statement describes a connection in a lattice structure with two types of sublattices: A and B. In this context, A(B) represents A-type lattice sites with neighboring B-type spins, and vice versa. The hypothesis states that the spins on the B-type sublattice are always the nearest neighbors of the spins on the A-type sublattice, and vice versa. This pattern is most likely due to the material's magnetic interactions or other properties.

This ensures translational symmetry through verifying that the spin's thermal expectation value remains constant throughout lattice. Translational symmetry means that the arrangement of atoms or spins is repeated at regular intervals. In this case, it means that the lattice structure remains constant no matter where it is located in the material. A spin's thermal expectation value is the projected average spin orientation at a given temperature. This statement suggests that, because of translational symmetry, the average spin orientation remains constant across the lattice, implying that the material's magnetic properties or other spin-related properties are consistent across its structure. Putting it together, the statement essentially describes the spatial arrangement of spins in a lattice structure, emphasizing the relationship between spins on different sublattices and the uniformity of spin-related properties across the lattice due to translational symmetry.

The features of antiferromagnetic spin waves discussed in this and the subsequent

sections are based on a two sublattice model with uniaxial anisotropy and a single exchange integral, J, coupled to nearest neighbors. The anisotropy effect is represented by a crystalline field, H_A, which is pointed in opposing directions for the two sublattices along the preferred axis. As an alternative to explicitly treating the higher-order spin wave interactions that cause the macroscopic anisotropy constant to decrease with increasing temperature, this field is permitted to be temperature dependent [41].

The antiferromagnetic state is degenerate for the isotropic Hamiltonian in Eq.(3.1) because the common direction of the ensuing antiparallel magnetic moments of the two sublattice is arbitrary. Anisotropy, which is more significant in an antiferromagnetic state than a ferromagnetic one, can remove degeneracy in any genuine antiferromagnetic crystal. An effective field must be used to introduce the anisotropy field. The spins on sublattice 1 at site A should be oriented in the $+z$-direction, whereas those on sublattice 2 at site B should be oriented in the $-z$-direction. Let's we consider the hypothetical field H_A in an antiferromagnetic crystal lattice. It is regarded as an anisotropy field in the $+z$-direction at sublattice 1 sites and in the $-z$-direction at sublattice 2. We therefore want to investigate the antiferromagnetic spin system governed by the Heisenberg Hamiltonian Formalism in the presence of an external applied field $\vec{H_{ex}} = H_0\hat{z}$ and an anisotropy field H_A.

$$\mathbf{H} = 2\sum_{j\ell} J_{j\ell}(S_j \cdot S_\ell - \gamma\sum_j \Big(H_A + H_0\Big) \cdot S_j + \gamma\sum_\ell \Big(H_A - H_0\Big) \cdot S_\ell \qquad (3.1)$$

where $\gamma = \dfrac{g\mu_B}{\hbar}$ the gyromagnetic ratio. The first term includes the AFM coupling between all neighbours, the second and third term characterize the Zeeman- and anisotropy part of the two sublattices, respectively.

In Eq.(3.1), H is the Hamiltonian for the AFM, $(J < 0)$ is the exchange constant, and $\mathbf{S}_j$ and $\mathbf{S}_\ell$ are the spins on the locations of the two nearest spins, A and B, respectively. H_0 represents the external magnetic field, whereas H_A is a positive number that approximates the influence of the crystal anisotropy energy. It has the property of having a positive magnetic moment, which aligns the spins on site A in the $+z$ direction and the spins on site B in the $-z$ direction. It introduced H_A primarily to stabilize spin arrays along a desired axis, the z axis, at each site [81, 53].

The spins are arranged on a D-dimensional hypercubic lattice with N sites, a total volume of $V = Na^D$, and a as the lattice spacing. The exchange integral $J_{j\ell}$ between nearest neighbor sites R_j and R_ℓ [56] spin mediates the antiferromagnetic interaction. Since the two sublattices will be analyzed separately, a set of spin operators for the sublattice j of "up" spins and the sublattice ℓ of "down" spins is needed for each sublattice. The spin raising and lowering operators in terms of the boson annihilation and creation operators are obtained by performing a Holstein-Primakoff transformation on the conventional spin operators.

As a result, antiferromagnetic spin wave theory may be compared to ferromagnetic treatment. The Holstein-Primakoff representation describes spin deviation from the ground level. It describes the spin operators on sublattice site A when the spin projection on the state is $+S$ using canonical boson generation and annihilation operators $a_j^\dagger$ and a_j, respectively. Because there are two sublattices, we must create two separate boson spaces, each a single sublattice. An antiferromagnetic model on a hypercubic lattice without external fields or anisotropies as in Fig.3.2, with lattice spacing a and nearest-neighbor interactions mediated by bonds described by the vectors δ_i (black arrows) [56]. The spins on the two surfaces (down and up arrows) interact through the connection $J_{j\ell} = J$.

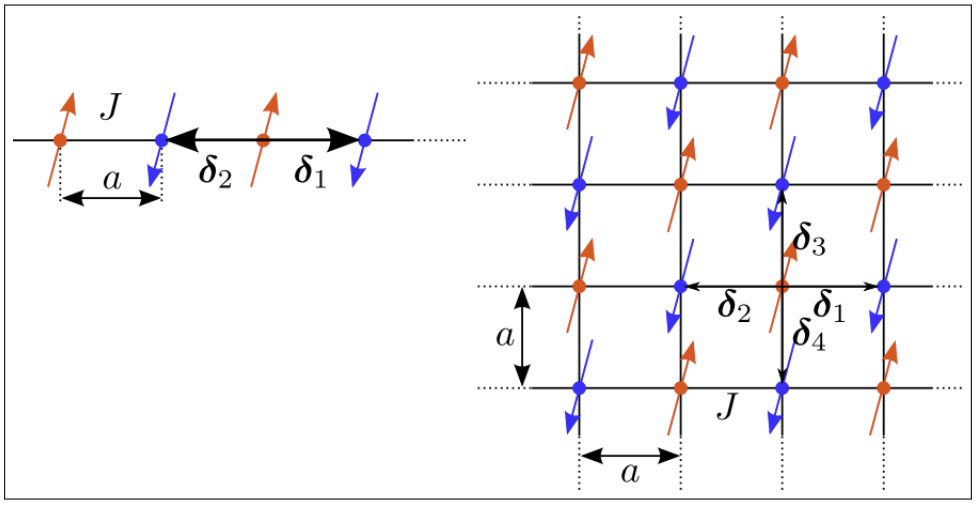

Figure 3.2: A model of hypercubic crystal structure of two sublattices interact by the coupling J,adapted from; adapted from [56]

In order to show translational invariance in the classical ground state using classical condensed-matter theory approaches, we need to select an alternative elementary cell, as shown in Fig.3.2. This modified cell contains two basis points, resulting in

a narrower Brillouin zone in momentum space and the formation of two spin-wave modes. Despite its simplicity, the Heisenberg model has multiple applications, describing phenomena such as ferromagnetism, ferrimagnetism, and antiferromagnetism [64, 7].

3.2 Heisenberg Hamiltonian Spin Model

The Heisenberg model is widely applicable to insulators and semiconductors. Calculating sublattice magnetization and other thermodynamic parameters requires complex lattice sums, which are frequently assessed using series expansions at both high and low temperatures. In this regard, an analytical investigation will be performed on an antiferromagnetic system's hypercubic lattice structure. The Heisenberg Hamiltonian for the antiferromagnetic system, formed of N-spins with nearest-neighbor interaction Eq.(3.2), may be stated in component form. From a broader point of view, the Heisenberg model accurately describes the reciprocal interaction of localized spin degrees of freedom in many-body systems. As a result, the conventional model Hamiltonian for the antiferromagnetic (AFM) hypercubic crystal lattice including sublattices A and B, including the appropriate Zeemann component and anisotropy field, is as follows:

$$\mathbf{H} = 2J\sum_{j\ell}(S_j^x S_\ell^x + S_j^y S_\ell^y + S_j^z S_\ell^z - \gamma\sum_j(\vec{h}_A\cdot\vec{S}_j) + \gamma\sum_j \vec{h}_B\cdot\vec{S}_\ell) \tag{3.2}$$

Where we have been represented $\vec{h}_A = \vec{H}_A + \vec{H}_0$ and $\vec{h}_B = \vec{H}_A - \vec{H}_0$.

The proper arrangement of Bose operators in the Hamiltonian is critical for building a quantitative quantum theory. To extend classical many-body theory to antiferromagnetic interactions, we use the Holstein and Primakoff (1940) transformation [36] on boson operators.

At low temperatures, the ground state is expected to exhibit long-range Néel order due to favourable anti-parallel alignment of spin orientations on sublattices A and B of the hypercubic lattice. The classical Néel state of the antiferromagnetic system, denoted as $|AFM\rangle$ with up and down spins on A and B sites, serves as the basis. Spin wave theory proposes that deviations from the standard N'eel state can be represented by bosonic excitations. The spin operator expression separates bosons on sublattices A and B with local bosonic creation and annihilation operators $a_j^\dagger$ and

$b_\ell^\dagger$, respectively.

The Holestein-Primakoff (HP) transformation makes it easier to rewrite the Heisenberg Hamiltonian. The antiferromagnetic Heisenberg formalism model can be expressed by an extension of the HP theory. Because quantum antiferromagnetic systems have different interacting magnetic properties than quantum ferromagnetic systems, the generalization of HP to these systems is quite useful. Our model is stated using raising and lowering operators of the type $S_j^{\pm} = S_j^x \pm iS_j^y$; the spin components are very useful [31] and may be written as follows:

$$\hat{S}^x{}_j\hat{S}^x{}_\ell + \hat{S}^y{}_j\hat{S}^y{}_\ell = \frac{1}{2}\hat{S}_j^\dagger\hat{S}_\ell^- + \frac{1}{2}\hat{S}_j^-\hat{S}_\ell^\dagger \tag{3.3}$$

Therefore, if the external magnetic field and anisotropy field along the z-direction, the Hamiltonian in Eq.(3.2) would be rewritten as

$$\mathbf{H} = 2J\sum_{j\ell}\{\frac{1}{2}(S_j^\dagger S_\ell^- + S_j^- S_\ell^\dagger) + S_j^z S_\ell^z\} - \sum_j \vec{h}_A \cdot S_j^z + \sum_\ell \vec{h}_B \cdot S_\ell^z \tag{3.4}$$

It should be noted that the commutator of two spin operators is an operator rather than just a complex number (c-number), since working directly with spin operators is much more difficult than working directly with the canonical bosonic (fermionic) creation and annihilation operators, whose commutators (anti-commutators) are simple c-numbers. It would be beneficial if one could formulate the spin operators in terms of such conventional fermionic or bosonic operators and work with those instead.

3.2.1 Holstein-Primakoff Transformation

To utilize classical condensed-matter theory techniques and achieve translational invariance in the classical ground state, we must choose a different elementary cell. As seen in Fig3.2, each cell has two basis points, resulting in a smaller Brillouin zone in both momentum space and energy, demonstrating two spin-wave modes. The spin interaction of spin operators is carefully determined using the expansion of the HP transformation. Magnetic spin operators are dispersed throughout a number of sites that correspond to a quasiparticle known as a magnon. They include creation and annihilation operators. Because numerous flipped spins can occur on a site (depending on total spin), multiple magnons can coexist in the same place, leading to the conclusion that these quasiparticles do not obey the Pauli exclusion principle.

This suggests that magnons behave as bosons. Typically, the bosonic operators a_j and b_ℓ are introduced during this process. The rising spin operator is coupled to the a_j operator, which causes a spin deviation for down-spins at sublattice site B. In contrast, the lowering spin operator relates to $a_j^\dagger$, reducing a spin deviation for up-spins at sublattice site A. The formulae below show these correlations [104, 36].

Sublattice A	Sublattice B
$S_j^+ = \left(\sqrt{2S - a_j^\dagger a_j}\right) a_j$	$S_\ell^+ = b_\ell^\dagger \left(\sqrt{2S - b_\ell^\dagger b_\ell}\right)$
$S_{aj}^- = a_j^\dagger \left(\sqrt{2S - a_j^\dagger a_j}\right)$	$S_\ell^- = \left(\sqrt{2S - b_\ell^\dagger b_\ell}\right) b_\ell$
$S_j^z = S - a_j^\dagger a_j$	$S_\ell^z = -(S - b_\ell^\dagger b_\ell)$

(3.5)

We must understand that separate boson operators, a_j and b_ℓ, have been specified for the sublattices A and B, respectively. The situation described in Eq.(3.5) does not allow for a complete solution to the Heisenberg model equation. To approximate the solution, the more complex spin operators are often converted to bosonic creation and annihilation operators in the second quantization. The commutation relations for the spin operators must be fulfilled for both the creation and annihilation operators to be bosonic. The indices j and ℓ correspond to the sites in A and B, respectively, where $a_j^\dagger$, a_j and $b_\ell^\dagger$, b_ℓ are the creation and annihilation operators for spin deviations at sites j, ℓ of sublattices A and B, respectively, that satisfy the boson commutation criteria.

$$\begin{aligned} [a_j, a_{j'}^\dagger] &= \delta_{jj'}, \qquad [a_j, a_j] = 0 \\ [b_\ell, b_{\ell'}^\dagger] &= \delta_{\ell\ell'}, \qquad [b_\ell, b_\ell] = 0 \end{aligned} \tag{3.6}$$

It should be noticed that expanding the square root of Eq.(**??**) is necessary for the Holstein-Primakoff transformation. This means that the Heisenberg model's term H has an unlimited total number of terms. Therefore, the transition makes sense if there is a physical reason to stop the infinite series. In this case, n_j can be reduced to its lowest powers since only a small number of magnons are activated at low temperatures. The operator for the magnon number at the location R_j is n_j. The most fundamental approximation in this context is the so-called spin-wave approximation, as stated in [75]. In spin wave theory, we suppose that the HP equations modify the Hamiltonian as

$$\langle a_\ell^\dagger a_\ell \rangle \ll 2S \qquad \langle b_\ell^\dagger b_\ell \rangle \ll 2S \tag{3.7}$$

Taking only the first term of expansion in the square roots, using the binomial expansions of the square roots, and maintaining terms to order $\frac{1}{S}$ [77] in the Hamiltonian. Substituting these approximations into the Hamiltonian Eq.3.4 and keeping terms up to six-order in creation/annihilation product of operators gives:

$$\begin{aligned}\mathbf{H} &= -4JNzS^2 - 2\gamma H_a NS \\ &+ 2JS\sum_{\langle j\ell\rangle}\{a_j b_\ell + a_j^\dagger b_\ell^\dagger + a_j^\dagger a_j + b_\ell^\dagger b_\ell\} + h_A\sum_j a_j^\dagger a_j + h_B\sum_\ell b_\ell^\dagger b_\ell \\ &- \frac{J}{2}\sum_{\langle j\ell\rangle}\{a_j b_\ell^\dagger b_\ell b_\ell + a_j^\dagger a_j a_j b_\ell + a_j^\dagger b_\ell^\dagger b_\ell^\dagger b_\ell + a_j^\dagger a_j^\dagger a_j b_\ell^\dagger + 4a_j^\dagger a_j b_\ell^\dagger b_\ell\} \\ &+ \frac{J}{8S}\sum_{\langle j\ell\rangle}\{a_j^\dagger a_j a_j b_\ell^\dagger b_\ell b_\ell + a_j^\dagger a_j^\dagger a_j b_\ell^\dagger b_\ell^\dagger b_\ell\} \\ &= \mathcal{H}^{(0)} + \mathcal{H}^{(2)} + \mathcal{H}^{(4)} + \mathcal{H}^{(6)} \end{aligned} \tag{3.8}$$

In this case, $H^{(n)}$ denotes words made up of products of n bosonic operators, meaning that each term has an even number of boson operators together with a variety of intra- and inter-sub-lattice couplings.

$$\mathcal{H}^{(0)} = -4JNzS^2 - 2\gamma H_a NS \tag{3.9}$$

The part of Hamiltonian $\mathcal{H}^{(2)}$ is quadratic in the spin deviation of creation and annihilation operators have the form

$$\mathcal{H}^{(2)} = 2JS\sum_{\langle j\ell\rangle}\{a_j b_\ell + a_j^\dagger b_\ell^\dagger + a_j^\dagger a_j + b_\ell^\dagger b_\ell\} + h_A\sum_j a_j^\dagger a_j + h_B\sum_\ell b_\ell^\dagger b_\ell \tag{3.10}$$

The part of Hamiltonian $\mathcal{H}^{(4)}$ which involve product of terms up to fourth order in boson creation and annihilation operators have the form

$$\mathcal{H}^{(4)} = -\frac{J}{2}\sum_{\langle j\ell\rangle}\{a_j b_\ell^\dagger b_\ell b_\ell + a_j^\dagger a_j a_j b_\ell + a_j^\dagger b_\ell^\dagger b_\ell^\dagger b_\ell + a_j^\dagger a_j^\dagger a_j b_\ell^\dagger + 4a_j^\dagger a_j b_\ell^\dagger b_\ell\} \tag{3.11}$$

In the last $\mathcal{H}^{(6)}$ is the terms containing at least a product of six a's or b's operators or their hermitian conjugates is

$$\mathcal{H}^{(6)} = \frac{J}{8S}\sum_{\langle j\ell\rangle}\{a_j^\dagger a_j a_j b_\ell^\dagger b_\ell b_\ell + a_j^\dagger a_j^\dagger a_j b_\ell^\dagger b_\ell^\dagger b_\ell\} \tag{3.12}$$

3.2.2 Fourier Transformation

Next, a transformation from localized field operators to collective boson operators that adhere to the commutation requirements is introduced, $[a_k, a_{k'}^\dagger] = [b_k, b_{k'}^\dagger] =$

$\delta(k-k')\quad [a_k, a_{k'}] = [b_k, b_{k'}] = 0$. It is instructive to write the Hamiltonian in terms of the unitary Fourier transformations of the boson operators a_j and b_ℓ, which are a_k and b_k respectively. Since Eq.(3.12), in its current form, clearly illustrates the coupling between nearby spins, we hypothesize that the basis states that diagonalize the Hamiltonian involve collective excitations of all the spins in the system. The Fourier transforms of the a_j and b_ℓ can be used to turn individual excitations into collective excitations. Using Fourier transform variables is required since the spin deviations are not restricted to one location on the lattice but rather spread across. The Hamiltonian section of the equation that is quadratic in the spin deviation of the creation and annihilation variables is then subjected to the introduction of spin wave variables using the Fourier-transform and the operators becomes:

$$\begin{aligned} a_j &= \frac{1}{\sqrt{N}}\sum_k e^{ik\cdot x_j} a_k \qquad & a_j^\dagger &= \frac{1}{\sqrt{N}}\sum_k e^{-ik\cdot x_j} a_k^\dagger \\ b_\ell &= \frac{1}{\sqrt{N}}\sum_k e^{-ik\cdot x_\ell} b_k \qquad & b_\ell^\dagger &= \frac{1}{\sqrt{N}}\sum_k e^{ik\cdot x_\ell} b_k^\dagger \end{aligned} \tag{3.13}$$

where N is the total number of spin sites and $\vec{k}$ is the wave number that runs over N in the first Brillouin zone of the lattice's reciprocal space. In order to ascertain the characteristics of the spin wave operators, the statistics of the excitations are essential. The operators we want must follow the boson commutation relations since magnons behave like bosons. The only non-zero commutators are $[a_k; a_{k'}^\dagger] = [b_k; b_{k'}^\dagger] = \delta_{k;k'}$, indicating that the commutation relations are typical bosonic. We pick the k-vectors that are located in the Brillouin zone connected to each sublattice. The Brillouin zone of the two sublattices is also similar because the two are identical.

Finally, the Hamiltonian in Eq.(3.8) is rewritten using the Fourier transform variables within the momentum space as (see detailin Appendix A-2):

$$\begin{aligned} \mathbf{H} = &-2NS(\omega_e + \omega_A) + \sum_k \{A_1^2(a_k b_k + a_k^\dagger b^\dagger) + A_2^2 a_k^\dagger a_k + A_3^2 b_k^\dagger b_k\} \\ &- A^{(4)} \sum_{k_1..k_4} \Big\{ \xi_1^{(4)} a_{k_1} b_{k_2}^\dagger b_{k_3} b_{k_4} + \xi_2^{(4)} a_{k_1}^\dagger a_{k_2} a_{k_3} b_{k_4} + \xi_3^{(4)} a_{k_1}^\dagger b_{k_2}^\dagger b_{k_3}^\dagger b_{k_4} \\ &\quad + \xi_4^{(4)} a_{k_1}^\dagger a_{k_2}^\dagger a_{k_3} b_{k_4}^\dagger + 4\xi_5^{(4)} a_{k_1}^\dagger a_{k_2} b_{k_3}^\dagger b_{k_4} \Big\} \\ &+ A^{(6)} \sum_{k_1...k_6} \Big\{ \xi_1^{(6)} a_{k_1}^\dagger a_{k_2} a_{k_3} b_{k_4}^\dagger b_{k_5} b_{k_6} + \xi_2^{(6)} a_{k_1}^\dagger a_{k_2}^\dagger a_{k_3} b_{k_4}^\dagger b_{k_5}^\dagger b_{k_6} \Big\} \end{aligned} \tag{3.14}$$

This section looks at the interaction of bosonic spin operators in an antiferromagnetic system, which is important for defining the dispersion relationship of antiferromagnetic spin waves, commonly known as magnons. In the next sections, we

will apply the Green function technique to decouple the boson operators defined in Eq.(3.14). This strategic method will allow us to derive the dispersion relation for spin waves with more accuracy.

3.3 Green's Function Equation

In this section we have presented the Green's function method, which is used to investigate spin waves in ferromagnetic, antiferromagnetic and non-collinear magnets. The method gives the temperature-dependence of the magnon spectrum and a compact expression which allows us to calculate the magnetization up to the transition temperature. To keep the method simple and tractable, we have used the Tyablikov decoupling scheme to reduce higher-order Green's functions. The dispersion relation can be explicitly obtained in simple cases.

Let A(t) and B(t') be two operators in the Heisenberg representation at times t and t', respectively. We define Green's function by

$$G_{AB}(t-t') = \langle\langle A(t);B(t')\rangle\rangle = i\theta(t-t')\langle[A(t),B(t')]\rangle \tag{3.15}$$

where

$$\theta(t-t') = \begin{cases} 1 & \text{if} \quad t > t' \\ 0 & \text{if} \quad t < t' \end{cases}$$

In spite of the complicated notation in its definition given above, Green's function is just a thermal average of a commutation relation between two operators. Green's function is connected, as will be seen below, to the physical properties of the system. So, depending on what we want to study, we choose the operators A(t) and B(t').

A useful feature of the Green function method is its applicability over the whole temperature range. Calculations of thermodynamic properties using Green functions have been found to be in good agreement with the results of non-interacting spin wave approximations at low temperatures and with the results of other statistical methods near the Néel temperature [109, 61].

In this study, the Green function technique is applied to the anisotropic Heisenberg exchange model of a two-sublattice antiferromagnet in order to obtain spin correlations, which can subsequently be utilized to determine thermodynamic properties.

The Green function approach estimates the sublattice magnetization $\langle S_i \rangle$ and internal energy (H) utilizing correlation functions using spin operator pairs.

The Green Function of the equation of motion is an effective mathematical tool for addressing spin waves [112]. To get the energy spectra of spin wave dispersion and the thermal expectation values of the spin interaction. We utilized Zubarev's Green function to describe the double-time temperature-dependent Green function method [121].

$$\begin{aligned} G_{lm}(t-t') &= \langle\langle S_l^{\dagger}(t); S_m^{-}(t')\rangle\rangle \\ &\equiv -i\theta(t-t')\langle [S_l^{\dagger}(t), S_m^{-}(t')]\rangle \end{aligned} \tag{3.16}$$

In most compounds, the magnetic atoms or ions form part of a crystalline lattice in which they are surrounded by other ions, the symmetry of the nearest-neighbor coordination being determined from the crystal structure. By means of the random-phase approximation (RPA) decoupling procedure [94, 112].

$$\langle\langle S_n^z S_l^{\dagger}; S_m^{-}\rangle\rangle \approx \langle S_n^z\rangle\langle\langle S_l^{\dagger}; S_m^{-}\rangle\rangle \tag{3.17}$$

Because of the translational symmetry, the thermal expectation value of the spin is uniform on each lattice. Under the assumptions,

$\langle S_a^z \rangle = \langle S^z \rangle_a = const$ for every point **a** on the a sublattice

and

$\langle S_b^z \rangle = \langle S^z \rangle_b = const$ for every point **b** on the b sublattice.

3.3.1 Equation-of-Motion Method for Operators

The Operator Equation-of-Motion method is based on the the standard quantum mechanical results for any operator A within the Heisenberg representation [8].

$$\begin{aligned} i\frac{d\mathbf{A}}{dt} &= \mathbf{AH} - \mathbf{HA} \\ \frac{d\mathbf{A}}{dt} &= -i[A, H] \end{aligned} \tag{3.18}$$

The Hamiltonian **H** is not time-dependent, but operator A is assumed to be. Each site- and time-labelled boson operator has a unique differential equation. We utilize the Fourier transform to convert the time representation to a frequency representation. The xy plane's symmetry enables us to perform a Fourier transformation from the site labels to a representation that includes the in-plane wave vector **k**. We find a set of coupled equations that employ boson operators comparable to those at the nearest neighbor site. These equations are recognized using a variety of indices.

3.3.2 Green Function Equation-of-Motion Method

The Green Function Equation-of-motion first defined from the double-time Green Function in terms of correlation Function between operators according to Zubarev (1960). The relation between correlation function and spectral intensities contained in the fluctuation-dissipation theorem. The static and dynamic properties of the system can be determined once the correlation function known.

The Green Function for arbitrary the operators $A(t)$ and $B(t)$ is defined as

$$G_{AB}(t,t') = \langle\langle A(t);B(t')\rangle\rangle \tag{3.19}$$

For a system with time-independent Hamiltonian H, the temperature-dependent Green's function involving two Bose operators A and B, is defined by

$$\begin{aligned} G_{AB}(t,t') &= \langle\langle A(t);B(t')\rangle\rangle = -i\langle TA(t)B(t')\rangle \\ &= -i\theta(t-t')\langle A(t)B(t')\rangle - i\theta(t'-t)\langle B(t')A(t)\rangle \end{aligned} \tag{3.20}$$

where $A(t)$ is the Heisenberg operator at time t; with $\theta(t-t')$ as the step function, and $\theta(t-t')$ being unity for positive t and zero for negative t; and the single bracket denotes an average with respect to the canonical density matrix of the system. We start from the definition of $G_{AB}(t-t')$ and the equation of motion for the operator $A(t)$ is found by differentiating the Green Function with respect to its time labels, say t it results:

$$\omega\langle\langle A;B\rangle\rangle_\omega = \frac{1}{2\pi}\langle[A,B]\rangle + \langle\langle[A,H];B\rangle\rangle_\omega \tag{3.21}$$

where ω is the angular frequency. This will be taken to represent the standard form of the equation of motion for real-time GFs. In a few special cases, the operator $[H,A]$ is straightforwardly related to the operator A, and then we can just solve the preceding equation of motion for the original GF $G_{A;B}(t')$. We will usually try to get an approximate solution by imposing a termination to the process after a chosen finite number of steps: this will involve looking for an approximation to simplify the GF that appears on the right-hand side of the last equation. This is usually called a decoupling approximation.

The second term on the right of Eq.(3.21) is a new Green Function. The equation of motion for this new Green function is found in the way and so on. A set of

coupled equations is solved in a manner analogous to that described for above operators. Eq.(3.21) represents an infinite hierarchy of coupled equations since each Green function on the right side is of higher order and satisfies a similar equation of motion. To solve this system of coupled equations, a decoupling approximation is needed to reduce the number of equations. We consider random-phase approximations, which are the most used decoupling approaches in ferro- and antiferromagnetism theory. Mathematical operations are performed within the framework of Green function decoupling techniques, with a focus on random-phase approximation (RPA). This approximation is particularly helpful in settings characterized by low temperatures, when spin alignment is almost perfect and deviations from it are negligible.

This approach is mainly based on the decoupling of equations of motion. Decoupling makes it possible to solve for the Green function in terms of both energy and the spectrum of excitation frequencies. The following equation summarizes the link between the Green functions and the corresponding correlation functions:

$$\langle B(t')A(t)\rangle = \lim_{\varepsilon\to 0}\int_{-\infty}^{\infty}\left[\langle\langle A;B\rangle\rangle_{E+i\varepsilon} - \langle\langle A;B\rangle\rangle_{E-i\varepsilon}\right]\frac{e^{-iE(t-t')}}{e^{\beta E}-1}dE \tag{3.22}$$

where A and B are the appropriate spin operators, t and t' are times, $\beta = \dfrac{1}{k_B T}$, k_B is Boltzmann's constant, and T is absolute temperature. Thermodynamic quantities of interest, such as, sublattice magnetization and internal energy, are obtained from these correlation functions.

The double-time temperature-dependent Green's function, $\langle\langle A(t);B(t')\rangle\rangle$, which involves the two Heisenberg operators $A(t)$ and $B(t')$, is a function of $(t-t')$ and may be Fourier transformed in relation to this variable. The transformation is denoted by $\langle\langle A;B\rangle\rangle_E$. E is a function of $E(\hbar\omega)$ and obeys the equation of motion. The average number of magnons and the system's dispersion relation can be readily determined using the Green function approach at $k = k'$. Reminding us that the double-time, temperature-dependent Green Function equation of motion in Eq.(3.21) H denotes the Hamiltonian of the system. We define $A = a_k$, $B = a_k^\dagger$ and [ ] is a commutation relation.

$$\omega_k\langle\langle a_k;a_{k'}^\dagger\rangle\rangle = \frac{\delta_{kk'}}{2\pi} + \langle\langle[a_k,H];a_{k'}^\dagger\rangle\rangle \tag{3.23}$$

Here ω_k the dispersion relation we want to calculate. The Kronecker delta function given by

$$\delta_{kk'} = \begin{cases} 1 & if \quad k = k' \\ 0 & otherwise \quad 0 \end{cases}$$

From Commutation relation and definition of Kronecker delta function we get the Green Function Equation of Motion for Heisenberg Hamiltonian becomes

$$\begin{aligned} \omega_k \langle\langle a_k; a_k^\dagger \rangle\rangle &= \frac{1}{2\pi} + \langle\langle [a_k, \mathbf{H}]; \mathbf{a_k^\dagger} \rangle\rangle \\ \omega_k \langle\langle a_k; a_k^\dagger \rangle\rangle &= \frac{1}{2\pi} + \langle\langle [a_k, H^{(0)}]; a_k^\dagger \rangle\rangle + \langle\langle [a_k, H^{(2)}]; a_k^\dagger \rangle\rangle \\ &\quad + \langle\langle [a_k, H^{(4)}]; a_k^\dagger \rangle\rangle + \langle\langle [a_k, H^{(6)}]; a_k^\dagger \rangle\rangle \end{aligned} \tag{3.24}$$

The Hamiltonian **H** has given in Eq.(3.14) of the form

$$\mathsf{H} = \mathcal{H}^{(0)} + \mathcal{H}^{(2)} + \mathcal{H}^{(4)} + \mathcal{H}^{(6)} \tag{3.25}$$

3.4 Decoupling of Operators

Since we will only take into account the most careful estimate, we have overlooked the equations for the higher Green's functions. A number of equations will be approximately decoupled so that the second Green's functions can be defined in terms of the first functions. We further draw attention to the fact that, as a result of translational invariance, the variables $\langle n_f \rangle = \langle a_f^\dagger a_{f'} \rangle$ relate to the average magnetization per site and are independent to the site index [100].

We proceed the calculation by substituting into the Green Function of Eq.(3.24), we may decouple (diagonalize) the total Hamiltonian of the form in Eq.(3.25), and obtain the following results by calculating $[a_k, H]$ at $k = k'$, $\delta_{kk'} = 1$.

$$\omega_k \langle\langle a_k; a_{k'}^\dagger \rangle\rangle = \frac{1}{2\pi} + \langle\langle [a_k, H^{(2)}]; a_k^\dagger \rangle\rangle + \langle\langle [a_k, H^{(4)}]; a_k^\dagger \rangle\rangle + \langle\langle [a_k, H^{(6)}]; a_k^\dagger \rangle\rangle \tag{3.26}$$

Substitution of the total Hamiltonian of various components of Eq.(3.25) and after long tedious calculation (see Appendix A) we obtain

$$\langle\langle a_k; a_k^\dagger \rangle\rangle = \frac{\omega_k + R'}{2\pi[\omega_k^2 + (R' - R)\omega_k - RR' + B^2 \Upsilon_k^2]} \tag{3.27}$$

where we have used

$$\begin{aligned} R &= \omega_e (1 - \frac{m_k}{NS}) + \omega_A + \omega_0 \\ R' &= \omega_e (1 - \frac{n_k}{NS}) + \omega_A - \omega_0 \\ B &= \frac{\omega_e}{2N^2 S^2} \left[2N^2 S^2 - NS(m_k + n_k) + n_k m_k \right] \end{aligned}$$

where $\omega_0 = \gamma H_0 \quad \langle a_k^\dagger a_k \rangle = \hat{n}_k$ and $\langle b_k^\dagger b_k \rangle = \hat{m}_k$

3.5 Dispersion Relation

We will focus on the initial approximation of the basic excitation interaction energy, leading to simple poles on the real axis in the one-particle Green's function described by Eq.(3.27). In this approach, primary excitations have an indefinite lifespan. The calculation of spin wave energies, corresponding to the poles of the Green function along the real axis [98], involves setting the denominator of Eq.(3.27) to 0. The influence of single-particle polarization on the real energy axis affects the elementary excitation spectrum, as represented by Green functions. In practical systems, the real energy axis is shortened, and the varying Fourier components of an operator on the upper and lower half planes of complex energy values weaken elementary excitations [31, 100]. Equating the Green function's;$\langle\langle a_k; a_k^\dagger \rangle\rangle$, denominator to zero provides (details in Appendix A), i.e.

$$\begin{aligned} 2\pi[\omega_k^2 + (R' - R)\omega_k - RR' + B^2\Upsilon_k^2] = 0 \\ \omega_k^2 + (R' - R)\omega_k - RR' + B^2\Upsilon_k^2 = 0 \end{aligned} \tag{3.28}$$

By considering the average of $\langle a_k^\dagger a_k \rangle$ and $\langle b_k^\dagger b_k \rangle$ are the expectation values for the number operators of independent bosons with dispersion relation ω_k in equilibrium, and can be replaced by the Bose-Einstein statistics for the occupation numbers because the two types of magnons have the same energy, i.e, $\langle a_k^\dagger a_k \rangle = \langle b_k^\dagger b_k \rangle \equiv \langle \hat{b}_k \rangle$. Thus, solving Eq.(3.28) by the completing the square method and long simplification yields

$$\begin{aligned} (\omega_k - \omega_0)^2 = \Big(\omega_A + \omega_e\Big)^2 - (\omega_e\Upsilon_k)^2 - 2\Big(\omega_e^2 + \omega_e\omega_A - (\omega_e\Upsilon_k)^2\Big)\frac{\langle b_k \rangle}{NS} \\ + \omega_e^2\Big(1 - 2\Upsilon_k^2\Big)\frac{\langle b_k \rangle^2}{N^2S^2} - \omega_e^2\Big(\frac{\langle b_k \rangle^3}{N^3S^3} + \frac{\langle b_k \rangle^4}{4N^4S^4}\Big)\Upsilon_k^2 \end{aligned} \tag{3.29}$$

The expectation value of $\bar{n}_k = \langle a_k^\dagger a_k \rangle$ can be interpreted as operator for the magnon number at given lattice site but at low temperature only a few magnons are excited. Since the operator $\bar{n}_k = \langle a_k^\dagger a_k \rangle$ is averaged over the entire system the over all errors in the energy will be small provided that the ratio of the excited magnons to the total number of sites is very small, i.e, $\frac{\langle a_k^\dagger a_k \rangle}{NS} < 1$, so that at low temperatures ($k_B T \ll J$, where J is the exchange interaction energy) the number of excitation states are very small sand $\langle n_k \rangle \ll S$. Thus we made an approximation of $\frac{\langle a_k^\dagger a_k \rangle}{NS} = \frac{\langle b_k \rangle}{NS} < 1$ and then above quadratic power of $\langle b_k \rangle$ in (3.29) can be neglected, yields

$$(\omega_k-\omega_0)^2=\Big(\omega_A+\omega_e\Big)^2-(\omega_e\Upsilon_k)^2-2\Big(\omega_e^2+\omega_e\omega_A-(\omega_e\Upsilon_k)^2\Big)\frac{\langle b_k\rangle}{NS}$$
$$+\omega_e^2\Big(1-2\Upsilon_k^2\Big)\frac{\langle b_k\rangle^2}{N^2S^2} \tag{3.30}$$

The magnonic spin wave propagates with wave length $\lambda=4a$ in the first Brillouin zone, which corresponding wave vector $k_m=\frac{2\pi}{\lambda}=\frac{\pi}{2a}$ [101]. Therefore; we can approximate, the geometry of the space lattice factor defined by $\Upsilon_k=\frac{1}{z}\sum_\delta e^{i\vec{k}.\vec{\delta}}$, where $\vec{\delta}$ are the vectors connecting closest neighbors in the opposite sublattice and only connected intersublattice exchange field. The geometrical structural factor for the hypercubic spherical zone is $\Upsilon_k=\frac{1}{D}\sum_{i=1}^{D}\cos\Big(\vec{k}_i.\vec{\delta}\Big)$, where D is the dimensionality [56], assumes a spherical Brillouin zone and approximated as $\Upsilon_k=\cos\Big(\frac{\pi k}{2k_m}\Big)$, where $k_m=\frac{\pi}{2a}$, and a is an effective lattice parameter that can be modified for different situations [52, 83]. Thus, Eq.(3.30) can be rewritten as

$$(\omega_k-\omega_0)^2=\omega_A^2+2\omega_e\omega_A+\omega_e^2\sin^2\Big(\frac{\pi k}{2k_m}\Big)-\Big[\omega_e\omega_A+\omega_e^2\sin^2\Big(\frac{\pi k}{2k_m}\Big)\Big]\frac{2\langle b_k\rangle}{NS}$$
$$+\omega_e^2\Big[\sin^2\Big(\frac{\pi k}{2k_m}\Big)-\cos^2\Big(\frac{\pi k}{2k_m}\Big)\Big]\frac{\langle b_k\rangle^2}{N^2S^2} \tag{3.31}$$

However, the linear approximation considerably simplified the energy-momentum conservation rules, allowing computations to be extended to higher order processes. A linear function was chosen to represent ω_k because it is the most straightforward way of describing magnon frequencies across the entire zone. In fact, we've run calculations using a nearly accurate spherical model as well.

We introduce the dimensionless anisotropy parameter $\alpha=\frac{\omega_A}{\omega_e}$ with the magnetic nearest neighbors' of z-numbers, then Eq.(3.31) becomes

$$(\omega_k-\omega_0)^2=\omega_e^2\Big\{\alpha^2+2\alpha+\sin^2\Big(\frac{\pi k}{2k_m}\Big)-2\Big[\alpha+\sin^2\Big(\frac{\pi k}{2k_m}\Big)\Big]\frac{\langle b_k\rangle}{NS}$$
$$+\Big[\sin^2\Big(\frac{\pi k}{2k_m}\Big)-\cos^2\Big(\frac{\pi k}{2k_m}\Big)\Big]\frac{\langle b_k\rangle^2}{N^2S^2}\Big\} \tag{3.32}$$

As we shall see, we can obtain the expression for the dispersion relation, the magnon numbers and other thermodynamic quantities of AFMs from Eq.(3.32).

Let's consider; again, the geometric space factor, Υ_k^2, which is defined as $\frac{1}{z}\sum_\delta e^{i\vec{k}\cdot\vec{\delta}}$; where the vector $\vec{\delta}$ denotes the distance between the nearest neighbors on the other sublattices, whereas $\vec{k}$ is the wave vector. in Eq.(3.30). This statement describes a specific circumstance employing a hypercubic lattice structure. An approximation

may be made when considering long wavelengths and the nearest neighbors represented by (z), resulting in $1-\Upsilon_k^2 \approx \frac{2}{z}a^2k^2$ [81]. When considering long wavelengths and nearest neighbor in a hypercubic lattice with a coordination number (z), the approximation $1-\Upsilon_k^2$ is particularly useful. This approximation reduces the formula to $\frac{2}{z}a^2k^2$, providing a simpler representation of the geometric space factor in this context. With this approximation Eq.(3.30) reduced to a simplified form, (detail in appendix A)

$$(\omega_k-\omega_0)^2 = \frac{\omega_e^2}{z}\Big\{z\Big(\alpha^2+2\alpha\Big)+2\mathrm{a}^2\mathrm{k}^2-2\Big(\mathrm{z}\alpha+2\mathrm{a}^2\mathrm{k}^2\Big)\frac{\langle \mathrm{b_k}\rangle}{\mathrm{NS}} - \Big(z-4a^2k^2\Big)\frac{\langle b_k\rangle^2}{N^2S^2}\Big\} \tag{3.33}$$

Summary of the Chapter

In this section, the spin wave theory of antiferromagnetism has been presented for the simple hypercubic lattice in multiple dimensions where anisotropy has been considered. The calculation then becomes more complicated and needs other approximations to decouple chains of operators to renormalize the harmonic, or free-magnon, spectrum. One can also use Green's function method which allows us to include implicitly magnon-magnon interactions below to the transition temperature (see Chapter 4). The method involves, however, some decoupling schemes which make the results near the transition less precise. Using this model, it has been possible to derive the dispersion relation of spin wave frequencies, and spin wave velocities. While these properties can in principle be found by classical means, this model provides quantum corrections as an expansion in the spin S which have been approximated an appropriate places. Even though the expansion can be taken to higher order terms, these involve considering the various interactions of magnons by performing various analytical techniques on complicated and non-diagonalisable Hamiltonians.

Chapter 4

Result and Discussion

We consider the effects of uniaxial anisotropy on the dispersion relation, temperature dependence of sublattice magnetization, heat capacity of antiferromagnetic compound with nearest- neighbor exchange interactions. The simplified model treated gives an explanation for the peculiar behavior of well known antiferromagnetic materials with finite anisotropy field and the exchange energy.

We conducted extensive mathematical calculations to fully understand the complex interplay between the anisotropy field and the dispersion relation. The calculations were methodically designed, with a particular emphasis on higher-order spin interactions, as discussed in the previous chapter. Using these advanced analytical methods, we want to uncover the complex mechanisms behind the anisotropy field's effect on the dispersion parameters of the antiferromagnetic system.

In antiferromagnetic compounds, the bond interaction between the magnetic ion's $3d$-orbitals and the s- or p-orbitals of the ligand atom adds to the anisotropy field [19, 22]. Because of these and other factors, antiferromagnetic materials have a fundamentally anisotropic field. Certainly, the production and source of anisotropy fields in antiferromagnetic materials are not entirely understood and require further investigation. In this section, we focus on the impact of the anisotropy field on antiferromagnetic parameters.

Uniaxial anisotropy is the directional dependency of a material's magnetic characteristics along a certain axis. In antiferromagnetic materials, uniaxial anisotropy has a significant impact on the dispersion relationship. The dispersion relation defines the connection between the energy of magnetic excitations (spin waves) and their

respective wave vectors. The combination of anisotropy and exchange interactions affects the dispersion relation, resulting in unique patterns in the magnetic excitation spectrum.

Sublattice magnetization in antiferromagnetic materials is a measure of magnetic order inside each sublattice of spins with opposing orientations. The temperature dependence of sublattice magnetization is a key parameter for determining these materials' thermodynamic behavior. As temperature fluctuates, the conflict between thermal excitation and magnetic order generates a complex connection. Uniaxial anisotropy varies this connection by changing the temperature at which the material changes from an ordered to a disordered magnetic state.

Heat capacity refers to the ability of antiferromagnetic materials to store thermal energy. The combination of magnetic and thermal contributions influences the heat capacity of antiferromagnetic compounds with nearest-neighbor exchange connections. Uniaxial anisotropy introduces an additional energy scale to compete with exchange interactions, resulting in a unique heat capacity profile. The unusual properties observed in well-known antiferromagnetic materials with finite anisotropy fields, such as the exchange energy, can be attributed to the delicate balance of two opposing variables.

In this section, our focus is directed towards the analysis and discussion of the results derived from the mathematical calculations concerning various physical quantities, including the dispersion relation and the influence of anisotropy fields on spin wave frequency, as well as other thermodynamic parameters pertinent to antiferromagnets.

Section 4.1 elaborates on the results obtained in Chapter 3, offering a detailed examination of both the dispersion relation and the effects of anisotropy fields, in accordance with the stated problem.

Section 4.2 undertakes a comprehensive analysis by juxtaposing our findings with previous studies and conducting a thorough exploration of the impacts of anisotropy fields on antiferromagnetic parameters.

In Section 4.3, we engage in a comprehensive and exhaustive discussion, aligning with the objectives outlined in the problem statement.

4.1 Effects of Anisotropy Field on Dispersion Relation

This section focuses into a comprehensive examination of the results obtained from theoretical calculations using higher-order six-products of bosonic operators. The primary objective is to investigate the question: "**What effect does the anisotropy field have on the dispersion relation of an antiferromagnetic system?**" We want to understand the complex dynamics underlying the interaction between the anisotropy field and the dispersion properties of the antiferromagnetic material by systematically combining rigorous theoretical analysis and the mathematical methods developed in the preceding chapter.

Antiferromagnetic materials show promise as low-power devices, making them excellent candidates for next-generation spintronic applications. The nature and disorder of inter-particle interactions influence the excitation localization effects. Magnetic materials' anisotropy field determines their suitability for spintronic devices used in data storage and transmission [111, 44].

4.1.1 Dispersion relation and Anisotropic field effect on Antiferromagnetic

Anisotropy exchange interaction is a combination of spin-orbit coupling and exchange interaction that is more essential in understanding the behavior of antiferromagnetic materials [67, 10]. Understanding the antiferromagnetic anisotropic field was considered to provide information on the system's high-temperature superconductivity, which would assist in spin wave dispersion investigation. The anisotropy field of exchange interactions determines the anisotropic properties of antiferromagnetic materials, meaning that anisotropy in these materials is due to their magnetocrystalline characteristics. Furthermore, the anisotropy constant is proportional to the extent of spin-orbit coupling [76]. In AF compound the bond interaction between the $3d$-orbitals of the magnetic ion and the p-orbitals of the ligand atom

attribute for anisotropy field [19, 22]. Because of these and other factors, AF materials have an inherent anisotropy field.

In this study a highly idealized Heisenberg model of antiferromagnetic spin interaction, which consisted of a three-dimensional array of fixed spins with cubic symmetry and fully isotropic exchange coupling between nearest neighbors is considered. This model incorporates key aspects such as nearest neighbor exchange interactions, uniaxial anisotropy, and external field effects in the z-direction. In a low-energy state, the sublattice splits into two distinct sublattices, each with opposing magnetic moments. As a result, all spins' nearest neighbors belong to the opposite sublattice. We assumed that the spins are placed in a 3-dimensional hypercubic lattice with spacing a of total volume $V = a^3N$ and N sites because the calculations were done nearly in spherical mode.

As the temperature rises, spins get more excited, resulting in extra spin waves. The higher eigenstates of the system are a combination of excited and unexcited systems. Using the superposition principle, any number of spin waves at a certain wave vector $\mathbf{k}$ may be excited. Spin waves (magnons) are classified as bosons due to their similarities to photons and phonons. Bose-Einstein statistics are used to include temperature into thermodynamic averages [86, 49].

In Eq's.(3.32 & 3.33), the quantity $\langle \mathbf{b}_k \rangle$ denotes the mean number of spin waves with wave vector $\mathbf{k}$ at excitation temperature T for a single mode and can be expressed as $\langle \mathbf{b}_k \rangle = (e^{\beta E_k} - 1)^{-1}$, where $\beta = (k_B T)^{-1}$ and E_k is the excitation energy. Each spin wave decreases the total spin by one unit from its saturation value NS, which affects the magnon numbers at temperature T. Thus, we approximate

$$NS\langle \mathbf{b}_k \rangle = \sum_k \frac{1}{e^{\beta E_k} - 1} = \int \frac{V}{(2\pi)^3} \frac{d^3\mathbf{k}}{e^{\beta E_k} - 1} \tag{4.1}$$

This is the average number of spin waves in thermal equilibrium with wave vector $\mathbf{k}$ at temperature T. When the chemical potential μ is assumed to be zero, a specific sample of the Bose-Einstein distribution function yields the number of bosons with energy $\hbar\omega_k$ in thermal equilibrium at temperature $\mathbf{T}$. The total number of bosons in thermal equilibrium, on the other hand, is not a variable that is independent. We calculate the integral at very low temperatures; because at extremely very low

temperature, only spin waves with vanishingly low excitation energies contribute significantly to the integral [5, 49, 47]. Only in the limit of small $\mathbf{k}$ does the energy of spin waves become vanishingly small; $E_k = \hbar\omega_k \approx Ck$, where C is a constant. Over the first Brillouin zone, the integration can be applied. By making change of variable $\mathbf{k} = (\frac{k_B T}{C})\mathbf{q}$ the integration results;

$$\langle \mathbf{b}_k \rangle = \frac{(k_B T/C)^3}{NS} \int \frac{V}{(2\pi)^3} \frac{d^3\mathbf{q}}{e^{\mathbf{q}} - 1} = \frac{\Theta^3}{NS} F(q) \tag{4.2}$$

Where we defined $F(q) = \int \frac{V}{(2\pi)^3} \frac{d^3\mathbf{q}}{e^{\mathbf{q}}-1}$ and $\Theta = \frac{k_B T}{C}$.

Thus the dispersion relation in Eq.(3.32) rewritten in the form

$$\begin{aligned}(\omega_k - \omega_0)^2 = \omega_e^2 \Big\{ \alpha_A^2 + 2\alpha + \sin^2\left(\frac{\pi k}{2k_m}\right) - 2\Big[\alpha + \sin^2\left(\frac{\pi k}{2k_m}\right)\Big] \frac{\Theta^3}{NS} F(\mathbf{q}) \\ + \Big[\sin^2\left(\frac{\pi k}{2k_m}\right) - \cos^2\left(\frac{\pi k}{2k_m}\right)\Big] \frac{\Theta^6}{(NS)^2} F^2(\mathbf{q}) \Big\}\end{aligned} \tag{4.3}$$

From the mathematical analysis of spin interaction of antiferromagnetic system bosonic creation and annihilation operators to the order of six products, we obtained a simplified dispersion relation of the form given in Eq.(4.3). This shows how the energy of the system deviates from the equilibrium value as the temperature of the exciting system rises from extremely small value. In antiferromagnetic interactions, we find that higher order spin interaction processes cause considerable thermal change of magnons. However, in the low-temperature approximation, the values on the right-hand side of Eq.(4.3) in the third part are negligible and can be ignored.

Let's look deeper at how the anisotropy field influences the dispersion relation. Describing the relationship between the anisotropy field and spin wave interaction inside a model is inherently intricate and difficult to define in physical terms. However, in our model's low-temperature approximation range, something unexpected occurs: the development of an anisotropy field component with an order proportional to the temperature cube. This approximation is important for studying the sensitive interaction of dispersion relation, anisotropy, and temperature, as seen below:

$$\Big(\omega_k - \omega_0\Big)^2 = \omega_e^2 \Big\{ \alpha^2 + 2\alpha + \sin^2\left(\frac{\pi k}{2k_m}\right) - 2\Big[\alpha + \sin^2\left(\frac{\pi k}{2k_m}\right)\Big] \frac{\Theta^3}{NS} F(\mathbf{q}) \Big\} \tag{4.4}$$

Using the approximation provided in Eq.(4.3), Eq.(3.33) can be simplified to the linear form:

$$(\omega_k - \omega_0)^2 = \frac{\omega_e^2}{z}\left\{z\left(\alpha^2 + 2\alpha\right) + 2\mathrm{a}^2\mathrm{k}^2 - 2\left(\mathrm{z}\alpha + 2\mathrm{a}^2\mathrm{k}^2\right)\frac{\Theta^3}{\mathrm{NS}}\mathrm{F}(\mathbf{q})\right\} \tag{4.5}$$

With this approximation created, we get the analytical ability to completely analyze and grasp the many relationships between these variables. The connections between them are graphically represented in the graphs below, which provide a better understanding of their interrelationships. By analyzing these figures, we may get insight into the interplay of anisotropy and temperature on the dispersion relation, exposing the complexities of their impact on overall system dynamics. We may get insights into the interactions of anisotropy and temperature on the dispersion relation, demonstrating the complexities of their influence on the overall dynamics of the system.

With this approximation in place, we get the analytical possibility to study and to understand the varied correlations between these variables, we plot a graph of dispersion as a function of wave vector according to Eq.(4.4) shown below:

Graph in Fig.4.1 indicates that the interaction of the anisotropy field and temper-

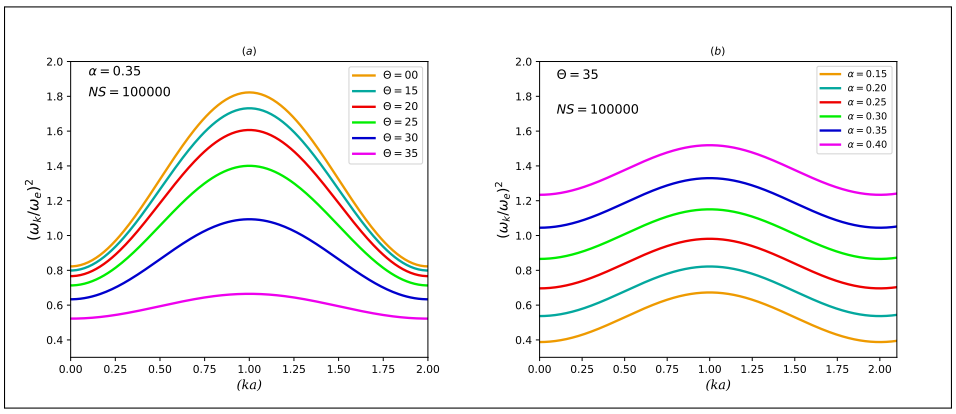

Figure 4.1: Sinusoidal dispersion relation of antiferromagnetics of (a) fixed anisotropy field and different values of temperature factorsm (b) fixed temperature factor and different values anisotropy field factors.

ature factor has a considerable impact on the dispersion of antiferromagnetic spin waves. This relationship is complex and requires a comprehensive analysis.

When we examine the effect of raising the temperature factor while keeping the anisotropy factor constant, we get an interesting finding. The amplitude of the sinusoidal spin wave dispersion relation gradually decreases, ultimately leading to an inversion. When the anisotropy factor is increased while the temperature factor remains constant, the dispersion relation appears by opening a gap and shifting upward, as shown in Fig.4.1b. The graph in Fig.4.1 shows that the anisotropy field factor and temperature factor have a significant influence on the dispersion of antiferromagnetic spin waves. This connection is complicated and needs a thorough investigation.

Fig.4.2 depicts according to Eq.(4.5) of the linear dispersion relationjkokk, which resemble the findings in Fig4.1 and emphasizes the consistency of the results.

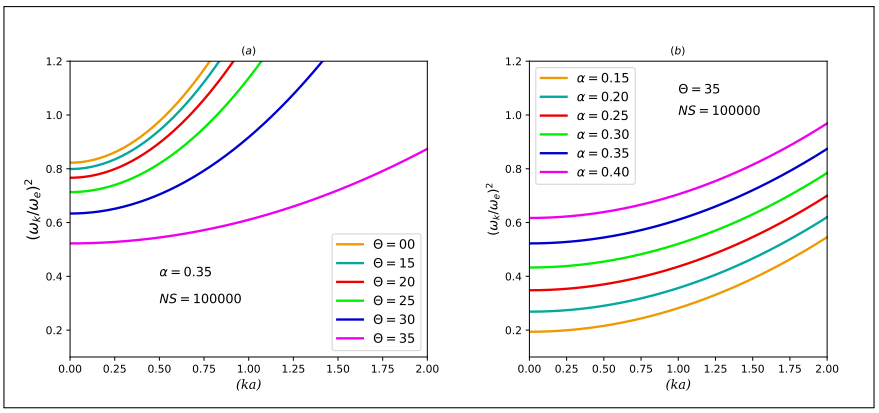

Figure 4.2: Linear dispersion relation of antiferromagnetics of (a) fixed anisotropy field and different values of temperature factor (b) fixed temperature factor and different values anisotropy field factors.

For different values of anisotropy and the temperature parameter, changes were continuously plotted on a graph, as shown in Fig.4.3. This was done simultaneously based on Eqs. (4.4) and (4.5). In such instances, the dispersion relation establishes an open gap and an upward shift, as seen in Fig.4.3. The graph in Fig.4.3(a) shows that when the temperature factor increases, the amplitude of the dispersion relation decreases until it reaches zero. As a result, the sinusoidal oscillation spectrum shifts downwards below the ordinate of the coordinate system, indicating an increase in the downward direction.

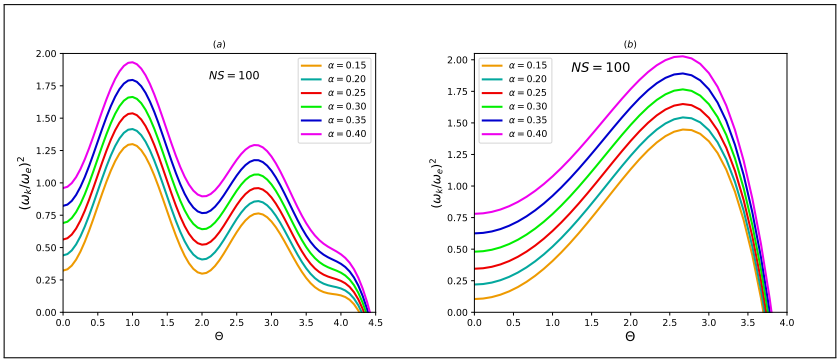

Figure 4.3: Dispersion relation of antiferromagnetics when both anisotropy field and temperature factors varies (a) sinusoidal (b) linear relations.

Furthermore, a linear approximation of the dispersion relation is shown in Fig.4.3(b), demonstrating its temperature dependence across a range of anisotropic field factors. As the temperature factor increases, the dispersion rises briefly before decreasing to zero and inverting. This remarkable discovery suggests that the system has complicated dynamics. Further research is needed to properly understand these findings and maybe identify new patterns in the area.

4.1.2 Dispersion Relation of selected Antiferromagnetic Materials

In this part, we will examine the theoretical foundations and practical applications of numerous transitional metal antiferromagnetic insulating materials. These materials have previously gained a lot of attention due to well-documented experimental and computational results. These materials are very fascinating conceptually. At temperatures below the Néel threshold, they exhibit a simple three-dimensional (3D) antiferromagnetic ordering with two sublattices. It is worth noting that the magnetic interactions of these materials are dominated by nearest neighbor exchange, with effective exchange fields of comparable magnitudes. This feature has been carefully investigated in studies undertaken by many scholars [90, 27, 84, 3].

Spins in most transitional complex metal compounds align along the easy axis or in another favored direction, in addition to the Heisenberg exchange, due to weak anisotropic interactions among individual ions. They have a substantial effect on the dispersion pattern around the Brillouin zones. The Hamiltonians of transition metal ions in an octahedral ligand environment use spin-orbit coupling to control both

ion and exchange field anisotropies. Manganese ions have a $3d^5$ structure, with a ground state term of ${}^6D_{5/2}$. It possesses a high spin angular momentum ($S = 5/2$), but no orbital angular momentum ($L = 0$). Crystal field anisotropy reduces as the number of multiplets rises. The magnetic Fe^{2+}-ions have a ground-state configuration of $3d^5({}^5D_4)$, with high orbital angular momentum and effective anisotropy caused by single-ion spin-orbit coupling.

The major exchange interaction occurs between nearest neighbor ions, followed by similar inter-sublattice exchange fields (H_E) and an easy axis anisotropy field (H_A). These exchange parameters may be represented in the context of the Heisenberg Hamiltonian, essentially limiting the exchange interaction to nearest neighbor inter-sublattice terms. This description uses bosonic operators for detailed analysis [102, 25, 78]. The exchange parameters for various antiferromagnetic compounds are listed below in table 4.1.

The well recognized and agreed exchange values of the transitional metal com-

Table 4.1: Exchange field values

Compound	Spin (S)	H_EkG	$H_A(kG)$	α	reference
MnF_2	5/2	526	10	0.0156	[86]
FeF_2	2	560	190	0.3393	[86]
$CsMnF_3$	5/2	350	7.965	0.0228	[60]
K_2MnF_4	5/2	602	2.35	0.0039	[9]
Rb_2MnF_4	5/2	551	2.59	0.0047	[9]
$Mn_2P_2S_6$	5/2	1060	0.0802	0.00076	[54]

pounds mentioned in Table 4.1 allowed us to better understand the impacts of anisotropy and temperature on antiferromagnetism dispersion in complex dynamics.

We plotted a dispersion relation graph as a function of wave vector, keeping temperature parameter constant and for varying values of anisotropy field factor. This was done for both the sinusoidal and linear connections specified in Eq.4.4 as shown in Fig.4.4.

Fig.4.4 depicts the dispersion relation as a function of wave vector for several transitional metal insulators, keeping temperature parameters constant and displaying both sinusoidal and linear correlations. The graph shows how the spectra of various materials split and gap substantially based on their anisotropy field values. Surprisingly, this separation follows a pattern identical to that seen in Fig.4.1. This

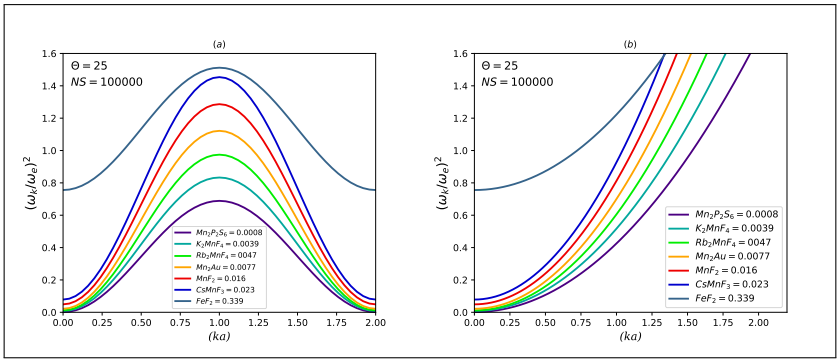

Figure 4.4: Dispersion relation of antiferromagnetics compounds at fixed temperature factor and different aninsotropy values (a) sinusoidal relation (b) linear relation.

explanation focuses on the most essential aspects of the presented graph, such as the defined temperature factors, the separation of spectra based on anisotropy field values, and the resemblance to the observed pattern in Fig.4.1.

We produced another graph displaying the dispersion relation as a function of wave vector for the same material seen in Fig.4.4, but this time with a temperature parameter value of $\Theta = 35$. Both sinusoidal and linear relationships were displayed, reflecting the configuration shown in Fig.4.5. This figure shows behavior similar to Fig.4.4, but with a lower amplitude of dispersion.

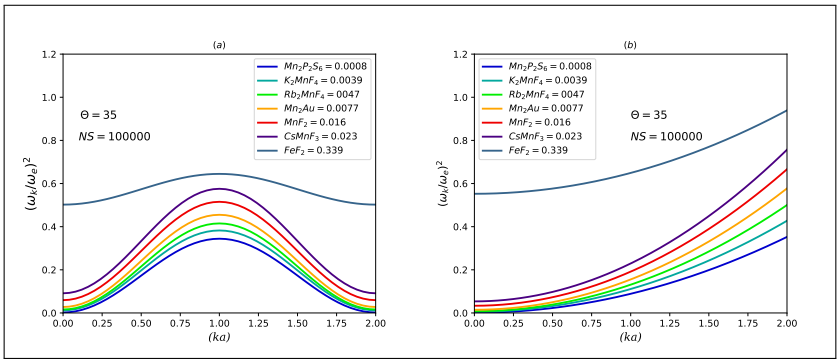

Figure 4.5: Dispersion relation of antiferromagnetics compounds at fixed temperature factor and different aninsotropy values (a) sinusoidal relation (b) linear relation.

A deeper analysis reveals that for temperature parameter values greater than 35, the dispersion inverts. These graphs of a specific material describe how the temperature parameter value has a major influence on the behavior of the dispersion relation, as

shown in the observed pattern.

To further understanding, we plotted a graph that depicts as Fig.4.6 of the dispersion relation as a function of temperature for several transitional metal insulators with known anisotropy fields. Fig.4.6(a) shows that when the temperature parameter increases, the amplitude of the sinusoidal dispersion relation gradually decreases until it reaches zero. This phenomenon causes a downward shift in the sinusoidal oscillation spectrum beneath the ordinate axis, suggesting a significant increase in the downward direction along the coordinate system.
In Fig.4.6(b) also shows a linear approximation of the dispersion relation, emphasizing its dependency on temperature across various materials for the anisotropy field component. As the temperature rises, the dispersion briefly increases before rapidly decreasing to zero and then reversing

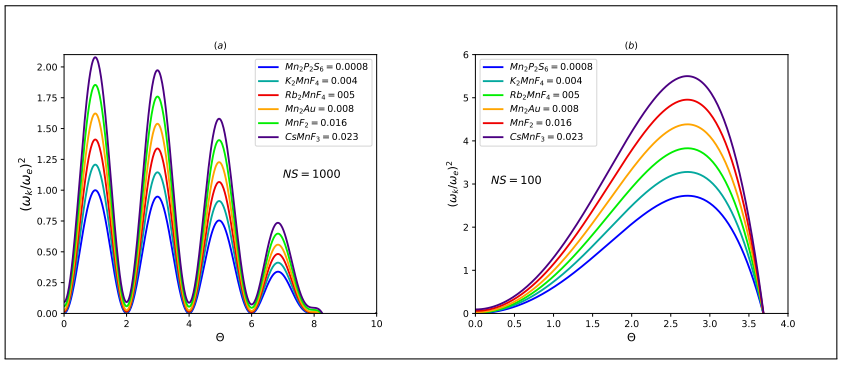

Figure 4.6: Dispersion relation of antiferromagnetics compounds at fixed temperature factor and different aninsotropy values (a) sinusoidal relation (b) linear relation.

To summarize the results of the analysis, note that the results of these studies are significant since they provide critical insights that require more investigation. The complex relation between anisotropy and temperature factors has a significant impact on the dispersion of antiferromagnetic spin waves. This emphasizes the need of conducting a thorough analysis to uncover the basic mechanisms at work and determine the probable consequences of the observed phenomenon.

4.2 Approximation of Dispersion and Magnon Number

As the temperature T approaches absolute zero, only spin waves with small excitation energies contribute insignificantly to the integral in Eq.(4.3). Consequently, the values of Θ^3 and Θ^6 become sufficiently small at low temperatures, and the ratios $\frac{\langle b_k \rangle^2}{N^2 S^2}$ may also become significantly small. This indicates that when the temperature rises, there are more excited spins. By assuming only a few spins excited with vanishingly small energy at low temperatures, the second and third terms in Eq.(4.3) can be neglected and the dispersion relation is reduced to a simpler form as

$$\left(\omega_k - \omega_0\right)^2 = \omega_e^2 \left\{ \alpha^2 + 2\alpha + \sin^2\left(\frac{\pi k}{2k_m}\right) \right\} \tag{4.6}$$

In special case of low temperature approximation the dispersion relation obtained in Eq.(4.6) is in line with research reported [88] and; in the absence of an external magnetic field ($H_0 = 0$), also agree with antiferromagnetic dispersion relation that various researchers have reported in [83, 84, 115]. The obtained dispersion relation in this work, also line up with those of [48, 86]. However, the linear approximation greatly simplifies the energy-momentum conservation principles, allowing computations to be extended to higher order systems. A linear function was used to represent ω_k since it is the simplest approach to describe magnon frequencies throughout the zone. In reality, we performed computations using a fairly correct spherical model as well. Then Eq.(4.6) becomes

$$\frac{\omega_k - \omega_0}{\omega_e} = \pm \sqrt{\left(\alpha^2 + 2\alpha + \sin^2(\frac{\pi}{2}\frac{k}{k_m})\right)} \tag{4.7}$$

A linear approximation greatly simplified the energy-momentum conservation rules, allowing the calculations to be extended to higher order processes. The function was chosen to represent ω_k since it is the most straightforward relation that describes the magnon frequencies over the entire zone. In fact, we calculated the results using a nearly perfect spherical model of excitation energy as a function of wave number $\mathbf{k}$ and anisotropic field frequency ω_A factor (i.e α). Thus magnon dispersion relation would be rewrite using an approximation provided in Eq.(3.33), we can rewrite Eq.(4.7) in the simpler form of

$$\omega_k = \omega_0 \pm \frac{\omega_e}{\sqrt{z}} \sqrt{z\alpha^2 + 2z\alpha + a^2 k^2} \tag{4.8}$$

The angular frequency spin wave corresponds to the excitation energy, which describes the quasi-particle the Magnon which carry a fixed amount of energy and lattice momentum and are spin-1, indicating it obey boson behaviour. Thus, magnons are small quantized energy corresponding to a specific decrease in magnetic strength that travels as a unit through a magnetic crystal. Therefore this form of spin-wave excitation energy can be written as

$$E_k = E_0 + \sum_k \hbar\omega_k \tag{4.9}$$

The magnon excitation energies then follow as a solution from the equation of motion; $\mathbf{E}(k) = \sum_k \hbar\omega_k$, is antiferromagnetic dispersion of spin wave interaction and $\langle \mathbf{b}_k \rangle$ is the expectation value of magnon numbers with wave vector $\vec{k}$. The Hamiltonian for excited spin-wave interaction can be expressed as

$$\mathcal{H}^{SW} = E_0 + \sum_k \hbar\omega_k a_k^\dagger a_k \tag{4.10}$$

The excitations of these uncoupled harmonic oscillators are called magnons as they represent the elementary magnetic excitation. The k-dependent energy of the magnons ω_k defines their dispersion relation.

The Green functions theory of Eq.(3.22) was used to estimate the number of excited magnons at temperature T in the magnon interaction, utilizing the magnon creation and annihilation operators $a_k = A(t)$ and $a_k^\dagger = B(t')$ as follows:

$$\langle a_k^\dagger a_k \rangle = \lim_{\varepsilon \to 0^+} i \int_{-\infty}^{\infty} \frac{1}{e^{\beta E} - 1} \Big(\langle\langle a_k; a_k^\dagger \rangle\rangle_{E+i\varepsilon} - \langle\langle a_k; a_k^\dagger \rangle\rangle_{E-i\varepsilon} \Big) e^{-iE(t-t')} dE \tag{4.11}$$

where "E" is the actual energy of the Green function, whose pole is on the real axis, and "epsilon (ε)" is the imaginary portion of energy on the complex plane, according to [121]. In the presence of a magnetic field, the eigenfrequency of the excited state energy of antiferromagnetic magnons is represented by $\omega_k = \omega_0 \pm \frac{\omega_e}{\sqrt{z}} \sqrt{z\alpha^2 + 2z\alpha + k^2 a^2}$. The equation of motion for the operator is

$$i\frac{da_k}{dt} = [a_k, \mathrm{H}^{sw}] \tag{4.12}$$

where H is the magnon system Hamiltonian in units of $\hbar = 1$, then

$$\Big[a_k, \mathrm{H}^{SW}\Big] = \Big[a_k, \hbar\omega_k a_k^\dagger a_k\Big] = \hbar\omega_k a_k \tag{4.13}$$

Using the Green Function equation of motion for operators given in Eq.(3.21) at magnon energy (E), Eq.(4.13) become

$$\langle\langle a_k; a_k^\dagger \rangle\rangle = \frac{1}{2\pi(E - \hbar\omega_k)} \tag{4.14}$$

Substituting Eq.(4.14) in the integrand of Eq.(4.11) and applying pole integration method (see appendix B-2), we obtain a final result

$$\langle a_k^\dagger a_k \rangle = \frac{1}{e^{\beta\hbar\omega_k} - 1} \tag{4.15}$$

where $\beta = \frac{1}{k_B T}$ and $\langle a_k^\dagger a_k \rangle = \langle n_k \rangle$, thus, for single magnon the mean number is

$$\langle n_k \rangle = \frac{1}{e^{\beta\hbar\omega_k} - 1} \tag{4.16}$$

This shows that there is a logarithmic relationship between the dispersion and the magnon number, and vice versa for the total magnon number. Any number of spin waves with a given k can be excited owing to the superposition principle. This implies that spin waves obey Bose-Einstein states, just like photons and phonons do. Consequently, the quantity of spin waves excited at temperature T will be

$$n = \sum_k \langle n_k \rangle = \sum_k \left(e^{\beta E_k} - 1 \right)^{-1} \tag{4.17}$$

The number of magnons evaluated using the dispersion law in Eq.(4.17) and the performing the summation over the possible values of k-allowed by the periodic boundary condition.

The number of magnons excited at a given temperature is determined by the Bose-Einstein factor $\langle n_k \rangle = (e^{\beta\hbar\omega_k - 1})^{-1}$ exploits in determining the sublattice magnetization, where $\beta = (k_B T)^{-1}$. Magnons have a single polarization for each values of wave number **k** and the total number of magnons excited at a temperature T, would be found by performing a sum over states, which is more readily done as a function of frequency ω_k. Making use of the density of state function $\rho(\omega_k)d\omega_k = \frac{V}{(2\pi)^3} k^2 (\frac{dk}{d\omega_k}) d\omega_k$, then, the weighted magnon density is found from $\sum_k \langle n_k \rangle = \int \langle n_k \rangle \rho(\omega_k) d\omega_k$. Using Eq.(4.8) for the frequency ω_k, into the density of states, after long algebraic simplification and some approximation; (see appendix B-2), we find a relation for magnon number density

$$\sum_k \langle n_k \rangle = \frac{N\sqrt{z^3}}{2\pi^2} \left\{ A_1 \zeta(1)\theta - A_2 \zeta(2)\theta^2 + 2A_3 \zeta(3)\theta^3 - 6A_4 \zeta(4)\theta^4 \right\} \tag{4.18}$$

where z is the number of nearest neighbor, $\theta = \frac{k_B T}{\hbar \omega_e}$ is a dimensionless normalized excitation temperature. The coefficient variables A_1, A_2, A_3, and A_4 in Eq.(4.18) are functions of external applied and anisotropy fields. $\zeta(n)$ is the Riemann zeta function.

Summary: The results obtained in this sub-section of uniaxial antiferromagnetic system with nearest neighbor exchange interaction are valuable for investigating the influence of anisotropy field on the dispersion relation, antiferromagnetic characteristics of magnetization, susceptibility, and heat capacity. The interplay of anisotropy and exchange interactions influences the dispersion relation, temperature-dependent sublattice magnetization, and heat capacity. This knowledge advances our understanding of the magnetic properties of antiferromagnetic materials, opening the way for specialized applications in fields such as information storage and magnetic sensors.

4.2.1 Dispersion Relation and Anisotropy Fields

To investigate the relationship between dispersion frequency and anisotropy field, we use Eq.(4.6) and produce a graph that plots the normalized dispersion relationship against the normalized wave number for various anisotropy factors. As a result, Fig.4.7 below depicts the normalized dispersion relation within the spherical Brillouin zone of an antiferromagnetic system at various anisotropy values.

According to this figure, the minima of the dispersion relation for an ideal antiferromagnetic material shift upward from the zero level as (α) (at a constant ω_e) increases. Additionally, it should be mentioned that, as α increases, the amplitude of angular frequency (ω_k) oscillations decreases relative to its amplitude at minima. This suggests that the strength of an anisotropic field causes an increase in antiferromagnetic dispersion that results in decrease of amplitude of oscillation. Further scrutiny reveals that the graph flattens as the anisotropic field strength rises.

Let's take a look at an ideal cubic lattice structure antiferromagnetic system and draw a graph using Eq.(4.8), as shown in Fig.4.8, to demonstrate the impact of an anisotropic field on the linearity of the dispersion relation.

In this figure, the dispersion relation show linear with an arbitrary unit of wave number (ka), (tick black line). The linear relation deviates from a straight line as

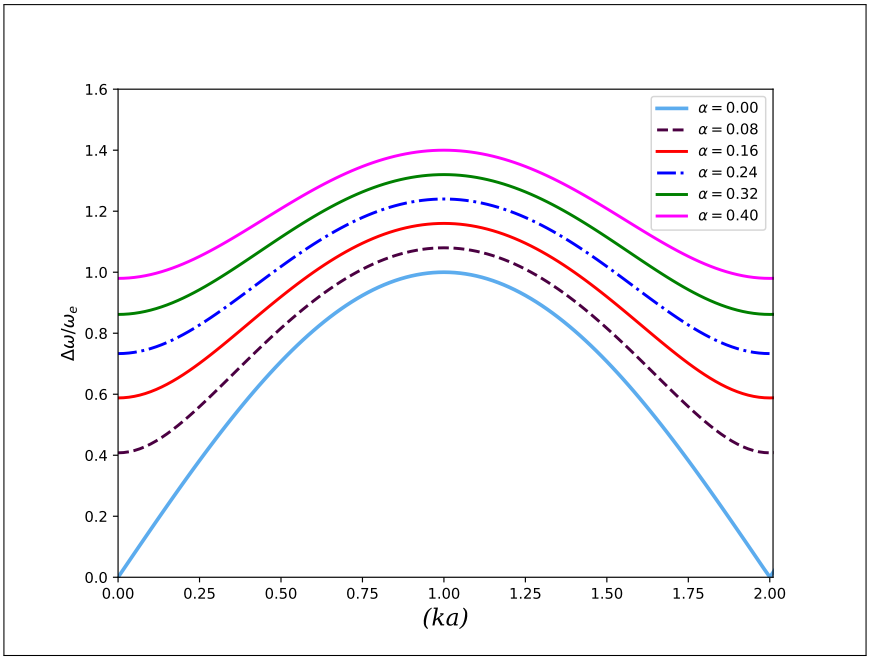

Figure 4.7: The sinusoidal curve of the dispersion relation ω_k, as a function of (ka), *where k is the wave vector and a is the lattice parameter in the first BZ.*

the α increases, with the wave number values close to the origin (i.e., $k = 0$). This shows that the non-linearity rises as the value of α increases. In general, a further scrutiny of Figs.4.7 and 4.8 reveal the flattening of the graph as α increases. Anisotropy fields have several sources and result from a variety of causes, including dipole-dipole interaction, magneto-crystal structure, bond interactions between ligands and magnetic atoms, spin-orbit interaction, and others. In antiferromagnetic materials serve primarily as a restoring force to external sources that disturb the system's stable order.

For further elaboration we shall next consider, a special antiferromagnetic materials of metal fluoride compounds with experimentally proven value of anisotropic and exchange field.

4.2.2 Dispersion Relation of Antiferromagnetic Fluoride Insulators

In this section, we will correlate theoretical analysis to practical implications for selected antiferromagnetic insulating fluoride materials FeF_2, MnF_2, and $RbMnF_3$, which have received a lot of attention in the past due to well-established experimental and computationally validated evidence. These three compounds show ba-

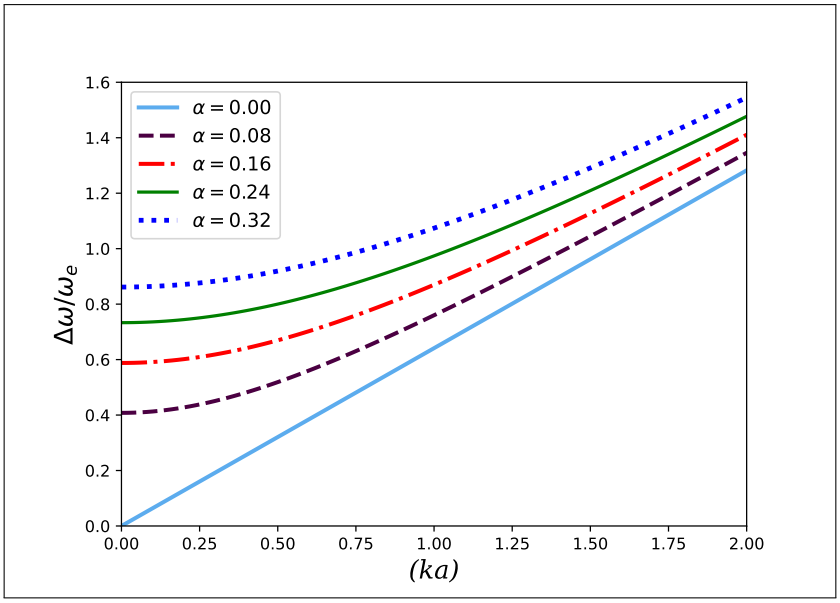

Figure 4.8: The linear dispersion of antiferromagnetic are plotted versus the wave number *(ka) in the first Brillouin zone*

sic 3-D antiferromagnetic ordering with two sublattices at temperatures below their Néel threshold. The cubic Perovskite structure of $RbMnF_3$ differs from the tetragonal rutile structure of the two compounds. With effective exchange fields of the same order of magnitude, their magnetic interactions are dominated by nearest neighbour exchange [84, 90, 27, 3].

The dispersion relation for antiferromagnetic system derived in Eq.(4.7) can characterize and thoroughly describe the dispersion relation for these antiferromagnetic materials explicitly and rewrite as:

$$\omega_k = \gamma H_0 \pm \frac{\gamma H_E}{\sqrt{z}} \sqrt{\left(\alpha^2 + 2\alpha + \sin^2(\frac{\pi}{2}\frac{k}{k_m})\right)} \tag{4.19}$$

where H_E is the effective exchange field connecting nearest neighbor inter-sublattice spins. The effective exchange parameter for MnF_2 has been obtained using inelastic neutron scattering experiments [86, 74, 113] with nearest neighbor exchange and similar inter-sublattice exchange fields (H_E). The magnetic Mn^{2+}-ions' ground state configuration is $3d^5(^6S_{5/2})$, which has a relatively low effective anisotropy field because it lacks orbital angular momentum and its value is nearly $H_A = 1.0$T [86, 74, 10] for MnF_2 and 4.5Oe for $RbMnF_3$ [78]. We listed the exchange field values in table 4.2 for our considerations [86, 90, 102, 78].

In the table.4.2, H_C represents a critical spin flip field. Antiferromagnetism exhibits a constant anisotropy field like exchange fields, cause the spins of two sublattices

Table 4.2: Exchange field values

	$H_E(T)$	$H_A(T)$	$H_c(T)$	α	$T_N(K)$
MnF_2	53.0	1.0	10.39	0.0185	68
FeF_2	55.5	19.0	49.70	0.3423	78
$RbMnF_3$	83.0	0.00045	0.027	0.0000054	83

to precess in opposite directions. To precess in the same direction, the spins need to make different-sized circles. If H_0 and H_A are smaller than H_E; and for small values of k in the long wave approximation, the dispersion relation in Eq.(4.19) could be again significantly simplified into the form of

$$\omega_k = \gamma H_0 \pm \frac{\gamma H_E}{\sqrt{z}} \sqrt{\left(z\alpha^2 + 2z\alpha + (\frac{\pi}{2}\frac{k}{k_m})^2\right)} \tag{4.20}$$

Based on the values listed in table 4.2, a dispersion relation for Eqs.(4.19 & 4.20) is plotted as in Fig.4.9 left and right panels, respectively, in an external magnetic field of $H_0 = 100$ kOe.

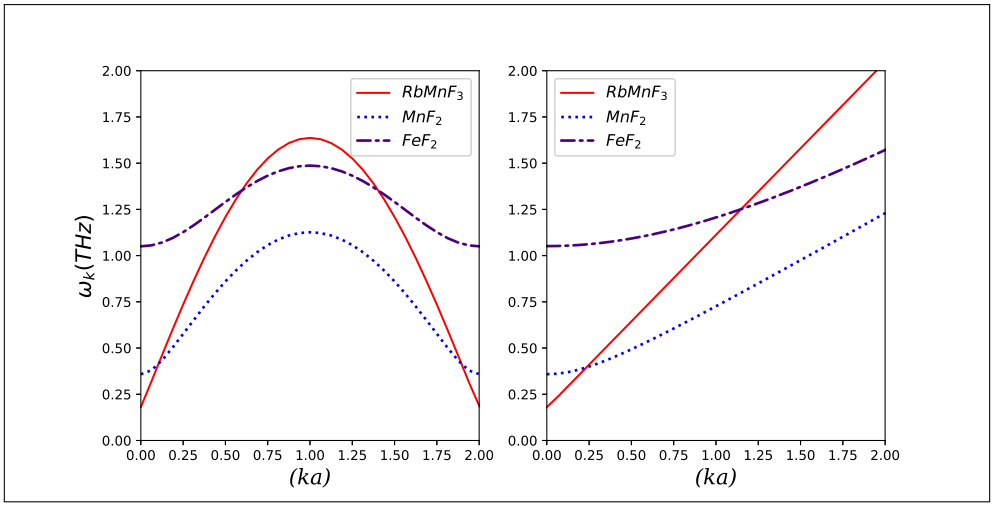

Figure 4.9: Dispersion of three antiferromagnetic materials of uniaxial symmetric crystal lattice, in the presence of magnetic field($H_0 \neq 0$).

Fig.4.9 represents the dispersion of antiferromagnetic materials of $RbMnF_3$, MnF_2 and FeF_2 in a spherical Brillouin zone. It is well known that, $RbMnF_3$ is a simple cubic structure [84, 78], MnF_2 and FeF_2 are body centered structure [86].

The diagrams in Fig.4.9 of these three materials in an external magnetic field exhibits similar behavior to the curve seen in Fig.4.7 despite each material have a

different anisotropic field strength. The minimum of dispersion for these crystals differ according to the value of α and shifts up, as can be seen. The graph in the left panel Fig.4.9 exhibit behavior resembling that of leading the dispersion to decrease to the curve in Fig.4.7. The amplitude of the dispersion, however, varies greatly perhaps due to their structure difference and the value of α. This leads the dispersion to decrease with increase in anisotropy field. Fig.4.9 demonstrate further that, as α increases, the linearity of the dispersion curve deviates toward the origin. Again, in the absence of an external magnetic field ($H_0 = 0$), we plot a dispersion graph using Eqs.(4.19 & 4.20) as shown in Fig.4.10.

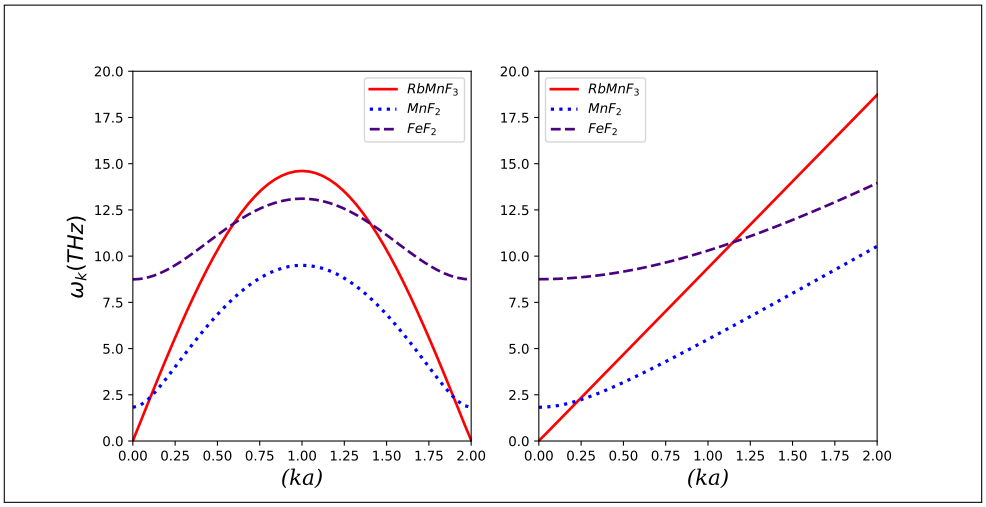

Figure 4.10: Dispersion of antiferromagnetics of uniaxial symmetric crystal lattice, in the absence of external field ($H_0 = 0$)

This figure illustrates a lower amount of dispersion minima compared to Fig.4.9 with Fig.4.9, indicating that the external magnetic field strengthens the dispersion relation. This demonstrates that anisotropy and exchange fields have a significant influence on dispersion in antiferromagnetic materials, pointing to magnetocrystalline structures as the source of anisotropic behavior. Our study's total dispersion results are consistent with antiferromagnetic materials analyzed in references [18, 23]. However, we analyze the impact of anisotropic fields in order to identify unusual events in our case.

Analogously, the anisotropy field can be viewed as a restoring force that keeps the antisymmetric spin alignment at the lowest possible energy. This external source must perform work and expend some energy to change stability [23]. The field may

increase spin-flopping, which breaks symmetry, decreasing the saturation of excited spins.

The effects of anisotropic field on amplitude of the dispersion and flattening of the curve is clearly observable for FeF_2, as shown in Figs.4.9 and 4.10, in agreement with the report revealing that the value of this field in the material is larger than that in MnF_2 and $RbMnF_3$ [96, 39, 95].

Using Eqs.(4.19 & 4.20) we have plotted a graph for the same material for further analysis on dispersion and anisotropy field (H_A), as shown in Fig.4.11.

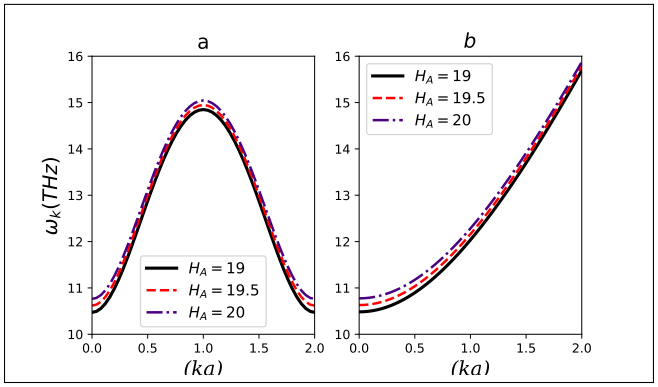

Figure 4.11: Dispersion of antiferromagnetic insulator, FeF_2, for a uniaxial symmetric crystal lattice, with an external magnetic field ($H_0 \neq 0$) (a) sinusoidal (b) linear

In this figure larger anisotropic field effect is clearly observed. Accordingly, as the field size rises, the dispersion curve creates a gap of the same nature which continues to match the trend of Figs.(4.7) & (4.8) plotted using the model in Eq.(4.7 & 4.8).

Anisotropy is always present in antiferromagnetism. In MnF_2 an effective anisotropy field of $8.8kOe$ by another work calculated which tends to keep the spins lined up. The effective anisotropy field in the $-z$ direction acting on the up spin whose magnetic moments are down and on the $+z$ direction acting on the down spins. Just as with the exchange fields; these fields will tend to make the spins of the two sublattice precess in opposite direction. In order to the spins precess in the same direction they must precess in different size of circle. Therefore, whether or not the spins are all in phase, i.e. even $\mathbf{k} = 0$, the spins, will precess and incline to

one another. This require to do work against the exchange field H_E as well as the anisotropy field H_A [48]. The work done according to Anderson's formalism for small **k** is

$$\begin{aligned} E_k &= \mp\hbar\omega_k \\ &= \mp\hbar\omega_0 - \hbar\frac{\omega_e}{\sqrt{z}}\sqrt{\left[\omega_A^2 + 2\omega_A\omega_e + (cons)a^2k^2\right]} \end{aligned} \tag{4.21}$$

In this equation the $\mp$ is for mode-1 and the $+$ is for mode-2. For a special case where $H_A = 0$ the work is reduced to

$$E_k = \hbar\omega_0 \pm (cons)ak \tag{4.22}$$

4.2.3 Antiferromagnetic Resonance of Fluoride Insulators

We take into account an AFM with two sublattices and an easy axis along $\vec{z}$. Two unit vectors, $\vec{m}_1$ and $\vec{m}_2$, are used to represent the orientations of the magnetic moments. Exchange interaction field, anisotropy field, and a magnetic field are believed to be in the direction that contribute to the precession of $\vec{m}_1$ and $\vec{m}_2$ [49]. The two sublattices' magnetization vectors, M_1 and M_2 where $|M_1| = |M_2| = M$, are pointed in the $+z$ and $-z$ directions, respectively, because of an anisotropy field, H_A. These two sublattices exhibit an exchange interaction relations formulas $H_E^{(1)} = -\lambda M_2$ and $H_E^{(2)} = -\lambda M_1$, where λ is a positive constant. We assume the Zeeman energy to be the governing term, indicating H_0 is powerful enough to align all moments in the direction of the external field. The first to create a fundamental formula for magnetization dynamics was Landau and Lifshitz [6], hence, the total force exerted on the two sublattice magnetization vectors is determined as follows:

$$\begin{aligned} H_{eff}^{(1)} &= -\lambda M_2 + H_A\hat{z} \\ H_{eff}^{(2)} &= -\lambda M_1 - H_A(-\hat{z}) \end{aligned} \tag{4.23}$$

In antiferromagnetism, we have two magnetization vectors and two equations of motion. In both, the time derivative of each sublattices total angular momentum equals the torque applied to the sublattice as given below

$$\begin{aligned} \frac{d\vec{M}_1}{dt} &= \gamma\left[\vec{M}_1 \times \mathbf{H}_{ef}\right] \\ \frac{d\vec{M}_2}{dt} &= \gamma\left[\vec{M}_2 \times \mathbf{H}_{ef}\right] \end{aligned} \tag{4.24}$$

Where γ is the magneto-mechanical ratio, M is the sub-lattice's total magnetic moment, and H_{eff} is the sum of the external and virtual fields acting on it. Let $H_E = \lambda M_1 \vec{z} = -\lambda M_2 \vec{z}$ and assume $M_1^{(x)}$, $M_2^{(x)}$, $M_1^{(y)}$, $M_2^{(y)}$ all that vary with $e^{i\omega t}$. The resonance frequencies are the eigenvalues of a matrix. After a simple algebraic simplification, a set of linear equations with $M_1^{(z)} = -M$ and $M_2^{(z)} = -M$ is obtained. The determinant equation is calculated by deducting [52] $M_1^+ = M_1^x + iM_1^y$ and $M_2^+ = M_2^x + iM_2^y$, so that

$$\begin{vmatrix} \gamma(H_A + H_E - \omega) & \gamma H_E \\ \gamma H_E & \gamma(H_A + H_E + \omega) \end{vmatrix} = 0 \tag{4.25}$$

Thus, the matrix of determinant offers antiferromagnetic resonance frequencies in the form of

$$\omega = \pm\gamma\Big[H_A(H_A + 2H_E)\Big]^{1/2} \tag{4.26}$$

When there is no external magnetic field and $\mathbf{k} = 0$ implies $\gamma_0 = 1$, and Eq.(4.21) coincide with Eq.(4.26). Excitation modes in a unit cell are as numerous as the constituent parts of the magnetic system. Antiferromagnetic system thus possesses two non-degenerate modes in the presence of external magnetic fields. In the simplest case, when a modest anisotropy field H_A is applied along the uni-axial axis, two circulating polarized modes frequently arise. According to Eq.(4.26), the spin wave frequencies are given in the presence of an external magnetic field (H_0) and an anisotropy field (H_A) at $k = 0$,

$$\omega_0 = \gamma H_0 \pm \gamma\sqrt{H_A(H_A + 2H_E)} \tag{4.27}$$

The origin of this mathematical relation can be traced back to Kittle and Nagmiya, who independently conducted a macroscopic examination of antiferromagnetic resonance [48, 49, 71, 51]. Eq.(4.26) demonstrates the frequency of the crystal lattice's natural mode. For the sample antiferromagnetic materials, this frequency value might be regarded as the upper bound of stability. The resonance frequency is $\omega_0 = \gamma H_c$, where H_c is the crucial value of the frequency for transition of the current stable phase, when there is no external magnetic field. When the magnetic field applied along the easy axis reaches the critical value, spin flopping takes place. With the anisotropy field, H_A and exchange field H_E can be used to approximate the

spin-flop critical field, which is given by $H_c \simeq \sqrt{H_A^2 + 2H_A H_E}$ [40, 70, 71]. When the external magnetic field engages against the internal exchange fields of the easy axis, the magnon interactions in the Brillouin zone decrease. The spin flip happens in the spherical model of resonance mode when the external field is almost equal to the critical field. Using table 4.2, an approximation of the AFMR frequency may be obtained by assuming the values of $\gamma = 176.0\ GHzT^{-1}$, and the spin-flop critical fields (H_c) are 10.3T and 49.89T, respectively, for MnF_2 and FeF_2. The frequencies are also 1.82THz and 8.75THz, respectively. We can see how the external field affects the sublattice spin precession and resonance frequencies of the sample materials plotted as in Fig.4.12.

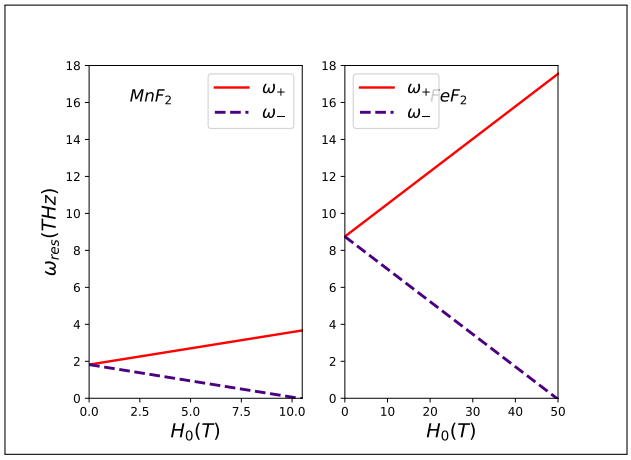

Figure 4.12: Antiferromagnetic resonance in MnF_2 and FeF_2 at external fields along the magnetic easy-axis. Below the spin-flop field H_C the magnetic resonance can occur for two different frequencies, one increasing (ω_{res}^{+}) and the other decreasing (ω_{res}^{-}) as H_0 increases; ω_{res} eventually approaches zero as $H_0 \Rightarrow H_c$)

This Figure shows that for the given specimen, the critical point of the spin flopped at an external field is nearly equal to the critical field, and a change in the resonance mode took place.

Summary: To recapitulate the effects of anisotropy on the dispersion relation, we see that as the magnitude of the uniaxial anisotropy field increases, so does the amplitude of the energy (energy) oscillation. This finding is consistent with data supported by well-established experimental and computational evidence used to investigate the dispersion relation equation. This shows that the anisotropy field has a major effect on the spin excitation energy of the antiferromagnetic spin interaction.

4.3 Effects of Anisotropy Field on Antiferromagnetic Parameters

In this subsection, we examined the results of theoretical and mathematical calculations involving bosonic operators, with the goal of addressing the problem statement; **'What is the impact of anisotropy field on thermodynamic parameters in an antiferromagnetic system?'** The objective here is to perform a thorough theoretical and mathematical examination of the data reported in Chapter 3, with an emphasis on the impact of the anisotropic field factor on important thermodynamic parameters including magnetization, susceptibility, and heat capacity.

This explanation gives a more concise and straightforward summary of the examination and the subsection's aims. It highlights the importance of theoretical and mathematical study and describes the thermodynamic characteristics of concern.

In the next part, we'll look at how these anisotropy fields affect thermodynamic parameters like antiferromagnetic magnon density, sublattice magnetization, and heat capacity in relation to excitation temperature and spin wave frequency. We will examine the influence of anisotropic fields on the magnetization and heat capacity properties of sublattice antiferromagnetic spin systems.

The bond interaction between the $3d$-orbitals of the magnetic ion and the s-or p-orbitals of the ligand atom in antiferromagnetic compound attribute for anisotropy field [19, 22]. As a result of these and other factors, anisotropy field is a fundamental property of antiferromagnetic materials. Certainly, the origin and source of anisotropy fields in antiferromagnetic materials are not entirely understood and require further investigation.

4.3.1 Effects of Anisotropy on Density of Magnon Mode(DMM)

To investigate the impact of anisotropy fields on magnon density, we made a graph (Fig.4.13) that shows the connection between magnon density and normalized excitation temperature (θ) using Eq. (4.18). The graph shows data for a magnetic field ($H_0 = 24,25$ T), antiferromagnetic exchange field ($H_E = 50$ T), and variable anisotropy field (α) in a perfect crystal lattice, as illustrated below. This figure (Fig.4.13), shows that the effects of anisotropy parameter strength on density of

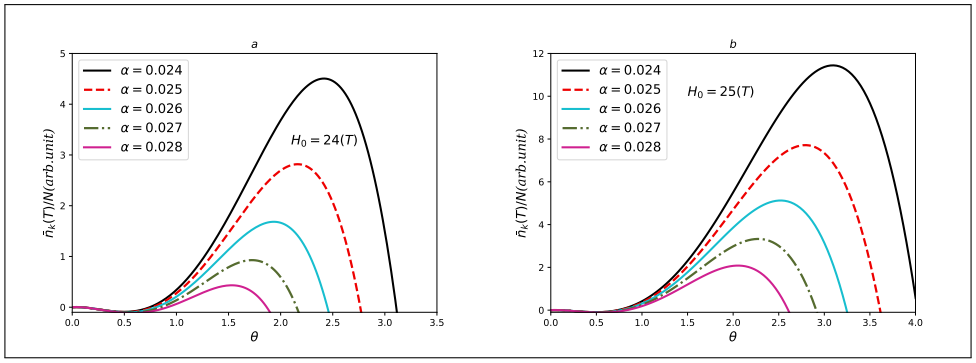

Figure 4.13: Density of magnon as a function of temperature at different anisotropic field and external magnetic fields at $H_0 = 24$ T as shown in the left panel and at $H_0 = 25$ T as shown in the right panel, in uniaxial direction.

magnon mode (DMM). According to this, DMM exhibit a decline until the normalized temperature (θ) rises to 0.6 and then rises up to a maximum peak for all anisotropy strengths with excitation temperature. While DMM reached its highest peak value, it displayed constant behavior for a few temperature intervals before dropping off quickly as the temperature increased. We notice that raising the value of "α" causes peak maxima to decrease in accordance.

The maximum peak value is affected differently by varying the applied magnetic field and anisotropy field strengths. At fixed magnetic field, increasing anisotropy value decreases the peak maxima,(see Fig.(4.13). When the magnetic field is increased, the level of peak maxima increases for a fixed value of the anisotropy field, (see Fig.4.13b).

It is worth noting that the peak maximum values recorded in connection to the anisotropy field effect, as shown in Fig.4.13, drop as the anisotropy value grows. Further examination reveals that the graph moves downward below the coordinate as anisotropy increases.

This shows that at temperature very near to absolute zero the spins of antiferromagnetic order aligned in opposite orientations(stable order). Due to the action of external source, the stable order is breaked and the spins become excited to interact each other. This may lead to an increase in their excited temperature and the magnon numbers rises. Just after all components excited, the increase in magnon number ceased and begin to fall with temperature. The anisotropy field suppresses

the increase of the magnon numbers.

To sum up, the anisotropy field suppresses the spins from being easily excited, as shown in all of the figures in this model.

4.3.2 Effects of Anisotropy on Magnetization

The description of staggered magnetization in words is necessary to understand why, in the simplest circumstances (1D lattice or square lattice), it may be mathematically described as a sum of the magnetic moment at each site with an alternating sign, as well as what a more comprehensive definition would be. It should be evident that the primary need is to use the site magnetic moments on the sublattices to construct a quantity that is not zero when antiferromagnetic order exists. The existence of staggered magnetization in a lattice indicates that the crystal can be divided into two or more interpenetrating sublattices, each with its own ordered magnetic moment. It is a phenomena observed in both antiferromagnetism and ferrimagnetism. In the former, the sublattice magnetic moments aggregate to zero, but in the later, there is a residual total magnetic moment.

For analytical solution of the temperature dependent magnetization (mean sublattice magnetization), we have to apply a transformation of the average magnon occupation number function $(e^{\beta\hbar\omega_k}-1)^{-1}$ in the continuum version [1]. The average magnetism at each site of all the sublattices, each properly rotated to align them all in the same direction, is summed to define staggered magnetization in a general sense that is valid for any lattice in any dimension. We may find the staggered magnetization order parameter by using:

$$M_{stag} = \sum_{i}^{A,B} (-1)^i \vec{S}_i^z \tag{4.28}$$

where $$(-1)^i = \begin{cases} 1 & \text{for} \quad i = A \\ -1 & \text{for} \quad i = B \end{cases}$$

Antiferromagnetic magnetization change the total S^z by ± 1, the effect on individual sublattices can be the statistical average. The ordered parameter could be considered as the staggered magnetization and the difference of the sublattice magnetization would be introduced as

$$\begin{aligned} M_{stg} &= \langle \sum_A S_A^z - \sum_B S_B^z \rangle \\ &= 2S - \sum_k \langle a_k^\dagger a_k \rangle - \sum_k \langle b_k^\dagger b_k \rangle \end{aligned} \tag{4.29}$$

At finite temperature $\langle a_k^\dagger a_k \rangle$ and $\langle b_k^\dagger b_k \rangle$ are boson numbers n_k expressed by the Bose-Einstein distribution.

The magnon numbers are not constant, in equilibrium, at a temperature T, they will be N_T for external energy is minimum. As a result the average number of occupation number $\langle n_k \rangle = a_k^\dagger a_k$ evaluated from Bose-Einstein distribution function $(e^{\beta\hbar\omega_k} - 1)^{-1}$. From the statistical quantum mechanics of energy distribution function, the magnetization of spin system approximated as $M(T,H) = \frac{1}{V}(\frac{\partial\Omega}{\partial H_0})_T$. A spin wave relation can help define magnetization as a function of temperature T, an external magnetic field, and an anisotropy field caused by a thermally induced spin wave. This may be written as:

$$M(T,H) = Ng\mu_B S\Big(1 - \frac{1}{NS}\sum_k \langle n_k \rangle\Big) \tag{4.30}$$

with magnon density $\sum_k n_k$ given by Eq.(4.18). The saturation magnetization is $M_0 = Ng\mu_B S$ when no magnons are activated, i.e. when $\langle n_k \rangle = 0 \quad$ for all $\mathbf{k}$ and is the moment for perfect alignment, and N is the number of atoms per unit volume [41, 42]. Therefore, at low temperature (not too high for small $\mathbf{k}$) the magnetization expression will be valid and we want to investigate the effects of anisotropic field strength in this region. The magnetic moments of the sublattices and of the antiferromagnetic material as a whole are determined in the usual method with the integrals being evaluated. A net magnetization exists only when H_0 is finite causing a difference in the two sublattice magnetic moments. The decrease in spontaneous sublattice magnetization, M, in the direction of equilibrium with rising temperature is proportional to the number of thermally excited magnons. Using Eq.(4.18) into Eq.(4.30) and after some algebraic manipulation and approximation provides (see appendix B_4)

$$M(T,H) = M_0\Big(1 - \frac{\sqrt{z^3}}{S}\Big\{0.0292A_1\theta - 0.0833A_2\theta^2 + 0.122A_3\theta^3 - 0.658A_4\theta^4\Big\}\Big) \tag{4.31}$$

To investigate the impact of the anisotropy field on magnetization, we set up a graph (Fig.4.14) showing the variation of magnetization with respect to the excitation temperature (θ) for different assumed anisotropy strength values. This study is based on the Eq.(4.31) provided below.

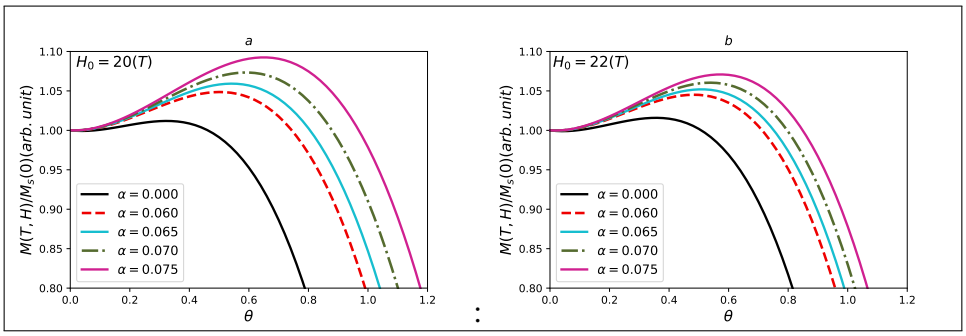

Figure 4.14: Magnetization as a function of excitation temperature at various values of anisotropy and applied magnetic fields: at $H_0 = 20T$, as shown in the left panel and at $H_0 = 22T$, as shown in the right panel, in uniaxial direction.

Fig.4.14 demonstrates that the temperature dependence of the net AF magnetization for an ideal isotropic magnetic crystal. The deviation of magnetization from the saturation value slowly increases and the gaps seem overlap with excitation temperature up to ($\theta = 0.2$). As the anisotropy field (α) increases, the magnetization above normalized temperatures of $\theta = 0.2$ increases and the gap opening becomes wider (see Fig.4.14a). When compared to absence of anisotropy the maximum peak and minima for each value of α there is shift up toward higher temperature side.

We observe from the same figure that increasing the values of α, at a fixed applied magnetic field, Shows increase in magnetization maxima and the gap between magnetization spectrum increased (see Fig.4.14a). On the other hand, for fixed value of α, increase of magnitude of applied external magnetic field decrease the gap between spectrum of magnetization (see 4.14b). This leads to realize that application of larger magnitude of magnetic field suppress the interchain spin interaction to reduce anisotropy gaps between the clusters.

Magnetization was plotted against temperature (θ) using a higher-order approximation of the spin wave dispersion equation. This was done to look into the effects of the anisotropic field on magnetization, which are illustrated Fig.4.15 below.

The magnetization as function of excitation temperature shown in Fig.4.15 indic-

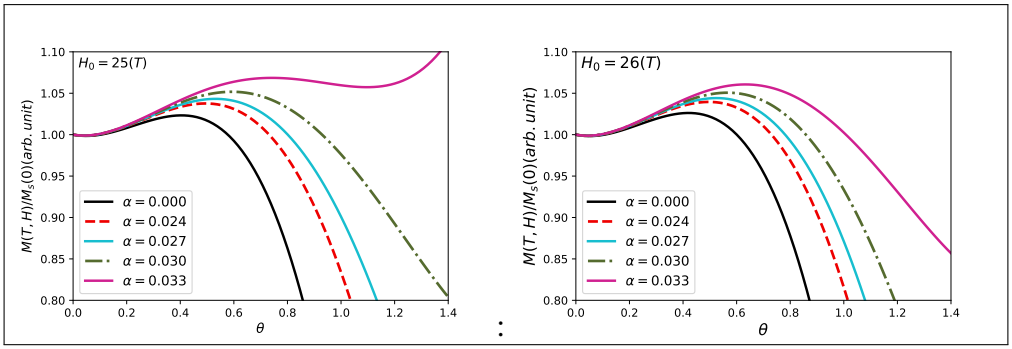

Figure 4.15: Magnetization as a function of excitation temperature at various values of anisotropy fields and applied magnetic fields at $H_0 = 25T$ as shown in the left panel and at $H_0 = 26T$ as shown in the right panel, in uniaxial direction.

ates that the magnetization curves identical trends of pattern as observed in Fig.4.14. The only difference observed in Fig.4.15, as anisotropy increase the spectrum of magnetization cluster move faster to shift upward.

The magnetization property shown in Figures (4.14 and 4.15) is affected by magnetic field, and at lower temperatures, applying a stronger magnetic field causes the gap in the magnetization cluster to be quenched. This indicates that the system's eigenvalue is shifted to a higher energy level by the magnetic field, which slows the magnetization's deviation with excitation temperature.

The magnetization involving various anisotropy fields is consistent with studies published in [97, 37]. The staggered magnetization curve flattens out with rising anisotropy, then rapidly increases with anisotropic field, and eventually drops as excitation temperature rises. This form shift points out the effect of spin flipping in low-temperature, anisotropic fields.

Applying an external magnetic field along the magnetic moment leads to an increase of the net magnetization with temperature. As the excitation temperature rises thermal energy effect overwhelms and the magnetization decreases with temperature. Anisotropy field show increment of magnetization. Further scrutiny indicates that increasing anisotropy field shift upward the magnetization curve.

It is worth noticing that increasing anisotropic field strength leads to an increase of the peak maxima of excitation temperature derivative of magnetization. In addition,

the antiferromagnetic magnetization is very sensitive to anisotropy field.

4.3.3 Antiferromagnetic Sublattice Susceptibility

The antiferromagnetic sublattice susceptibility quantifies an antiferromagnetic material's sublattice response to an applied magnetic field. It reflects the sublattice's ability to magnetize under the influence of a magnetic field. Often, the antiferromagnetic sublattice susceptibility is represented by a tensor, which accounts for the material's anisotropic response to the magnetic field. It serves as a crucial parameter for comprehending the magnetic properties of antiferromagnetic materials and can provide valuable insights into their behavior. Susceptibility is a measure of a material's responsiveness to an external magnetic field, while anisotropy quantifies the strength of a material's preferred direction of magnetization. Within the context of antiferromagnetic materials, the anisotropy field plays a significant role in influencing the behavior of the sublattices and their sensitivity to an external magnetic field.

In magnetic systems, the magnetic energy $(M \cdot H)$ is a crucial parameter. The magnetization, M, is determined by taking the negative of the first derivative of energy, E with respect to the magnetic field; H, $M = -\frac{\partial E}{\partial H}$. Of particular interest for magnetic systems is the magnetic energy $M \cdot H$. Magnetic susceptibility is often thought to be the zero field limit of dM/dH, which corresponds to the local slope of the M-H curve. Thus, taking the derivative of the magnetization, M with respect to the magnetic field, H gives the magnetic susceptibility, χ.

$$\chi = \frac{M_s\sqrt{z^3}}{SH_E}\left\{0.029A_1^{'}\theta - 0.083A_2^{'}\theta^2 + 0.122A_3^{'}\theta^3\right\} \tag{4.32}$$

Where the coefficients of $A_1^{'}$, $A_2^{'}$ and $A_3^{'}$ are functions of anisotropy fields.
A susceptibility curve was plotted using Eq.(4.32) as shown in Fig.4.16 with various anisotropy field strength values.
Fig.4.16 demonstrates that upon increasing the temperature from zero, the susceptibility, χ rises from zero to a peak value and then rapidly declines to a negligible level. Therefore, a phase transition temperature is the temperature at which a discontinuity occurs in χ or where it reaches its maximum value.

As illustrated in Fig.4.16, the antiferromagnetic susceptibility of the system is strongly influenced by the anisotropy field and normalized temperature. The magnetic sus-

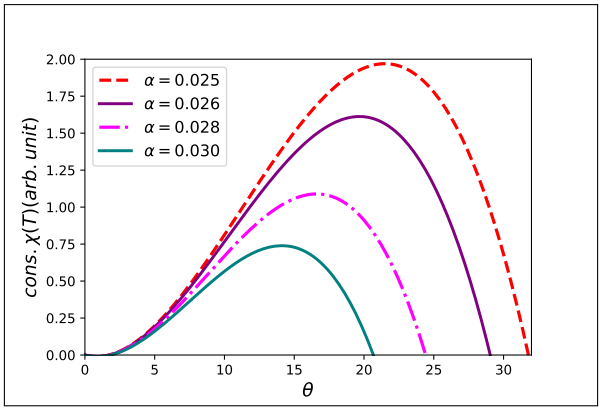

Figure 4.16: The system's antiferromagnetic susceptibility vs. normalized temperature, θ at various anisotropy factors.

ceptibility graph plotted based on our Heisenberg model of dispersion relation exhibits a similar trend to those found in previous studies [62, 28] that did not consider the anisotropy field. Fig.4.16 reveals that the maximum peak decreases with increasing anisotropy values.

This observation can be attributed to the enhanced stability of antiferromagnetic order induced by increasing anisotropy, leading to the suppression of the susceptibility peak. Additionally, the increased anisotropy could reduce thermal fluctuations, further contributing to the decrease in the maximum peak. Another crucial aspect to consider is the impact of anisotropy on magnetic interactions within the material. It is likely that increasing anisotropy alters magnetic interactions, resulting in a shift in susceptibility behavior. This is a significant finding and could have implications for our understanding of the behavior of antiferromagnetic materials. Further investigation and analysis of this trend could provide valuable insights into the underlying mechanisms at play.

4.3.4 Antiferromagnetic Heat Capacity

Heat capacity, a fundamental thermodynamic parameter, has a relationship with the ensemble's internal energy $U(T,\omega_k)$. Antiferromagnetic spin interactions' contribution to an ensemble's heat capacity ($C(T) = \frac{dU(\omega_k,T)}{dT}$) may be derived from the system's internal energy [35, 85]. The internal energy of an ensemble of antiferromagnetic magnons (bosons) may be represented as Debyes' type of heat capacity at finite temperature T (not too high for small k), and it can be determined by analyzing

the system's internal energy, which is provided by:

$$U(\omega,T) = 2\sum_{k}\hbar\omega_k\langle n_k\rangle \tag{4.33}$$

In which the average number of thermally excited magnons of wave vector **k** is $\langle n_k\rangle = (e^{\beta\hbar\omega_k}-1)^{-1}$. The factor of 2 is the result of counting the sublattice A and sublattice B types of spin excitations.

The gradient of antiferromagnetic magnons as function of temperature, which is more phonon like, calculated from the dispersion relation and the density of states (DOS) model. The dispersion relation in low temperature limit has a parabolic form $E \propto 2JzS(ak)$, this results in a density of states $D(\omega) \propto \omega$, which has a similarity to free electrons in 3 dimensions, and the total internal energy related to the magnon density of state by

$$U(\omega,T) = 2\frac{4\pi V}{(2\pi)^3}\int_0^{\infty}\frac{\hbar\omega_k}{e^{\beta\hbar\omega_k}-1}k^2dk \tag{4.34}$$

Thus, the magnetic heat capacity could be introduced by using Eq.(4.18) with some algebraic simplification and approximation as

$$C(T) = \frac{Nk_B}{2\pi^2}\sqrt{z^3}\left\{2A_1\zeta(2)\theta - 6A_2\zeta(3)\theta^2 + 24A_3\zeta(4)\theta^3 - 120A_4\zeta(5)\theta^4\right\} \tag{4.35}$$

The effects of the anisotropy field on the magnon heat capacity, MHC have been presented as a function of normalized temperature and for different anisotropy values in Fig.4.17 based on Eq.(4.35) at extremely low temperature(near absolute zero) approximations.

Fig.4.17 illustrates the theoretical predictions for the antiferromagnetic heat capacity at very low normalized temperatures, θ under various anisotropy fields and applied magnetic fields. At low temperatures, the magnon heat capacity increases with normalized temperature, peaks, and then decreases with increasing normalized temperature. These curves are consistent with previous research findings, regardless of the specific model or calculation method employed [58, 114, 37, 93].

Again, we plotted the MHC as a function of normalized temperature θ at various anisotropy levels using Eq.(4.35), as shown in Figs.4.18.

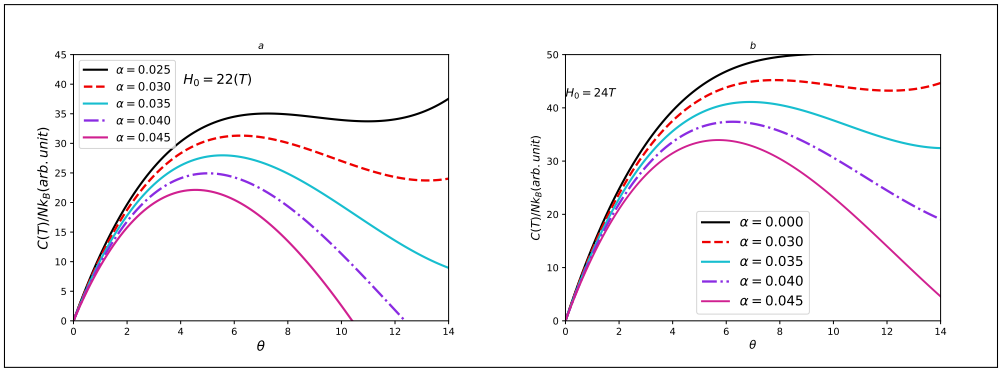

Figure 4.17: Heat capacity as a normalized temperature for different anisotropic field and applied magnetic fields: at $H_0 = 22$ T as shown in the left panel and at $H_0 = 24$ T as shown in the right panel, in uniaxial direction.

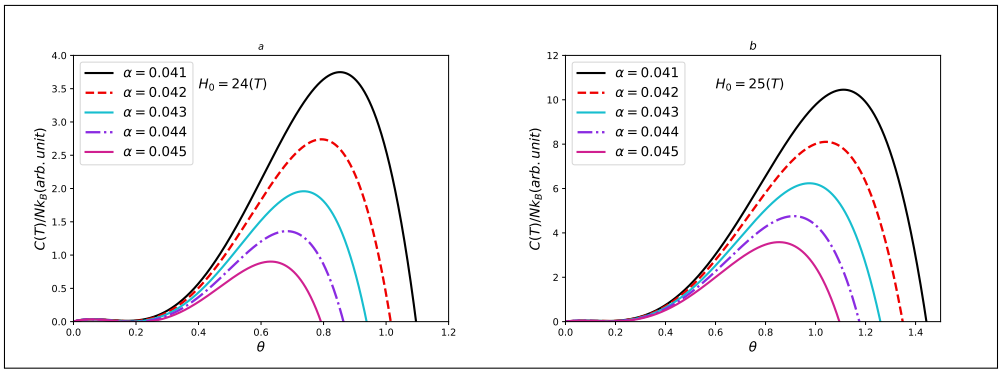

Figure 4.18: The heat capacity varies with normalized temperature for different anisotropic fields and applied magnetic fields. This is demonstrated in the left panel for $H_0 = 24$ T and in the right panel for $H_0 = 25$ T, both in the uniaxial direction.

The plots illustrate how the antiferromagnetic system's heat capacity changes with normalized temperature for different values of the anisotropy field α and applied magnetic field. The heat capacity increases gradually in the low-temperature region for almost all values of α and applied field. Subsequently, a gap emerges, and the highest peak is reached independently. Compared to the other variables, a higher α value corresponds to a lower maximum peak. This indicates that the anisotropy field strength, α and the maximum peak value are inversely related. The effect of the anisotropy field on the parameters of antiferromagnetic magnon heat capacity at a fixed magnetic field is depicted in Fig.4.18. Increasing a reduces the maximum peak and narrows the gap. After reaching its maximum peak, MHC exhibits constant behavior for a few temperature intervals before rapidly decreasing with increasing normalized temperature. As α increases, all peaks shift towards lower

temperatures and their rates of change decrease.

Upon closer examination, it is observed that the heat capacity dips below the x-axis as α increases. Conversely, for fixed values of α, increasing the applied field strength also augments the peak heat capacity. As the temperature rises, the region of maximum heat capacity stabilizes briefly before rapidly declining. This behavior can be attributed to the Schottky anomaly effect [32].

Understanding the relationship between heat capacity, temperature, and anisotropic field strength in antiferromagnetic materials may provide information on their thermodynamic properties and stability. The relationship between anisotropic field strength and peak spin excitation heat capacity is explained by spin order stability. As the anisotropy field strength grows, so does spin order stability, making the material more resistant to temperature-induced changes. This reduced susceptibility, resulting by decreased sensitivity to temperature variations, may prevent the maximum spin-excitation heat capacity peak. Stronger anisotropy fields effectively ”secure in” the spin order to minimize volatility.

Addressing this connection can give important insights into the thermodynamic behavior and temperature tolerance of antiferromagnetic materials. It also emphasizes the importance of anisotropy field strength in determining these materials' stability and reactivity to external perturbation. Further investigation of this connection has the potential to improve our understanding of the thermodynamic features of antiferromagnetic materials as well as their potential applications in a variety of disciplines.

4.4 Anisotropy Field and Antiferromagnetic Parameters of Transition metal Compounds

Transition metal fluoride compounds are commonly regarded as the better materials for testing and improving magnetic models. Because of their lack of electronic delocalization and often significant insulating characteristics, understanding their magnetic behavior is easier than comprehending oxides and sulfides. Early research on exchange constants and structural properties, as well as Néel theories for anti-

ferromagnetism and ferrimagnetism, relied on three-dimensional fluoride materials [9, 71].

4.4.1 Antiferromagnetic Sublattice Magnetization

Using Eqs.(4.31), we attempted to visualize the sublattice magnetization of an ideal antiferromagnetic material while varying the anisotropy field values. The resulting plot is depicted in the graph below

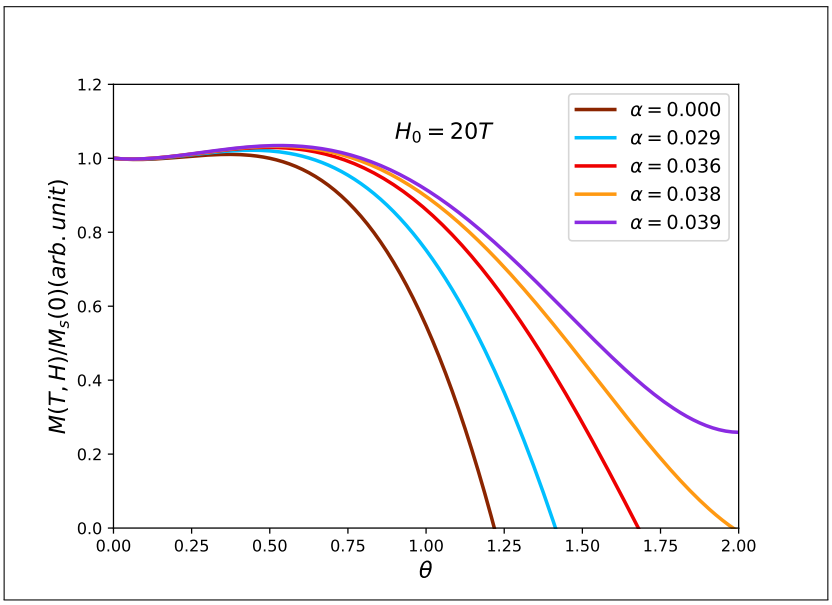

Figure 4.19: Magnetization as a fuction of excitation temerature at different anisotropy factors

Figure 4.19 demonstrates the temperature-dependent behavior of antiferromagnetic sublattice magnetization within an ideal isotropic magnetic crystal. A different pattern emerges when we analyze the link between temperature, anisotropy, and magnetization in the observed figure. At low normalized excitation temperatures, the magnetization curves first exhibit an intriguing feature: they appear to overlap, establishing a consistent pattern for all anisotropy values. This early stage reveals a region in which the effect of anisotropy on magnetization is roughly indistinguishable, allowing for a basic knowledge of magnetic behavior within this temperature range.

When the anisotropy field (α) is enhanced, a transformational process occurs. As the normalized temperature rises, the magnetization rises noticeably, and a notice-

able gap forms, implying a change from the behavior found in the lower temperature region. This change shows the strong influence of anisotropy on the magnetic response, implying a more pronounced alignment of magnetic moments as anisotropy increases.

To acquire a better understanding of the effect of anisotropy, we performed a comparison study using an anisotropy field that lacked known values. In this setting, we noticed a modest but substantial variation between the peak values for each scenario. These peaks migrated to higher temperature ranges before gradually decreasing and returning to the axis. This modest change emphasizes the complicated interplay between anisotropy and temperature, demonstrating how the introduction of anisotropy modifies the temperature-dependent magnetization profile. These discoveries add to a better understanding of the complicated dynamics that govern magnetic behavior in isotropic magnetic crystals.

Using the formulation in Eqs.(4.32 & 4.35), we tried to visualize the relation of susceptibility and heat capacity of an ideal antiferromagnetic material while changing the anisotropy field values we plotted the figure shown belw Fig.4.20.

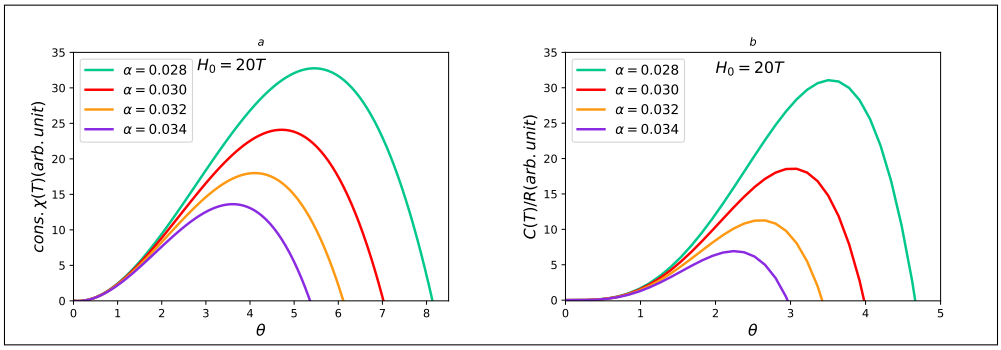

Figure 4.20: Susceptibilitty (a), heat capacity (b) as a function of normalized temperature for different anisotropic fields and applied magnetic fields.

We plotted antiferromagnetic susceptibility as a function of normalized temperature and varied the anisotropy field factors. The resultant graph showed a unique pattern: as the normalized temperature climbed, so did the susceptibility, reaching a peak maximum. The graph then stopped growing, showing constant values across a narrow temperature range. Following this, the graph observed a fast decline. Notably, we noticed that the maximum peak amplitude dropped as the anisotropic field

factor increased.

This effect may be described as the excitation temperature rises, the stable order of antiferromagnetic spin alignment is disturbed, resulting in an increase in magnetism. When all spin orders break, a maximum is achieved. A phase transition may then occur, resulting in a drop in the graph that shows this process.

In accordance with the system's underlying physics, the behavior of an antiferromagnetic system's heat capacity with normalized temperature frequently follows a similar pattern to the antiferromagnetic susceptibility.

When the heat capacity of an antiferromagnetic system is shown as a function of normalized temperature, it often follows the same pattern as the susceptibility. As the normalized temperature increases, so does the heat capacity, eventually reaching a maximum. This is followed by a constant over a small temperature range, after which the heat capacity rapidly declines. This behavior may be explained in terms of the energy required to disturb the antiferromagnetic order in the system. At low temperatures, the antiferromagnetic system exists in its ground state, with well-ordered spins. As the temperature rises, thermal energy destroys the ordered situation, increasing heat capacity. The peak maximum in heat capacity corresponds to the point at which thermal energy is sufficient to disrupt the antiferromagnetic order, resulting in a phase transition or a change in spin configuration.

In conclusion, the results in Figs.(4.20 (a) & (b)) show that the influence of an anisotropy field on the susceptibility and heat capacity of an antiferromagnetic system is larger as the anisotropy field increases at a fixed exchange field. Specifically, we notice that the peak decreases as the anisotropy field rises. This indicates that, theoretically, maintaining a constant anisotropy field while increasing the exchange field value would result in an increase in the maximum peak and a corresponding upward shift.

4.4.2 Anisotropy on Antiferromagnetic Transition Metal Compounds

Many studies focus on transition metal compounds (TMCs) due to their complex physics [82]. They also play a critical part in the operation of many energy and tech-

nology gadgets. TMCs' diverse structural properties and d-electron configurations enable a wide range of functionalities, resulting in their widespread application. The localized-d- electrons in transition metal atoms produce considerable local magnetic moments, and most TMCs exhibit magnetic ordering, including ferro-, ferri- and antiferromagnetism. Transition metals, in particular, have antiferro- or ferri-magnetic properties due to superexchange coupling between local cation moments with p orbitals. Unlike ferromagnetic materials, antiferromagnetic TMCs allow for a large variety of spin configurations.

The magnetic properties of transition metal compounds with relatively basic structures were studied both experimentally and theoretically. Their magnetic properties came from their series structure KMF_3, which has a perovskite structure. In the majority of structures, the M-ion was divalent and covered all of the transitional metal ions that made up the single crystal. These materials gave a lot of information on super-exchange and anisotropy mechanisms since the M-ions were placed on the simple cubic lattice with the F^-ion in the centre of each two neighbouring M^{2+}ions. This feature of transitional metal compound structure provided a large prospective supply of antiferromagnetic materials.

In our investigation of the magnetization and heat capacity of the antiferromagnetic transition compound Mn_2Au, we explored the exchange field between sublattices, which was established by susceptibility measurements, as well as an anisotropy field, which was predicted using theoretical second-order anisotropies.The values found for Mn2Au were given in [12, 13], with $H_E = 1300$ T and $H_A = 10$ T.

By exploring different antiferromagnetic insulating fluoride materials, such as FeF_2, MnF_2, Rb_2MnF_4, $RbFeF_4$,, and others, we want to correlate theoretical findings with practical consequences. There has always been a strong emphasis on established experimental and computationally validated results. These compounds have fundamental 3-d antiferromagnetic ordering with two sublattices below their Néel threshold temperatures. They adopt the tetragonal rutile crystal lattice structure with effective exchange fields of equal size, and their magnetic interactions are predominantly controlled by nearest neighbor exchanges [84, 3].

At low temperatures, the antiferromagnetic compound $RbMnF_3$ has a simple cubic crystal structure, while $CsMnF_3$ exhibits a hexagonal structure with strong axial anisotropy. At low temperatures, the latter has a two-sublattice structure with a space group of $P6_3/mmc$ and a magnetic unit cell that is identical to the chemical unit cell. Susceptibility measurements at low temperatures show that the exchange field H_E is 350kOe, and the axial anisotropy along the c-axis is $H_A = 7.5$ kOe [60].

We listed the exchange field values in table 4.3 for these of our consideration [102, 78, 9, 60, 3].

The thermodynamic features of antiferromagnetic ensembles with low temperature

Table 4.3: Exchange field values

Compound	S	H_E(kG)	$H_A(kG)$	α	$T_N(K)$	reference
MnF_2	5/2	526	10	0.0156	68	[86]
$RbMnF_3$	5/2	830	0.00045	0.000045	83	[9]
$CsMnF_3$	5/2	350	7.965	0.0228	54	[60]
K_2MnF_4	5/2	602	2.35	0.0039	42	[9]
Rb_2MnF_4	5/2	551	2.59	0.0047	38	[9]
$Mn_2P_2S_6$	5/2	1060	0.0802	0.00076	78	[54]

dependence were investigated using the total density of states spin wave spectrum. In other words, the density of states was the defining characteristic of a spin wave interaction ensemble. The density of states was then utilized to calculate antiferromagnetic properties such as magnetization and heat capacity.

The figure below illustrates the magnetization as a function of excitation temperature (θ) for different antiferromagnetic materials made of transitional metal compounds, making use of Eq.(4.32).

Fig.(4.21) displays the temperature dependence of the antiferromagnetic (AF) magnetization for different transitional metal compounds with approximately hexagonal crystals. At very low temperatures, all materials' magnetization curves appear to overlap. However, when excitation temperature rises, a gap appears in the magnetization deviation, with a scattered pattern and a maximum peak corresponding to the larger anisotropy field.

Furthermore, when the temperature rises, the magnetization peak increases in comparison to the low-temperature region. It is worth noting that the exchange field

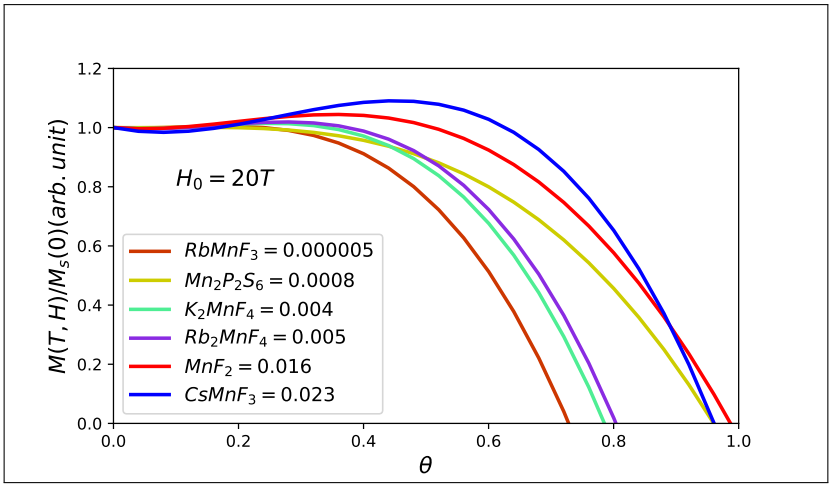

Figure 4.21: Magnetization as a function of excitation tamperature transitional metal compounds at an applied magnetic field $H_0 = 20$ T

has a substantial influence on magnetization a change, with materials with a greater exchange field showing a slight upward shifting of the highest peak towards the coordinate axis, followed by a slow return to baseline.

In order to comprehend the effect of intrinsic antiferromagnetic fields on susceptibility, we plotted the susceptibility (dM/dH) at limited dH around the external applied magnetic field H_0 as a function of normalized temperature for various antiferromagnetic materials.

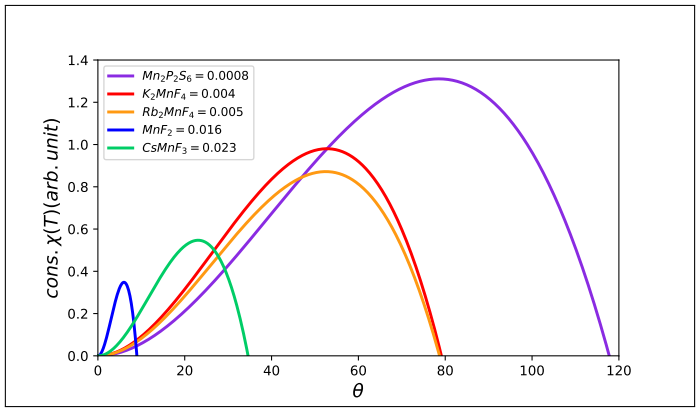

Figure 4.22: The system's antiferromagnetic susceptibility vs. normalized temperature, θ at various different antiferromagnetic compounds.

Fig.4.22 illustrates the relationship between susceptibility and normalized temperature (θ). The peak maxima demonstrate dispersion and separation with antiferromagnetic materials. It is important to note that the exact positions of the peak max-

ima are influenced by both the anisotropy factor and the quantity of the exchange field. Notably, higher exchange field values produce significantly larger maximum peaks on the graph. This finding stresses the role of the exchange field value in the development of peak maxima in susceptibility vs normalized temperature graphs.

The magnon heat capacity (MHC) as a function of excitation temperature and for various antiferromagnetic materials plotted below.

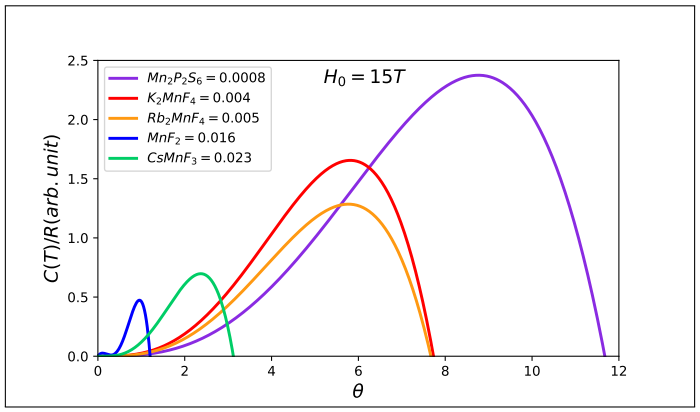

Figure 4.23: Heat capacity as normalized temperature for different antiferromagnetic compounds at $H_0 = 15$ T, in uniaxial direction model.

Fig.(4.23) illustrates the magnon heat capacity(MHC) vs normalized temperature (θ) for various antiferromagnetic materials. The heat capacity of antiferromagnetic materials is shown in the low-temperature approximation using Eq.(4.35). Individual heat capacity peaks appear and are dispersed in accordance with the unique properties of antiferromagnetic materials. The dispersion and separation of heat capacity peaks is similar to the behavior found with antiferromagnetic susceptibility. The anisotropy factor and exchange field have an influence on maximum heat capacity peaks.

It is observed that a higher exchange field value of an antiferromagnetic material results in greater peak maxima in the heat capacity graph (see $Mn_2P_2S_6$). This highlights the importance of the exchange field value in determining the appearance of peak maxima in the heat capacity vs normalized temperature plot. The result is consistent with the prior observation that the anisotropy field suppresses maximum peaks while the exchange field magnifies them.

Increased anisotropic field parameter has implications for lowering the susceptibility peak and minimizing thermal fluctuations, leading in improved antiferromagnetic stability. Changes in anisotropy change magnetic interactions, which in turn affect susceptibility and heat capacity. Peak values decrease with increasing anisotropy; nevertheless, with a constant anisotropy field, increasing the exchange field shifts and amplifies the peaks. The observations show that peak amplitude is impacted by both anisotropy and exchange fields. Higher excitation temperatures disrupt antiferromagnetic alignment, increasing magnetism and perhaps indicating a phase change, as seen by the abrupt drop in the graph.

Overall, the anisotropy field has a significant impact on the properties of antiferromagnetic materials, emphasizing its importance in understanding their behavior and prospective applications.

4.5 Discussion

In this research, we employed a uniaxial Heisenberg Hamiltonian Spin wave model, which serves as a robust framework for investigating quantum antiferromagnets. This theoretical approach allows us to derive the excitation energy spectrum from the stable state, commonly referred to as the ground state.

Our model incorporates the Heisenberg Hamiltonian alongside the Zeeman and anisotropy energy terms. To simplify the analysis, we aligned the spin easy axis with the Z-axis, and the anisotropy energy field was treated as one-ion anisotropy. Additionally, we assumed spin values ($S \geq 1$) and restricted the exchange interaction to occur solely between spins belonging to different sublattices, known as intersublattice interaction.

In the Heisenberg Hamiltonian model, outlined in Eqs.(3.4 & 3.8), we introduced higher-order terms involving up to six products of bosonic operators to appropriately explain spin wave interactions. Eq.(3.31) provides a simplified dispersion relation obtained from rigorous calculation and the Green's function approach.
The results derived in Eqs.(4.4 & 4.6) proviede information on the dispersion relation for the higher-order product of bosonic operator interactions, which was

developed using the Heisenberg Hamiltonian model and certain mathematical assumptions. These equations provide a basis for understanding how the energy of these interactions varies with momentum. Certain approximations minimize the complicated interactions between bosonic operators, resulting in a more realistic representation of their behavior via the derived dispersion relation. This full relationship is required to understand the dynamics of bosonic systems and anticipate their physical properties.
The dispersion relation differs from those published in earlier studies by [83, 84, 115, 86], which disregard higher-order terms above quadratic. The model considers the influence of anisotropic field factor and temperature parameter term on the dispersion relation (angular frequency) stated in Eq.(4.4).

The model used shows that the interaction between anisotropy and temperature has a considerable effect on the dispersion relation, emphasizing their complex impact on the dynamics of the antiferromagnetic system. We observed that changing anisotropy levels and increasing temperature increase the sinusoidal amplitude of the dispersion relation until it reaches zero. As a result, the oscillation spectrum moves downward, displaying the system's complex dynamics.

In the case of low temperatures and long wavelengths, several approximations have been employed to simplify the dispersion relation stated in Eq.(4.7). This mathematical model is consistent with previous studies conducted by [83, 84, 115, 86]. This study involves plotting a dispersion relation as a function of wave vector to demonstrate the effect of an anisotropy field at various magnitudes. Our results clearly show how the anisotropy field affects the dispersion properties of antiferromagnetic spin waves.

The use of a linear approximation considerably simplifies the dispersion relation, which is consistent with the research results of [51, 49, 48, 71]. This linearized dispersion relation simplifies the application of energy-momentum conservation laws to higher-order systems. The linear function (ω_k) was chosen to represent the dispersion because it accurately describes magnon frequencies in the Brillouin zone, as detailed in Eq.(4.7) and (4.8). These equations explicitly show how dispersion depends on both the anisotropy field and the wave vector.

In the analysis of the antiferromagnetic spin wave model, we examined various graphs by varying the anisotropy field parameter and observed the following:

1.**Dispersion Relation vs. Wave Vector Parameter**:
The graph of the dispersion relation as a function of the wave vector parameter was plotted for different magnitudes of the anisotropy field parameter. We observed that as the anisotropy parameter increases, the amplitude of the sinusoidal dispersion relation decreases.

2. **Magnetization vs. Excitation Temperature**:
The graph showing magnetization as a function of excitation temperature for different values of the anisotropy field parameter revealed a slight increase in the maximum peak as the anisotropy parameter increases.

3. **Magnetic Susceptibility vs. Excitation Temperature**:
When plotting magnetic susceptibility against excitation temperature, we noted that the maximum peak decreases with each increase in the anisotropy parameter value.

4. **Magnetic Heat Capacity vs. Normalized Excitation Temperature**:
Finally, the graph of magnetic heat capacity versus normalized excitation temperature indicated a decrease in the peak maxima for different values of the anisotropy field parameter.

The results presented here emphasize the importance of the anisotropy field parameter in determining the behavior of antiferromagnetic materials under varied situations.

The results reveal that the approximation-derived dispersion relation significantly corresponds with prior investigations, especially in circumstances involving extremely low temperatures and long wavelengths. Furthermore, our findings highlight the critical significance of the anisotropy field in antiferromagnetic interactions. Notably, as the magnitude of the uniaxial anisotropy field increases, the amplitude of energy oscillations (dispersion) decreases. This finding demonstrates that the anisotropy field has an substantial impact on the spin excitation energy inside the

antiferromagnetic spin interaction, stressing its significance in defining the system's behavior.

Chapter 5

Summary and Recommendation

5.1 Summary

In this thesis, we investigated the effects of an anisotropic field on an antiferromagnetic system, utilizing the Heisenberg Hamiltonian model to explore spin-wave interactions. Our objective was to better comprehend genuine antiferromagnetics and the dispersion relation of higher order product of bosonic operator aberrations from predicted behavior caused by spin wave interaction processes.
We employed the Holstein-Primakoff (HP) transformation to turn spin operators into boson operators, which allowed us to investigate magnon interactions. Using the Green Function approach, calculate the dispersion relation for spin wave propagation.

The results of the thesis In examining the antiferromagnetic spin wave model, we altered the anisotropy field parameter, revealing useful insights for both theoretical and practical physics. In summary:

1.Dispersion Relation: As the anisotropy parameter increases, the amplitude of the sinusoidal dispersion relation decreases.
2. Magnetization: The maximum peak of magnetization slightly increases with higher anisotropy parameter values.
3. Magnetic Susceptibility: The peak of magnetic susceptibility decreases as the anisotropy parameter increases.
4. Magnetic Heat Capacity: The peak maxima of magnetic heat capacity decrease for increasing values of the anisotropy field parameter.

These findings illustrate the influence of the anisotropy field parameter on the magnetic properties of antiferromagnetic materials.

5.2 Recommendation

This thesis investigates the interactions of antiferromagnetic spin waves in a low-dimensional spin system. This topic of research is occasionally judged unsatisfactory due to worries about its contribution to a better understanding of these relationships. Despite their beautiful look in antiferromagnetic systems, anisotropy field effects have limited practical use due to their low working temperatures and modest impacts. This emphasizes the need for more research to fully realize its

Spin wave research has enormous potential for application in magnetism and antiferromagnetics teaching and advisory procedures. It is critical that educators and mentors thoroughly investigate the consequences of anisotropy in various disciplines. By integrating spin wave research concepts, they may be able to improve the depth and relevance of their teaching and instruction, resulting in increased learning and growth for students and researchers.

It is advised that researchers use the study's findings to evaluate the practical uses of antiferromagnetic materials. These findings provide important insights into the design and setup of devices using such materials. By taking this information into consideration, researchers may increase the efficacy and efficiency of their efforts, increasing the practical application of antiferromagnetic materials.

The study's implications provide both incentive and a platform for additional investigation and review. Academics should use these implications as a motivation and starting point for future study on this topic, taking into consideration bi- or tri-anisotropy fields. Building on the facts and concepts presented in this study, further research can help to widen and increase knowledge of the issue.

For institutions, the outcome contributes to

- encourage curricular development and research,

- including magnetic research and
- develop inter-disciplinary programs.

For Researchers

- The model can be used for research in spintronics and quantum computing, expanding our understanding of antiferromagnetic properties.
- It can also be applied to practical applications such as data storage and magnetic sensors by varying parameters and materials.

Practitioners find it beneficial to

- Optimizing AFM materials and understanding anisotropy's impact on magnetic properties.
- enhance magnetic device design and performance.

Future work aims to focus on

- the effects of bi-directional anisotropy fields,
- changing exchange fields, and
- different crystal structures are discussed.

References

[1] ACHLEITNER, J. (2011). Magnetization and magnon excitation energies of the magnetic semiconductors eute and euo on the basis of the renormalized spin wave theory. *arXiv preprint arXiv:1103.1831*. 76

[2] ARTMAN, J., MURPHY, J. & FONER, S. (1965). Magnetic anisotropy in antiferromagnetic corundum-type sesquioxides. *Physical Review*, **138**, A912. 25

[3] ARTS, A. & DE WIJN, H. (1990). Spin waves in two-dimensional magnetic systems: Theory and applications. In *Magnetic Properties of Layered Transition Metal Compounds*, 191–229, Springer. 58, 67, 88, 89

[4] ASHCROFT, N.W. & MERMIN, N.D. (2022). *Solid state physics*. Cengage Learning. 122

[5] ASHCROFT, N.W., MERMIN, N.D. *et al.* (1976). *Solid state physics*. holt, rinehart and winston, new york London. 55, 122

[6] ATXITIA, U., HINZKE, D. & NOWAK, U. (2016). Fundamentals and applications of the landau–lifshitz–bloch equation. *Journal of Physics D: Applied Physics*, **50**, 033003. 71

[7] AUERBACH, A. (1998). *Interacting electrons and quantum magnetism*. Springer Science & Business Media. 38

[8] AVAN, P. & COHEN-TANNOUDJI, C. (1977). Two-level atom saturated by a fluctuating resonant laser beam. calculation of the fluorescence spectrum. *Journal of Physics B: Atomic and Molecular Physics*, **10**, 155. 44

[9] BANCI, L., BENCINI, A., BENELLI, C., BOHRA, R., DANCE, J.M., GATTESCHI, D., JAIN, V., MEHROTRA, R., TRESSAUD, A., WOOLLEY, R. *et al.* (1982). Relationships between structure and low-dimensional magnetism in fluorides. In *Structures versus Special Properties*, 87–146, Springer. 59, 85, 89

[10] BARAK, J., JACCARINO, V. & REZENDE, S. (1978). The magnetic anisotropy of mnf2 at 0 k. *Journal of Magnetism and Magnetic Materials*, **9**, 323–332. 53, 67

[11] BARMAN, A., GUBBIOTTI, G., LADAK, S., ADEYEYE, A.O., KRAWCZYK, M., GRÄFE, J., ADELMANN, C., COTOFANA, S., NAEEMI, A., VASYUCHKA, V.I. *et al.* (2021). The 2021 magnonics roadmap. *Journal of Physics: Condensed Matter*, **33**, 413001. 4, 5

[12] BARTHEM, V., COLIN, C., MAYAFFRE, H., JULIEN, M.H. & GIVORD, D. (2013). Revealing the properties of mn2au for antiferromagnetic spintronics. *Nature communications*, **4**, 2892. 88

[13] BHATTACHARJEE, N., SAPOZHNIK, A., BODNAR, S.Y., GRIGOREV, V.Y., AGUSTSSON, S.Y., CAO, J., DOMINKO, D., OBERGFELL, M., GOMONAY, O., SINOVA, J. *et al.* (2018). Nèel spin-orbit torque driven antiferromagnetic resonance in mn 2 au probed by time-domain thz spectroscopy. *Physical review letters*, **120**, 237201. 7, 88

[14] BLUNDELL, S. (2001). *Magnetism in condensed matter*. OUP Oxford. 22

[15] BONBIEN, V., ZHUO, F., SALIMATH, A., LY, O., ABBOUT, A. & MANCHON, A. (2021). Topological aspects of antiferromagnets. *Journal of Physics D: Applied Physics*, **55**, 103002. 4

[16] BONILLA, M., KOLEKAR, S., MA, Y., DIAZ, H.C., KALAPPATTIL, V., DAS, R., EGGERS, T., GUTIERREZ, H.R., PHAN, M.H. & BATZILL, M. (2018). Strong room-temperature ferromagnetism in vse2 monolayers on van der waals substrates. *Nature nanotechnology*, **13**, 289–293. 3

[17] CHENG, R., DANIELS, M.W., ZHU, J.G. & XIAO, D. (2015). Ultrafast switching of antiferromagnets via spin-transfer torque. *Physical Review B*, **91**, 064423. 6

[18] CHOTORLISHVILI, L., WANG, X.G., DYRDAŁ, A., GUO, G.H., DUGAEV, V., BARNAŚ, J. & BERAKDAR, J. (2022). Rectification of the spin seebeck current in noncollinear antiferromagnets. *Physical Review B*, **106**, 014417. 69

[19] CHOWDHURY, S.R. & MISHRA, S. (2017). Heavy ligand atom induced large magnetic anisotropy in mn(ii) complexes. *Phys. Chem. Chemical Physics*, **19**, 16914–16922. 51, 54, 74

[20] COEY, J. & MAZALEYRAT, F. (2023). History of magnetism. *Reference Module in Materials Science and Materials Engineering*. 1

[21] CULLITY, B.D. & GRAHAM, C.D. (2011). *Introduction to magnetic materials*. John Wiley & Sons. 24

[22] DENNIS, C., JACKSON, A., BORCHERS, J., GRUETTNER, C. & IVKOV, R. (2018). Correlation between physical structure and magnetic anisotropy of a magnetic nanoparticle colloid. *Nanotechnology*, **29**, 215705. 51, 54, 74

[23] DOS SANTOS, F.J., DOS SANTOS DIAS, M. & LOUNIS, S. (2020). Modeling spin waves in noncollinear antiferromagnets: Spin-flop states, spin spirals, skyrmions, and antiskyrmions. *Physical Review B*, **102**, 104436. 69

[24] DUTTA, S., CHANG, S.C., KANI, N., NIKONOV, D.E., MANIPATRUNI, S., YOUNG, I.A. & NAEEMI, A. (2015). Non-volatile clocked spin wave interconnect for beyond-cmos nanomagnet pipelines. *Scientific reports*, **5**, 9861. 7

[25] ENGELSBERG, M., REZENDE, S. & SOARES, E. (1979). 19f spin-lattice relaxation in antiferromagnets with the perovskite structure. *Journal of Applied Physics*, **50**, 1929–1931. 59

[26] ENZ, U. (1982). Magnetism and magnetic materials: Historical developments and present role in industry and technology. *Handbook of Ferromagnetic Materials*, **3**, 1–36. 1

[27] ERICKSON, R.A. (1953). Neutron diffraction studies of antiferromagnetism in manganous fluoride and some isomorphous compounds. *Physical Review*, **90**, 779. 58, 67

[28] FARIDFAR, M. & VAHEDI, J. (2022). Thermodynamic behavior of spin-1 heisenberg chain: a comparative study. *Journal of Superconductivity and Novel Magnetism*, **35**, 519–528. 81

[29] FOWLER, R.H. (1949). *Statistical thermodynamics*. Cambridge University Press. 23

[30] FUKAMI, S., LORENZ, V.O. & GOMONAY, O. (2020). Antiferromagnetic spintronics. *Journal of Applied Physics*, **128**. 4

[31] GEFFE, C.A. (2010). *Study of Photoinduced Ferromagnetism in Diluted Magnetic Semiconductor (Ga, Mn) As*. Ph.D. thesis, Addis Ababa University. 39, 48

[32] GOPAL, E. (2012). *Specific heats at low temperatures*. Springer Science & Business Media. 84

[33] GUEMARD, V. & MANCHON, A. (2022). Unified formulation of interfacial magnonic pumping from noncollinear magnets. *Physical Review B*, **105**, 054433. 3

[34] HARRISON, R.J. (1950). The quantum theory of antiferromagnetism. 24

[35] HENDRIKSEN, P.V., LINDEROTH, S. & LINDGÅRD, P.A. (1993). Finite-size modifications of the magnetic properties of clusters. *Physical Review B*, **48**, 7259. 81

[36] HOLSTEIN, T. & PRIMAKOFF, H. (1940). Field dependence of the intrinsic domain magnetization of a ferromagnet. *Physical Review*, **58**, 1098. 38, 40

[37] HONECKER, A., BRENIG, W., TIWARI, M., FEYERHERM, R., BLECKMANN, M. & SÜLLOW, S. (2022). Numerical interchain mean-field theory for the specific heat of the bimetallic ferromagnetically coupled chain compound mnni (no2) 4 (en) 2 (en= ethylenediamine). *Molecules*, **27**, 6546. 79, 82

[38] HUANG, B., CLARK, G., NAVARRO-MORATALLA, E., KLEIN, D.R., CHENG, R., SEYLER, K.L., ZHONG, D., SCHMIDGALL, E., MCGUIRE, M.A., COBDEN, D.H. *et al.* (2017). Layer-dependent ferromagnetism in a van der waals crystal down to the monolayer limit. *Nature*, **546**, 270–273. 3

[39] HUTCHINGS, M., RAINFORD, B. & GUGGENHEIM, H. (1970). Spin waves in antiferromagnetic fef2. *Journal of Physics C: Solid State Physics*, **3**, 307. 70

[40] JACCARINO, V., KING, A., MOTOKAWA, M., SAKAKIBARA, T. & DATE, M. (1983). Temperature dependence of fef2 spin flop field, journal of magnetism and magnetic materials. *Journal of Magnetism and Magnetic Materials*, **31**, 1117 –1118. 73

[41] JOENK, R. (1962). Magnetic field dependence of thermodynamic properties of antiferromagnets; adiabatic magnetization. *Physical Review*, **128**, 1634. 36, 77, 128

[42] JOENK, R. (1963). Adiabatic magnetization of antiferromagnets. *Journal of Applied Physics*, **34**, 1097–1098. 77, 128

[43] JOHANSEN, Ø. (2019). *Antiferromagnetic Insulator Spintronics*. Ph.D. thesis, Norwegian University of Science and Technology(NTNU). ix, 14, 15, 16

[44] JOHNSON, M., BLOEMEN, P., DEN BROEDER, F. & DE VRIES, J. (1996). Magnetic anisotropy in metallic multilayers. *Reports on Progress in Physics*, **59**, 1409. 53

[45] JUNGWIRTH, T., MARTI, X., WADLEY, P. & WUNDERLICH, J. (2016). Antiferromagnetic spintronics. *Nature nanotechnology*, **11**, 231–241. 5, 7

[46] KAMRA, A., AGRAWAL, U. & BELZIG, W. (2017). Noninteger-spin magnonic excitations in untextured magnets. *Physical Review B*, **96**, 020411. 16

[47] KEFFER, F. (1966). Spin waves. In *Ferromagnetism/Ferromagnetismus*, 1–273, Springer. 55

[48] KEFFER, F. & KITTEL, C. (1952). Theory of antiferromagnetic resonance. *Physical Review*, **85**, 329. 8, 62, 71, 72, 93

[49] KEFFER, F., KAPLAN, H. & YAFET, Y. (1953). Spin waves in ferromagnetic and antiferromagnetic materials. *American Journal of Physics*, **21**, 250–257. 8, 54, 55, 71, 72, 93

[50] KIMEL, A., IVANOV, B., PISAREV, R., USACHEV, P., KIRILYUK, A. & RASING, T. (2009). Inertia-driven spin switching in antiferromagnets. *Nature Physics*, **5**, 727–731. 6

[51] KITTEL, C. (1951). Theory of antiferromagnetic resonance. *Physical Review*, **82**, 565. 72, 93

[52] KITTEL, C. (2021). *Introduction to solid state physics Eighth edition*. 49, 72, 121

[53] KITTEL, C. & FONG, C.Y. (1963). *Quantum theory of solids*, vol. 5. Wiley New York. 36

[54] KOBETS, M., DERGACHEV, K., GNATCHENKO, S., KHATSÂ€™KO, E., VYSOCHANSKII, Y.M. & GURZAN, M. (2009). Antiferromagnetic resonance in mn2p2s6. *Low Temperature Physics*, **35**, 930–934. 59, 89

[55] KOOLS, J. (2020). *Inducing spin dynamics in antiferromagnetic NiO*. Ph.D. thesis, Eindhoven University of Technology, 2020. ix, 6

[56] KREISEL, A. (2011). *Spin-wave calculations for Heisenberg magnets with reduced symmetry*. Ph.D. thesis, Frankfurt am Main, Johann Wolfgang Goethe-Univ., Diss., 2011. ix, 37, 49, 121

[57] KRUGLYAK, V., DEMOKRITOV, S. & GRUNDLER, D. (2010). Magnonics. *Journal of Physics D: Applied Physics*, **43**, 26400. 7

[58] LE, P., HOI, B. & YARMOHAMMADI, M. (2018). Magnon-impurity interaction effect on the magnonic heat capacity of the lieb lattice. *AIP Advances*, **8**, 125317. 82

[59] LEE, C.H., ANBALAGAN, A.K., CHANG, T.W., FAN, C.L., CHUNG, J.C. & CHIEN, S.C. (2019). The exchange bias effect on single layer of fe-rich ferh thin film. *Materials Letters*, **254**, 309–311. 7

[60] LEE, K., PORTIS, A. & WITT, G. (1963). Magnetic properties of the hexagonal antiferromagnet csmn f 3. *Physical Review*, **132**, 144. 59, 89

[61] LEE, K.H. & LIU, S. (1967). Green's-function method for antiferromagnetism. *Physical Review*, **159**, 390. 26, 27, 29, 43, 117

[62] MARUTHI, R., GHOSH, S., SEEHRA, M.S., JOSHI, D.C., CHOWDHURY, M.R., MEDWAL, R., RAWAT, R.S., WEISE, B. & THOTA, S. (2021). Magnetic field-temperature phase diagram, exchange constants and specific heat exponents of the antiferromagnet mnnb2o6. *Journal of Physics: Condensed Matter*, **33**, 345801. 81

[63] MATHUR, N.D. (2003). Magnetic materials: Fundamentals and device applications. 1

[64] MATTIS, D.C. (2012). *The theory of magnetism I: Statics and Dynamics*, vol. 17. Springer Science & Business Media. 38

[65] MOHN, P. (2002). *Magnetism in the solid state: an introduction*, vol. 134. Springer Science & Business Media. 13

[66] MOOK, A., HENK, J. & MERTIG, I. (2019). Thermal hall effect in noncollinear coplanar insulating antiferromagnets. *Physical Review B*, **99**, 014427. 3

[67] MORIYA, T. (1960). Anisotropic superexchange interaction and weak ferromagnetism. *Physical Review*, **120**, 91. 53

[68] MORIYA, T. (1964). Ferro-and antiferromagnetism of transition metals and alloys. *Solid State Communications*, **2**, 239–243. 14

[69] MORIYA, T. (1965). Ferro-and antiferromagnetism of transition metals and alloys. *Progress of Theoretical Physics*, **33**, 157–183. 14, 17

[70] NAGAI, O. & YOSHIMORI, A. (1961). Spin waves in mnf2 and the inelastic scattering of neutrons. *Progress of Theoretical Physics*, **25**, 595–602. 73

[71] NAGAMIYA, T. (1951). Theory of antiferromagnetism and antiferromagnetic resonance absorption, i. *Progress of Theoretical Physics*, **6**, 342–349. 72, 73, 85, 93

[72] NÉEL, L. (1971). Magnetism and local molecular field. *Science*, **174**, 985–992. 17, 26

[73] NĚMEC, P., FIEBIG, M., KAMPFRATH, T. & KIMEL, A.V. (2018). Antiferromagnetic opto-spintronics. *Nature Physics*, **14**, 229–241. 5

[74] NIKOTIN, O., LINDGÅRD, P.A. & DIETRICH, O. (1969). Magnon dispersion relation and exchange interactions in mnf2. *Journal of Physics C: Solid State Physics*, **2**, 1168. 67

[75] NOLTING, W. & BREWER, W.D. (2008). *Fundamentals of many-body physics*. Springer. 40

[76] O'GRADY, E.A. (2020). Anisotropy in antiferromagnets. *Journal of Applied Physics*, **128**, 040901. 53

[77] OGUCHI, T. (1960). Theory of spin-wave interactions in ferro-and antiferromagnetism. *Physical Review*, **117**, 117. 41

[78] ORTIZ, J.L., GUERRA, G.F., MACHADO, F. & REZENDE, S. (2014). Magnetic anisotropy of antiferromagnetic rb mn f 3. *Physical Review B*, **90**, 054402. 59, 67, 68, 89

[79] PASHKIN, A., SELL, A., KAMPFRATH, T. & HUBER, R. (2013). Electric and magnetic terahertz nonlinearities resolved on the sub-cycle scale. *New Journal of Physics*, **15**, 065003. 6

[80] PRABHAKAR, A. & STANCIL, D.D. (2009). *Spin waves: Theory and applications*, vol. 5. Springer. 22

[81] QUINN, J.J. & YI, K.S. (2009). *Solid state physics: principles and modern applications*. Springer Science & Business Media. 36, 50

[82] RAO, C.N.R. (1989). Transition metal oxides. *Annual Review of Physical Chemistry*, **40**, 291–326. 15, 87

[83] REZENDE, S. & WHITE, R. (1976). Multimagnon theory of antiferromagnetic resonance relaxation. *Physical Review B*, **14**, 2939. 8, 49, 62, 93

[84] REZENDE, S. & WHITE, R. (1978). Spin-wave lifetimes in antiferromagnetic rbmn f 3. *Physical Review B*, **18**, 2346. 58, 62, 67, 68, 88, 93

[85] REZENDE, S., RODRÍGUEZ-SUÁREZ, R., ORTIZ, J.L. & AZEVEDO, A. (2014). Thermal properties of magnons and the spin seebeck effect in yttrium iron garnet/normal metal hybrid structures. *Physical Review B*, **89**, 134406. 81

[86] REZENDE, S.M., AZEVEDO, A. & RODRÍGUEZ-SUÁREZ, R.L. (2019). Introduction to antiferromagnetic magnons. *Journal of Applied Physics*, **126**, 151101. 3, 8, 54, 59, 62, 67, 68, 89, 93

[87] RODRIGUEZ, J., OK, H., XIA, Y.M., DEBRUNNER, P., HINRICHS, B., MEYER, T. & PACKARD, N. (1996). Mössbauer spectroscopy of the spin-coupled fe3+- fe2+ center of reduced uteroferrin. *The Journal of Physical Chemistry*, **100**, 6849–6862. 16

[88] ROSS, P., SCHREIER, M., LOTZE, J., HUEBL, H., GROSS, R. & GOENNENWEIN, S.T. (2015). Antiferromagentic resonance detected by direct current voltages in mnf2/pt bilayers. *Journal of Applied Physics*, **118**, 233907. 62

[89] SAIDAOUI, H.B.M. & MANCHON, A. (2016). Spin orbit torque in disordered antiferromagnets. *arXiv preprint arXiv:1606.04261*. ix, 35

[90] SANDERS, R., JACCARINO, V. & REZENDE, S. (1978). Magnetic polariton, impurity mode enhancement, and superradiance effects in fef2. *Solid State Communications*, **28**, 907–910. 58, 67

[91] SANG-WOOK, C., MANFRED, F., WEIDA, W., LAURENT, C. & VALERY, K. (2020). Seeing is believing: visualization of antiferromagnetic domains. *NPJ Quantum Materials*, **5**. 5

[92] SATOH, T., CHO, S.J., IIDA, R., SHIMURA, T., KURODA, K., UEDA, H., UEDA, Y., IVANOV, B., NORI, F. & FIEBIG, M. (2010). Spin oscillations in antiferromagnetic nio triggered by circularly polarized light. *Physical review letters*, **105**, 077402. 6

[93] SEKI, K. & YUNOKI, S. (2020). Thermodynamic properties of an s= 1 2 ring-exchange model on the triangular lattice. *Physical Review B*, **101**, 235115. 82

[94] SELZER, S. & MAJLIS, N. (1982). Theory of the surface magnetization profile and the low-energy, spin-polarized, inelastic electron scattering off insulating ferromagnets at finite t. *Physical Review B*, **26**, 404. 44

[95] SHAPIRA, Y. (1971). Observation of antiferromagnetic phase transitions by ultrasonic techniques. *Journal of Applied Physics*, **42**, 1588–1594. 70

[96] SHAPIRA, Y. & FONER, S. (1970). Magnetic phase diagram of mn f2 from ultrasonic and differential magnetization measurements. *Physical Review B*, **1**, 3083. 70

[97] STREMPFER, J., RÜTT, U., BAYRAKCI, S., BRÜCKEL, T. & JAUCH, W. (1993). Magnetic properties of transition metal fluorides m f 2 (m= mn, fe, co, ni) via high-energy photon diffraction. *Physical Review B*, **69**, 014417. 79

[98] SYROMYATNIKOV, A. (2022). Elementary excitations in spin-1 2 antiferromagnets on the triangular lattice. *Physical Review B*, **105**, 144414. 48

[99] TAHIR-KHELI, R., CALLEN, H. & JARRETT, H. (1966). Magnetic ordering in cubic crystals with first and second neighbor exchange. *Journal of Physics and Chemistry of Solids*, **27**, 23–32. 117

[100] TIABLIKOV, S.V. (2013). *Methods in the quantum theory of magnetism*. Springer. 47, 48

[101] TOPP, J., DUERR, G., THURNER, K. & GRUNDLER, D. (2011). Reprogrammable magnonic crystals formed by interacting ferromagnetic nanowires. *Pure and Applied Chemistry*, **83**, 1989–2001. 49, 121

[102] TSOGBADRAKH, N., TUVJARGAL, N., FENG, C., DAVAASAMBUU, J. & TEGUS, O. (2019). Insulator–half metallic transition by the tetragonal distortion: A first-principles study of strain-induced perovskite rbmnf _3. *arXiv preprint arXiv:1905.08959*. 59, 67, 89

[103] TZSCHASCHEL, C., OTANI, K., IIDA, R., SHIMURA, T., UEDA, H., GÜNTHER, S., FIEBIG, M. & SATOH, T. (2017). Ultrafast optical excitation of coherent magnons in antiferromagnetic nio. *Physical Review B*, **95**, 174407. 6

[104] UTERMOHLEN, F.G. (2021). *Magnetic Properties of Two-Dimensional Honeycomb-Lattice Materials*. The Ohio State University. 40

[105] WADLEY, P., HILLS, V., SHAHEDKHAH, M., EDMONDS, K., CAMPION, R., NOVÁK, V., OULADDIAF, B., KHALYAVIN, D., LANGRIDGE, S., SAIDL, V. *et al.* (2015). Antiferromagnetic structure in tetragonal cumnas thin films. *Scientific reports*, **5**, 17079. 7

[106] WADLEY, P., HOWELLS, B., ŽELEZNÝ, J., ANDREWS, C., HILLS, V., CAMPION, R.P., NOVÁK, V., OLEJNÍK, K., MACCHEROZZI, F., DHESI, S. *et al.* (2016). Electrical switching of an antiferromagnet. *Science*, **351**, 587–590. 7

[107] WANG, X., ZHANG, H. & WANG, X. (2018). Topological magnonics: A paradigm for spin-wave manipulation and device design. *Physical Review Applied*, **9**, 024029. 3

[108] WANG, Z. (2017). *Spin waves in magnetic thin films: new types of solitons and electrical control*. Ph.D. thesis, Colorado State University. 7, 8

[109] WINTUCKEY, E. & FLAX, L. (1971). Theory of the two sublattice heisenberg antiferromagnet. Tech. rep. 15, 43

[110] WU, H., ZHANG, H., WANG, B., GROSS, F., YANG, C.Y., LI, G., GUO, C., HE, H., WONG, K., WU, D. *et al.* (2022). Current-induced néel order switching facilitated by magnetic phase transition. *Nature communications*, **13**, 1629. 6

[111] XIE, Y., ZHAN, Q., HU, Y., HU, X., CHI, X., ZHANG, C., YANG, H., XIE, W., ZHU, X., GAO, J. *et al.* (2020). Magnetocrystalline anisotropy imprinting of an antiferromagnet on an amorphous ferromagnet in ferh/cofeb heterostructures. *NPG Asia Materials*, **12**, 67. 53

[112] XUE, D., GAO, M., KONG, Y. & LI, F. (1994). Spin wave theory of anisotropie two-sublattice heisenberg ferrimagnets. *physica status solidi (b)*, **184**, 215–224. 44

[113] YAMANI, Z., TUN, Z. & RYAN, D. (2010). Neutron scattering study of the classical antiferromagnet mnf2: a perfect hands-on neutron scattering teaching course. *Canadian Journal of Physics*, **88**, 771 – 797. 67

[114] YARMOHAMMADI, M. (2016). Magnon heat capacity and magnetic susceptibility of the spin lieb lattice. *Journal of Magnetism and Magnetic Materials*, **417**, 208–213. 82

[115] YOSIDA, K. (1996). *Theory of magnetism.: Edition en anglais*, vol. 122. Springer Science & Business Media. 20, 26, 62, 93

[116] YUAN, H. & WANG, X. (2017). Magnon-photon coupling in antiferromagnets. *Applied Physics Letters*, **110**. 2

[117] ZAKERI, K. (2014). Elementary spin excitations in ultrathin itinerant magnets. *Physics Reports*, **545**, 47–93. 8

[118] ŽELEZNỲ, J., WADLEY, P., OLEJNÍK, K., HOFFMANN, A. & OHNO, H. (2018). Spin transport and spin torque in antiferromagnetic devices. *Nature Physics*, **14**, 220–228. 5

[119] ZHUO, F., LI, H., MANCHON, A. *et al.* (2021). Topological phase transition and thermal hall effect in kagome ferromagnets. *Physical Review B*, **104**, 144422. 5

[120] ZHUO, F., LI, H., CHENG, Z. & MANCHON, A. (2022). Magnonic metamaterials for spin-wave control with inhomogeneous dzyaloshinskii–moriya interactions. *Nanomaterials*, **12**, 1159. 5

[121] ZUBAREV, D.N. (1960). Double-time green functions in statistical physics. *Soviet Physics Uspekhi*, **3**, 320. 44, 63, 124

Appendix A

A.1 Heisenberg-Hamiltonian model

The Heisenberg Hamiltonian in the antiferromagnetic (AFM) of hypercubic crystal lattice with sublattices A and B accompanying with Zeemann terms, is expressed as:

$$\begin{aligned}\mathcal{H} =& 2\sum_{\langle \ell m\rangle} J_{\ell m}\vec{S}_\ell.\vec{S}_m - \gamma(H_0+H_A)\sum_\ell S^z_\ell \\ &+ \gamma(H_A-H_0)\sum_m S^z_m \end{aligned} \tag{A.1}$$

where $\vec{S}_\ell$ is the spin operator at site A, $\vec{S}_m$ is at site B and J is the exchange constant between ions at site A and B, which is assumed to be a function of only the distance between the ions.
We choose the number $h_{A/B} = \gamma(H_A \pm H_0)$, where H_A is the infinitesimal anisotropic field required to specify the orientation of the up and down sublattices, respectively. Hence, the function simplifies (A.1) to

$$\mathcal{H} = 2\sum_{\langle \ell m\rangle} J_{\ell m}\vec{S}_\ell\vec{S}_m - \gamma h_A\sum_\ell S^z_\ell + \gamma h_{\mathbf{B}}\sum_m S^z_m \tag{A.2}$$

The spin interactions can be expressed in terms of the spin raising and lowering operators as

$$\mathbf{H} = J\sum_{\ell m}\{(S^\dagger_\ell S^-_m + S^-_\ell S^\dagger_m) + 2S^z_\ell S^z_m\} - h_A\sum_\ell S^z_\ell + h_B\sum_m S^z_m \tag{A.3}$$

We use the Holstein-Primakoff transformation to map the localized spin operators for the system of spin moments on the lattice to the canonical bosonic creation and annihilation operators of site A and B given below as

$$A \Rightarrow \begin{cases} S^+_\ell &= (\sqrt{2S - a^\dagger_\ell a_\ell})a_\ell \\ S^-_\ell &= a^\dagger_\ell(\sqrt{2S - a^\dagger_\ell a_\ell} \\ S^z_\ell &= S - a^\dagger_\ell a_\ell \end{cases}$$

and

$$B \Rightarrow \begin{cases} S_m^+ &= b^\dagger(\sqrt{2S - b_m^\dagger b_m}) \\ S_m^- &= (\sqrt{2S - b_m^\dagger b_m})b_m \\ S_m^z &= -(S - b_m^\dagger b_m) \end{cases}$$

At low temperature, the number of excitation about the ground state is very small ($\langle a^\dagger a\rangle = \langle \hat{n}\rangle \ll S$), so we can expand underradical of HP transformation equation in the Binomial expansion to the first order in the form of

$$A \Rightarrow \begin{cases} S_\ell^+ &= \sqrt{2S}(1 - \frac{a_\ell^\dagger}{2S} a_\ell)a_\ell \\ S_\ell^- &= a_\ell^\dagger \sqrt{2S}(1 - \frac{a_\ell^\dagger a_\ell}{2S}) \\ S_\ell^z &= S - a_\ell^\dagger a_\ell \end{cases}$$

and

$$B \Rightarrow \begin{cases} S_m^+ &= b^\dagger \sqrt{2S}(1 - \frac{b_m^\dagger b_m}{2S}) \\ S_m^- &= (\sqrt{2S}(1 - \frac{b_m^\dagger b_m}{2S})b_m \\ S_m^z &= -(S - b_m^\dagger b_m) \end{cases}$$

Substitution of the HP trnaformed equations of int the respective values of spin operators for each spin site in (A.3) and after some algebraic simplification we get

$$\begin{aligned} S_\ell^\dagger S_m^- &= 2Sa_j b_l - \frac{a_j b_l^\dagger b_l b_l}{2} - \frac{a_j^\dagger a_j a_j b_l}{2} + \frac{a_j^\dagger a_j a_j b_l^\dagger b_l b_l}{8S} + \ldots) \\ S_\ell^- S_m^\dagger &= 2Sa_j^\dagger b_l^\dagger - \frac{a_j^\dagger b_l^\dagger b_l^\dagger b_l}{2} - \frac{a_j^\dagger a_j^\dagger a_j b_l^\dagger}{2} + \frac{a_j^\dagger a_j^\dagger a_j b_l^\dagger b_l^\dagger b_l}{8S} + \ldots) \\ S_\ell^z S_m^z &= -S^2 + Sa_j^\dagger a_j + Sb_l^\dagger b_l - a_j^\dagger a_j b_l^\dagger b_l \end{aligned} \tag{A.4}$$

and the Zeeman term interation also expressed as

$$-h_A \sum_\ell S_\ell^z + h_B \sum_m S_m^z = -2\gamma H_a NS + h_A \sum_\ell a_\ell^\dagger a_\ell + h_B \sum_m b_m^\dagger b_m \tag{A.5}$$

Now we substitute (A.4) and (A.5) into the Heisenberg antiferromagnetic (A.3) we obtain

$$\begin{aligned} \mathbf{H} = &-2NS(\omega_e + \omega_A) + 2JS \sum_{\langle \ell m\rangle} \{a_\ell b_m + a_\ell^\dagger b_m^\dagger + a_\ell^\dagger a_\ell + b_m^\dagger b_m\} + h_A \sum_\ell a_\ell^\dagger a_\ell + h_B \sum_m b_m^\dagger b_m \\ &- \frac{J}{2} \sum_{\langle \ell m\rangle} \{a_\ell b_m^\dagger b_m b_m + a_\ell^\dagger a_\ell a_\ell b_m + a_\ell^\dagger b_m^\dagger b_m^\dagger b_m + a_\ell^\dagger a_\ell^\dagger a_\ell b_m^\dagger + 4a_\ell^\dagger a_\ell b_m^\dagger b_m\} \\ &+ \frac{J}{8S} \sum_{\langle \ell m\rangle} \{a_\ell^\dagger a_\ell a_\ell b_m^\dagger b_m b_m + a_\ell^\dagger a_\ell^\dagger a_\ell b_m^\dagger b_m^\dagger b_m\} \end{aligned} \tag{A.6}$$

A.1.1 Fourier Transform

Using Fourier transform, we can express bosonic space operators interms of momentum space vector by

$$a_j = \frac{1}{\sqrt{N}}\sum_k e^{ik\cdot x_j}a_k \qquad a_j^\dagger = \frac{1}{\sqrt{N}}\sum_k e^{-ik\cdot x_j}a_k^\dagger$$
$$b_l = \frac{1}{\sqrt{N}}\sum_k e^{-ik\cdot x_l}b_k \qquad b_l^\dagger = \frac{1}{\sqrt{N}}\sum_k e^{ik\cdot x_l}b_k^\dagger \tag{A.7}$$

where N is the total number of spin sites and $\vec{k}$ is the wave number that runs over N in the first Brillouin zone of the lattice's reciprocal space.

Fourier Transform of $H^{(2)}$

Substitution of (A.7) into

$$\mathcal{H}^{(2)} = 2JS\sum_{\langle jl\rangle}\{a_jb_l + a_j^\dagger b_l^\dagger + a_j^\dagger a_j + b_l^\dagger b_l\} + h_A\sum_j a_j^\dagger a_j + h_B\sum_l b_l^\dagger b_l$$

and after algebraic simplification one gets

$$\begin{aligned}H^{(2)} =& \omega_e\sum_{k_1k_2}\{\triangle(k_2-k_1)\Upsilon_{k_2}a_{k_1}b_{k_2} + \triangle(k_2-k_1)\Upsilon_{-k_2}a_{k_1}^\dagger b_{k_2}^\dagger + \triangle(k_2-k_1)a_{k_1}^\dagger a_{k_2}\\ &+\triangle(k_2-k_1)b_{k_1}^\dagger b_{k_2} + h_A\sum_{k_1k_2}\triangle(k_2-k_1)a_k^\dagger a_k + h_B\sum k_1k_2\triangle(k_2-k_1)b_{k_1}^\dagger b_{k_2}\end{aligned} \tag{A.8}$$

We have been used in the Hamiltonian; $\sum_j e^{i(k'-k).r_j} = N\delta_{k-k'}$ and, where necessary, the summation k as $-k$. We can approximation $k\cdot\delta \ll 1$ for big wave length. Here, we introduced the concept of Υ_k, a structural/geometric component that depends on the crystal structure and is defined as $\Upsilon_k = z^{-1}\sum_\delta e^{ik\cdot\delta}$, where δ is the vector connecting the closest neighbor in the opposite direction, and $\sum_j\sum_\delta = zN$. If we recall from the delta function condition that the lattice point in the center of symmetry is $\Upsilon_k = -\Upsilon_k$, then we have

$$\triangle(|k_2-k_1|) = \begin{cases}1 & when \quad k_1 = k_2\\ 0 & otherwise \quad 0\end{cases}$$

In this case

$$\begin{aligned}H^{(2)} &= \omega_e\sum_k\{\Upsilon_k a_kb_k + \Upsilon_k a_k^\dagger b_k^\dagger + a_k^\dagger a_k + b_k^\dagger b_k\} + \sum_k\{h_A a_k^\dagger a_k + h_B b_k^\dagger b_k\}\\ &= \sum_k\{A_1^2(a_kb_k + a_k^\dagger b^\dagger) + A_2^2 a_k^\dagger a_k + A_3^2 b_k^\dagger b_k\}\end{aligned} \tag{A.9}$$

where $A_1^{(2)} = \omega_e\Upsilon_k$, $A_2^{(2)} = \gamma h_A$ and $A_3^{(2)} = \gamma h_B$.

Fourier Transform of $H^{(4)}$

The Fourier transform of $H^{(4)}$ by substitution of (A.7) into

$$\mathcal{H}^{(4)} = -\frac{J}{2}\sum_{\langle jl\rangle}\{a_j b_l^\dagger b_l b_l + a_j^\dagger a_j a_j b_l + a_j^\dagger b_l^\dagger b_l^\dagger b_l + a_j^\dagger a_j^\dagger a_j b_l^\dagger + 4a_j^\dagger a_j b_l^\dagger b_l\}$$

and algebraic simplification yields

$$\begin{aligned}
\mathcal{H}^{(4)} &= -\frac{Jz}{2N}\sum_{k_1..k_4}\Big\{\Delta(k_1-k_2-k_3+k_4)\Upsilon_{(-k_2+k_3+k_4)}a_{k_1}b_{k_2}^\dagger b_{k_3}b_{k_4} - \Delta(k_1-k_2-k_3+k_4)\Upsilon_{k_4}a_{k_1}^\dagger a_{k_2}a_{k_3}b_{k_4} \\
&- \Delta(k_1-k_2-k_3+k_4)\Upsilon_{(-k_2-k_3+k_4)}a_{k_1}^\dagger b_{k_2}^\dagger b_{k_3}^\dagger b_{k_4} - \Delta(k_1+k_2-k_3-k_4)\Upsilon_{-k_4}a_{k_1}^\dagger a_{k_2}^\dagger a_{k_3}b_{k_4}^\dagger\Big\} \\
&- \frac{2Jz}{N}\sum_{k_1\ldots k_4}\Delta(k_1-k_2-k_3+k_4)\Upsilon_{(-k_3+k_4)}a_{k_1}^\dagger a_{k_2}b_{k_3}^\dagger b_{k_4} \\
&= -A^{(4)}\sum_{k_1..k_4}\Big\{\xi_1^{(4)}a_{k_1}b_{k_2}^\dagger b_{k_3}b_{k_4} + \xi_2^{(4)}a_{k_1}^\dagger a_{k_2}a_{k_3}b_{k_4} + \xi_3^{(4)}a_{k_1}^\dagger b_{k_2}^\dagger b_{k_3}^\dagger b_{k_4} \\
&+ \xi_4^{(4)}a_{k_1}^\dagger a_{k_2}^\dagger a_{k_3}b_{k_4}^\dagger + 4\xi_5^{(4)}a_{k_1}^\dagger a_{k_2}b_{k_3}^\dagger b_{k_4}\Big\}
\end{aligned} \tag{A.10}$$

Fourier Transform of $H^{(6)}$

I final, the Fourier transform of $H^{(4)}$ by substitution (A.7) into

$$\mathcal{H}^{(6)} = \frac{J}{8S}\sum_{\langle jl\rangle}\{a_j^\dagger a_j a_j b_l^\dagger b_l b_l + a_j^\dagger a_j^\dagger a_j b_l^\dagger b_l^\dagger b_l\}$$

and rigorous algebraic simplification yields

$$\mathbf{H}^{(6)} = A^{(6)}\sum_{k_1\ldots k_6}\Big\{\xi_1^{(6)}a_{k_1}^\dagger a_{k_2}a_{k_3}b_{k_4}^\dagger b_{k_5}b_{k_6} + \xi_2^{(6)}a_{k_1}^\dagger a_{k_2}^\dagger a_{k_3}b_{k_4}^\dagger b_{k_5}^\dagger b_{k_6}\Big\} \tag{A.11}$$

where we have been used $A^{(4)} = \dfrac{\omega_e}{4NS}$ and $A^{(6)} = \dfrac{\omega_e}{(4NS)^2}$

Thus, the total Hamiltonian can rewrite as

$$\begin{aligned}
\mathbf{H} &= -2NS(\omega_e+\omega_A) + \sum_k\{A_1^2(a_k b_k + a_k^\dagger b^\dagger) + A_2^2 a_k^\dagger a_k + A_3^2 b_k^\dagger b_k\} \\
&- A^{(4)}\sum_{k_1..k_4}\Big\{\xi_1^{(4)}a_{k_1}b_{k_2}^\dagger b_{k_3}b_{k_4} + \xi_2^{(4)}a_{k_1}^\dagger a_{k_2}a_{k_3}b_{k_4} + \xi_3^{(4)}a_{k_1}^\dagger b_{k_2}^\dagger b_{k_3}^\dagger b_{k_4} \\
&+ \xi_4^{(4)}a_{k_1}^\dagger a_{k_2}^\dagger a_{k_3}b_{k_4}^\dagger + 4\xi_5^{(4)}a_{k_1}^\dagger a_{k_2}b_{k_3}^\dagger b_{k_4}\Big\} \\
&+ A^{(6)}\sum_{k_1\ldots k_6}\Big\{\xi_1^{(6)}a_{k_1}^\dagger a_{k_2}a_{k_3}b_{k_4}^\dagger b_{k_5}b_{k_6} + \xi_2^{(6)}a_{k_1}^\dagger a_{k_2}^\dagger a_{k_3}b_{k_4}^\dagger b_{k_5}^\dagger b_{k_6}\Big\}
\end{aligned} \tag{A.12}$$

where

$$\begin{aligned}
\xi_1^{(4)} &= \Delta(k_1-k_2-k_3+k_4)\Upsilon_{(-k_2+k_3+k_4)} \\
\xi_1^{(4)} &= \Delta(k_1-k_2-k_3+k_4)\Upsilon_{k_4} \\
\xi_3^{(4)} &= \Delta(k_1-k_2-k_3+k_4)\Upsilon_{(-k_2-k_3+k_4)} \\
xi_4^{(4)} &= \Delta(k_1+k_2-k_3-k_4)\Upsilon_{-k_4} \\
\xi_5^{(4)} &= \Delta(k_1-k_2-k_3+k_4)\Upsilon_{(-k_3+k_4)} \\
\xi_1^{(6)} &= \Delta(k_1-k_2-k_3-k_4+k_5+k_6)\Upsilon_{(-k_4+k_5+k_6)} \\
\xi_2^{(6)} &= \Delta(k_1+k_2-k_3-k_4-k_5+k_6)\Upsilon_{(-k_4-k_5+k_6)}
\end{aligned}$$

Thus, we obtain a total Hamiltonian of the form

$$\mathbf{H} = \mathcal{H}^{(0)} + \mathcal{H}^{(2)} + \mathcal{H}^{(4)} + \mathcal{H}^{(6)} \tag{A.13}$$

Where wehave used in in the general form (A.9) as

$$\begin{aligned}
\mathrm{H}^{(0)} =& -2NS(\omega_e+\omega_A) \\
\mathcal{H}^{(2)} =& \sum_k \{A_1^2(a_k b_k + a_k^\dagger b^\dagger) + A_2^2 a_k^\dagger a_k + A_3^2 b_k^\dagger b_k\} \\
\mathcal{H}^{(4)} =& -A^{(4)} \sum_{k_1..k_4} \Big\{ \xi_1^{(4)} a_{k_1} b_{k_2}^\dagger b_{k_3} b_{k_4} + \xi_2^{(4)} a_{k_1}^\dagger a_{k_2} a_{k_3} b_{k_4} + \xi_3^{(4)} a_{k_1}^\dagger b_{k_2}^\dagger b_{k_3}^\dagger b_{k_4} \\
& + \xi_4^{(4)} a_{k_1}^\dagger a_{k_2}^\dagger a_{k_3} b_{k_4}^\dagger + 4\xi_5^{(4)} a_{k_1}^\dagger a_{k_2} b_{k_3}^\dagger b_{k_4} \Big\} \\
\mathbf{H}^{(6)} =& A^{(6)} \sum_{k_1 \ldots k_6} \Big\{ \xi_1^{(6)} a_{k_1}^\dagger a_{k_2} a_{k_3} b_{k_4}^\dagger b_{k_5} b_{k_6} + \xi_2^{(6)} a_{k_1}^\dagger a_{k_2}^\dagger a_{k_3} b_{k_4}^\dagger b_{k_5}^\dagger b_{k_6} \Big\}
\end{aligned} \tag{A.14}$$

A.2 Green Function Technique

The mathematics of the double time-temperature dependent Green functions has been given by Zubarev [1960], and by Bonch-Bruevich and Tyablikov[1962] to whom we refer for details. The features of this technique are relevant to the present work. The Green Function, $\langle\langle A(t); B(t')\rangle\rangle$ is defined as

$$\langle\langle A(t); B(t')\rangle\rangle = -\frac{i}{\hbar}\Theta(t-t')\langle[A(t); B(t')]\rangle \tag{A.15}$$

where $A(t)$ is the Heisenberg operator referred to time t, i,e,

$$A(t) = e^{i\frac{H}{\hbar}t} A e^{-i\frac{H}{\hbar}t} \tag{A.16}$$

and where H is the systems' Hamiltonian.

Differentiating the Green Function in (A.15) with respect to t we get

$$i\hbar\frac{d}{dt}\langle\langle A(t);B(t')\rangle\rangle = \delta(t-t')\langle[A(t),B(t')]\rangle + \langle\langle[A(t),H];B(t')\rangle\rangle \tag{A.17}$$

If the Hamiltonian is not explicitly time dependent, the Green function (is a function of $t-t'$) and may; therefore, be Fourier transformed with respect to this quantity. The transform is a function of $E=\hbar\omega$ and may be denoted by $\langle\langle A;B\rangle\rangle_E$. It may be shown to satisfy the equation of motion (see Zubarev (1960)).

$$\hbar\omega\langle\langle A;B\rangle\rangle = \frac{1}{2\pi}\langle[A,B]\rangle + \langle\langle[A,H];B\rangle\rangle_E \tag{A.18}$$

The Green function $\langle\langle A(t);B(t')\rangle\rangle$ in general involves Green functions of higher order than the original $\langle\langle A(t);B(t')\rangle\rangle$ except, of course, for the trivial cases of non interacting systems where exact solutions can be obtained. It is possible to linearize (A.18) by a suitable de-coupling approximation techniques.

Another equation which we shall require from Green function theory is that defining the relationship between $\langle\langle A;B\rangle\rangle_E$ and its related correlation function (B(t')A(t)). This may be written

$$\langle B(t')A(t)\rangle = \lim_{\varepsilon\to+0} i\int_{-\infty}^{\infty}\frac{\langle\langle A;B\rangle\rangle_{\omega+i\varepsilon} - \langle\langle A;B\rangle\rangle_{\omega-i\varepsilon}}{e^{\beta\hbar\omega}-1}e^{-i\omega(t-t')}d\omega \tag{A.19}$$

In the operator form of Green Function equation of motion has the form $\omega\langle\langle A;B\rangle\rangle = \frac{\langle[A,B]\rangle}{2\pi} + \langle\langle[A,H];B\rangle\rangle$, we define $A=a_k$, $B=a_k^\dagger$ and [ ] is a commutation relation and (A.18) can rewrite as

$$\begin{aligned}\omega_k\langle\langle a_k;a_{k'}^\dagger\rangle\rangle &= \frac{\langle[a_k,a_{k'}^\dagger]\rangle}{2\pi} + \langle\langle[a_k,H];a_{k'}^\dagger\rangle\rangle \\ \omega_k\langle\langle a_k;a_{k'}^\dagger\rangle\rangle &= \frac{\delta_{kk'}}{2\pi} + \langle\langle[a_k,H];a_{k'}^\dagger\rangle\rangle\end{aligned} \tag{A.20}$$

The Kronicker delta function given by

$$\delta_{kk'} = \begin{cases} 1 & if \quad k=k' \\ 0 & otherwise \quad 0 \end{cases}$$

From Commutation relation and definition of Kronicker delta function we get the Green Function Equation of Motion for Heisenberg Hamiltonian become

$$\begin{aligned}\omega_k\langle\langle a_k;a_k^\dagger\rangle\rangle &= \frac{1}{2\pi} + \langle\langle[a_k,\mathcal{H}];a_k^\dagger\rangle\rangle \\ \omega_k\langle\langle a_k;a_k^\dagger\rangle\rangle &= \frac{1}{2\pi} + \langle\langle[a_k,H^{(0)}];a_k^\dagger\rangle\rangle + \langle\langle[a_k,H^{(2)}];a_k^\dagger\rangle\rangle \\ &\quad + \langle\langle[a_k,H^{(4)}];a_k^\dagger\rangle\rangle + \langle\langle[a_k,H^{(6)}];a_k^\dagger\rangle\rangle\end{aligned} \tag{A.21}$$

In applying operator methods of Green function equation of motion we use the random phase approximation consists of the re-placement $\langle\langle S_l^z S_j^\dagger; S_i^-\rangle\rangle \to \langle S_l^z\rangle\langle\langle S_j^\dagger; S_i^-\rangle\rangle$ [99]. Furthermore, the Green Function of the form $\langle\langle S_j^\dagger S_j^- S_\ell^\dagger; B\rangle\rangle$ and $\langle\langle S_j^- S_j^\dagger S_\ell^\dagger; B\rangle\rangle$ are reasonably decoupled in symmetric form $\langle\langle S_j^\dagger S_j^- S_\ell^\dagger; B\rangle\rangle_{j\neq\ell} \quad \Rightarrow \quad \rangle S_j^\dagger S_j^-\rangle\langle\langle S_\ell^\dagger; B\rangle\rangle + \rangle S_j^- S_\ell^\dagger\rangle\langle\langle S_j^\dagger; B\rangle\rangle$ where has been $\langle S_\ell^\dagger S_\ell^\dagger = 0$, is used because $\langle S_\ell^\dagger S_\ell^\dagger$ is not diagonal in the total z component of the spin [61]. Thus, the calculation proceed for magnon energy deviation up to the order of products of 6-boson operats interactions as follows

$$\begin{aligned}
\omega_k\langle\langle a_k; a_{k'}^\dagger\rangle\rangle =& \frac{\langle[a_k, a_{k'}^\dagger]\rangle}{2\pi} + \langle\langle[a_k, \hat{H}]; a_{k'}^\dagger\rangle\rangle \\
\omega_k\langle\langle a_k; a_{k'}^\dagger\rangle\rangle =& \frac{1}{2\pi} + \langle\langle[a_k, H^{(0)}]; a_k^\dagger\rangle\rangle + \langle\langle[a_k, H^{(2)}]; a_k^\dagger\rangle\rangle + \langle\langle[a_k, H^{(4)}]; a_k^\dagger\rangle\rangle + \langle\langle[a_k, H^{(6)}]; a_k^\dagger\rangle\rangle
\end{aligned} \tag{A.22}$$

But we note that $\langle\langle[a_k, H^{(0)}]; a_k^\dagger\rangle\rangle = 0$
For convenience let solve separately

$$\begin{aligned}
\langle\langle[a_k, H^{(2)}]; a_k^\dagger\rangle\rangle =& A_1^{(2)}\langle\langle[a_k, a_k b_k]; a_k^\dagger\rangle\rangle + A_1^{(2)}\langle\langle[a_k, a_k^\dagger b_k^\dagger]; a_k^\dagger\rangle\rangle + A_2^{(2)}\langle\langle[a_k, a_k^\dagger a_k]; a_k^\dagger\rangle\rangle + A_3^{(2)}\langle\langle[a_k, b_k^\dagger b_k]; a_k^\dagger\rangle\rangle \\
=& A_1^{(2)}\langle\langle[a_k, a^\dagger]b_k^\dagger; a_k^\dagger\rangle\rangle + A_2^{(2)}\langle\langle[a_k, a_k^\dagger]a_k; a_k^\dagger\rangle\rangle \\
\langle\langle[a_k, H^{(2)}]; a_k^\dagger\rangle\rangle =& A_1^{(2)}\langle\langle b_k^\dagger; a_k^\dagger\rangle\rangle + A_2^{(2)}\langle\langle a_k; a_k^\dagger\rangle\rangle
\end{aligned} \tag{A.23}$$

Where we represent $A_1^{(2)} = 2JzS\Upsilon_k, \quad A_2^{(2)} = \gamma(H_a + H_0), \quad A_3^{(2)} = \gamma(H_a - H_0)$

$$\begin{aligned}
\langle\langle[a_k, H^{(4)}]; a_k^\dagger\rangle\rangle =& A_1^{(2)}\langle\langle[a_k, a_{k_1} b_{k_2}^\dagger b_{k_3} b_{k_4}]; a_k^\dagger\rangle\rangle + A_2^{(2)}\langle\langle[a_k, a_{k_1}^\dagger a_{k_2} a_{k_3} b_{k_4}]; a_k^\dagger\rangle\rangle + A_3^{(2)}\langle\langle[a_k, a_{k_1}^\dagger b_{k_2}^\dagger b_{k_3}^\dagger b_{k_4}]; a_k^\dagger\rangle\rangle \\
&+ A_4^{(2)}\langle\langle[a_k, a_{k_1}^\dagger a_{k_2}^\dagger a_{k_3} b_{k_4}^\dagger]; a_k^\dagger\rangle\rangle + A_5^{(2)}\langle\langle[a_k, a_{k_1}^\dagger a_{k_2} b_{k_3}^\dagger b_{k_4}]; a_k^\dagger\rangle\rangle \\
=& A_2^{(2)}\langle\langle[a_k, a_{k_1}^\dagger]a_{k_2} a_{k_3} b_{k_4}; a_k^\dagger\rangle\rangle + A_3^{(2)}\langle\langle[a_k, a_{k_1}^\dagger]b_{k_2}^\dagger b_{k_3}^\dagger b_{k_4}; a_k^\dagger\rangle\rangle + A_4^{(2)}\langle\langle[a_k, a_{k_1}^\dagger]a_{k_2}^\dagger a_{k_3} b_{k_4}^\dagger; a_k^\dagger\rangle\rangle \\
&+ A_4^{(2)}\langle\langle[a_k, a_{k_2}^\dagger]a_{k_1}^\dagger a_{k_3} b_{k_4}^\dagger; a_k^\dagger\rangle\rangle + A_5^{(2)}\langle\langle[a_k, a_{k_1}^\dagger]a_{k_2} b_{k_3}^\dagger b_{k_4}; a_k^\dagger\rangle\rangle \\
=& A_2^{(2)}\langle\langle a_{k_2} a_{k_3} b_{k_4}; a_k^\dagger\rangle\rangle + A_3^{(2)} b_{k_2}^\dagger b_{k_3}^\dagger b_{k_4}; a_k^\dagger\rangle\rangle + A_4^{(2)}\langle\langle a_{k_2}^\dagger a_{k_3} b_{k_4}^\dagger; a_k^\dagger\rangle\rangle \\
&+ A_4^{(2)}\langle\langle a_{k_1}^\dagger a_{k_3} b_{k_4}^\dagger; a_k^\dagger\rangle\rangle + A_5^{(2)}\langle\langle a_{k_2} b_{k_3}^\dagger b_{k_4}; a_k^\dagger\rangle\rangle \\
=& A_2^{(2)}\langle a_{k_2} a_{k_3}\rangle\langle\langle b_{k_4}; a_k^\dagger\rangle\rangle + A_3^{(2)}\langle b_{k_2}^\dagger b_{k_4}\rangle\langle\langle b_{k_3}^\dagger; a_k^\dagger\rangle\rangle + A_3^{(2)}\langle b_{k_3}^\dagger b_{k_4}\rangle\langle\langle b_{k_2}^\dagger; a_k^\dagger\rangle\rangle \\
&+ A_4^{(2)}\langle a_{k_2}^\dagger a_{k_3}\rangle\langle\langle b_{k_4}^\dagger; a_k^\dagger\rangle\rangle + A_4^{(2)}\langle a_{k_1}^\dagger a_{k_3}\rangle\langle\langle b_{k_4}^\dagger; a_k^\dagger\rangle\rangle + A_5^{(2)}\langle b_{k_3}^\dagger b_{k_4}\rangle\langle\langle a_{k_2}; a_k^\dagger\rangle\rangle \\
=& A_3^{(2)} m_k\langle\langle b_{k_3}^\dagger; a_k^\dagger\rangle\rangle + A_3^{(2)} m_k\langle\langle b_{k_2}^\dagger; a_k^\dagger\rangle\rangle + A_4^{(2)} n_k\langle\langle b_{k_4}^\dagger; a_k^\dagger\rangle\rangle + A_4^{(2)} n_k\langle\langle b_{k_4}^\dagger; a_k^\dagger\rangle\rangle + A_5^{(2)} m_k\langle\langle a_{k_2}; a_k^\dagger\rangle\rangle \\
\langle\langle[a_k, H^{(4)}]; a_k^\dagger\rangle\rangle =& 2(A_3^{(2)} m_k + A_4^{(2)} n_k)\langle\langle b_k^\dagger; a_k^\dagger\rangle\rangle + A_5^{(2)} m_k\langle\langle a_k; a_k^\dagger\rangle\rangle \\
\langle\langle[a_k, H^{(4)}]; a_k^\dagger\rangle\rangle =& 2A\Upsilon_k(m_k + n_k)\langle\langle b_k^\dagger; a_k^\dagger\rangle\rangle + 4Am_k\langle\langle a_k; a_k^\dagger\rangle\rangle
\end{aligned} \tag{A.24}$$

This equation is evaluated at points $k_1 = k_2 = k_3 = k_4 = k$ and representing $\langle a_k^\dagger a_k\rangle$ by $\langle n_k\rangle$ and $\langle b_k^\dagger b_k\rangle$ by $\langle m_k\rangle$, and also $A_1^2 = A_2^2 = A_3^2 = A_4^2 = -\frac{Jz}{2N}\Upsilon_k = A\Upsilon_k$, $A_5^2 = -2\frac{Jz}{N}$.

$$
\begin{aligned}
\langle\langle [a_k, H^{(6)}]; a_k^\dagger \rangle\rangle =& A_1^{(6)} \langle\langle [a_k, a_{k_1}^\dagger a_{k_2} a_{k_3} b_{k_4}^\dagger b_{k_5} b_{k_6}]; a_k^\dagger \rangle\rangle + A_2^{(6)} \langle\langle [a_k, a_{k_1}^\dagger a_{k_2}^\dagger a_{k_3} b_{k_4}^\dagger b_{k_5}^\dagger b_{k_6}]; a_k^\dagger \rangle\rangle \\
=& A_1^{(6)} \langle\langle [a_k, a_{k_1}^\dagger] a_{k_2} a_{k_3} b_{k_4}^\dagger b_{k_5} b_{k_6}; a_k^\dagger \rangle\rangle + A_2^{(6)} \langle\langle [a_k, a_{k_1}^\dagger] a_{k_2}^\dagger a_{k_3} b_{k_4}^\dagger b_{k_5}^\dagger b_{k_6}; a_k^\dagger \rangle\rangle \\
&+ A_2^{(6)} \langle\langle [a_k, a_{k_2}^\dagger] a_{k_1}^\dagger a_{k_3} b_{k_4}^\dagger b_{k_5}^\dagger b_{k_6}; a_k^\dagger \rangle\rangle \\
=& A_1^{(6)} \langle\langle a_k a_{k_3} b_{k_4}^\dagger b_{k_5} b_{k_6}; a_k^\dagger \rangle\rangle + 2A_2^{(6)} \langle\langle a_k^\dagger a_{k_3} b_{k_4}^\dagger b_{k_5}^\dagger b_{k_6}; a_k^\dagger \rangle\rangle \\
=& 2A_2^{(6)} \langle a_k^\dagger a_k \rangle \langle\langle b_{k_4}^\dagger b_{k_5}^\dagger b_{k_6}; a_k^\dagger \rangle\rangle + 2A_2^{(6)} \langle b_{k_4}^\dagger b_{k_6} \rangle \langle\langle a_k^\dagger a_{k_3} b_{k_5}^\dagger; a_k^\dagger \rangle\rangle \\
&+ 2A_2^{(6)} \langle b_{k_5}^\dagger b_{k_6} \rangle \langle\langle a_k^\dagger a_{k_3} b_{k_4}^\dagger b_{k_6}; a_k^\dagger \rangle\rangle \\
=& 4A_2^{(6)} n_k m_k \langle\langle b_k^\dagger; a_k^\dagger \rangle\rangle + 2A_2^{(6)} n_k m_k \langle\langle b_k^\dagger; a_k^\dagger \rangle\rangle + 2A_2^{(6)} n_k m_k \langle\langle b_k^\dagger; a_k^\dagger \rangle\rangle \\
\langle\langle [a_k, H^{(6)}]; a_k^\dagger \rangle\rangle =& 8A_2^{(6)} n_k m_k \langle\langle b_k^\dagger; a_k^\dagger \rangle\rangle
\end{aligned} \tag{A.25}
$$

In this equation we represnt $A_1^6 = A_2^6 = \frac{Jz}{8N^2S}\Upsilon$.

Substituting the results of (A.23), (A.24) and (A.25) into (A.20) one gets

$$
\begin{aligned}
\omega_k \langle\langle a_k; a_k^\dagger \rangle\rangle =& \frac{1}{2\pi} + \langle\langle [a_k, H^{(2)}]; a_k^\dagger \rangle\rangle + \langle\langle [a_k, H^{(4)}]; a_k^\dagger \rangle\rangle + \langle\langle [a_k, H^{(6)}]; a_k^\dagger \rangle\rangle \\
=& \frac{1}{2\pi} + A_1^1 \langle\langle b_k^\dagger; a_k^\dagger \rangle\rangle + A_2^1 \langle\langle a_k; a_k^\dagger \rangle\rangle + 2A\Upsilon_k (m_k + n_k) \langle\langle b_k^\dagger; a_k^\dagger \rangle\rangle + 4Am_k \langle\langle a_k; a_k^\dagger \rangle\rangle \\
&+ 8A_2^{(6)} n_k m_k \langle\langle b_k^\dagger; a_k^\dagger \rangle\rangle \\
=& \frac{1}{2\pi} + \left[A_1^1 + 2A\Upsilon_k (m_k + n_k) + 8A_2^{(6)} n_k m_k\right] \langle\langle b_k^\dagger; a_k^\dagger \rangle\rangle + \left[A_2^1 + 4Am_k\right] \langle\langle a_k; a_k^\dagger \rangle\rangle \\
=& \frac{1}{2\pi} + \frac{2Jz}{2N^2S^2} \left[2N^2S^2 - NS(m_k + n_k) + n_k m_k\right] \Upsilon_k \langle\langle b_k^\dagger; a_k^\dagger \rangle\rangle + \left[2JzS + \gamma(H_a + H_0)\right. \\
&\left. - 2\frac{JzS}{NS} m_k\right] \langle\langle a_k; a_k^\dagger \rangle\rangle \\
\omega_k \langle\langle a_k; a_k^\dagger \rangle\rangle =& \frac{1}{2\pi} + B\Upsilon_k \langle\langle b_k^\dagger; a_k^\dagger \rangle\rangle + R \langle\langle a_k; a_k^\dagger \rangle\rangle
\end{aligned} \tag{A.26}
$$

Here we replaced again

$$
\begin{aligned}
B =& \frac{\omega_e}{2N^2S^2} [2N^2S^2 - NS(m_k + n_k) + n_k m_k] \\
R =& \omega_e (1 - \frac{m_k}{NS}) + \omega_A + \omega_0
\end{aligned}
$$

Again we calculate for $\langle\langle b_k^\dagger; a_k^\dagger \rangle\rangle$ using operator methods of Green Function (A.20) as

$$
\begin{aligned}
\omega_k \langle\langle b_k^\dagger; a_k^\dagger \rangle\rangle =& \langle\langle [b_k^\dagger, \hat{H}]; a_k^\dagger \rangle\rangle \\
\omega_k \langle\langle b_k^\dagger; a_k^\dagger \rangle\rangle =& \langle\langle [b_k^\dagger, H^{(2)}]; a_k^\dagger \rangle\rangle + \langle\langle [b_k^\dagger, H^{(4)}]; a_k^\dagger \rangle\rangle + \langle\langle [b_k^\dagger, H^{(6)}]; a_k^\dagger \rangle\rangle
\end{aligned} \tag{A.27}
$$

Solve each separately for convenience

1.

$$\begin{aligned}
\langle\langle[b_k^\dagger, H^{(2)}]; a_k^\dagger\rangle\rangle =& A_1^{(2)}\langle\langle[b_k^\dagger, a_k b_k]; a_k^\dagger\rangle\rangle + A_1^{(2)}\langle\langle[b_k^\dagger, a_k^\dagger b_k^\dagger]; a_k^\dagger\rangle\rangle + A_2^{(2)}\langle\langle[b_k^\dagger, a_k^\dagger a_k]; a_k^\dagger\rangle\rangle \\
&+ A_3^{(2)}\langle\langle[b_k^\dagger, b_k^\dagger b_k]; a_k^\dagger\rangle\rangle \\
=& A_1^1\langle\langle[b_k^\dagger, b_k]a_k; a_k^\dagger\rangle\rangle + A_3^1\langle\langle[b_k^\dagger, b_k]b_k^\dagger; a_k^\dagger\rangle\rangle \\
\langle\langle[b_k^\dagger, H^{(2)}]; a_k^\dagger\rangle\rangle =& -A_1^1\langle\langle a_k; a_k^\dagger\rangle\rangle - A_3^1\langle\langle b_k^\dagger; a_k^\dagger\rangle\rangle
\end{aligned} \tag{A.28}$$

2.

$$\begin{aligned}
\langle\langle[b_k^\dagger, H^{(4)}]; a_k^\dagger\rangle\rangle =& A_1^{(2)}\langle\langle[b_k^\dagger, a_{k_1} b_{k_2}^\dagger b_{k_3} b_{k_4}]; a_k^\dagger\rangle\rangle + A_2^{(2)}\langle\langle[b_k^\dagger, a_{k_1}^\dagger a_{k_2} a_{k_3} b_{k_4}]; a_k^\dagger\rangle\rangle + A_3^{(2)}\langle\langle[b_k^\dagger, a_{k_1}^\dagger b_{k_2}^\dagger b_{k_3}^\dagger b_{k_4}]; a_k^\dagger\rangle\rangle \\
&+ A_4^{(2)}\langle\langle[b_k^\dagger, a_{k_1}^\dagger a_{k_2}^\dagger a_{k_3} b_{k_4}^\dagger]; a_k^\dagger\rangle\rangle + A_5^{(2)}\langle\langle[b_k^\dagger, a_{k_1}^\dagger a_{k_2} b_{k_3}^\dagger b_{k_4}]; a_k^\dagger\rangle\rangle \\
=& A_1^{(2)}\langle\langle[b_k^\dagger, b_{k_3}]a_{k_1} b_{k_2}^\dagger b_{k_4}; a_k^\dagger\rangle\rangle + A_1^{(2)}\langle\langle[b_k^\dagger, b_{k_4}]a_{k_1} b_{k_2}^\dagger b_{k_3}; a_k^\dagger\rangle\rangle + A_2^{(2)}\langle\langle[b_k^\dagger, b_{k_4}]a_{k_1}^\dagger a_{k_2} a_{k_3} b_{k_4}; a_k^\dagger\rangle\rangle \\
&+ A_4^{(2)}\langle\langle[b_k^\dagger, b_{k_4}]a_{k_1}^\dagger b_{k_2}^\dagger b_{k_3}^\dagger; a_k^\dagger\rangle\rangle + A_5^{(2)}\langle\langle[b_k^\dagger, b_{k_4}]a_{k_1}^\dagger a_{k_2} b_{k_3}^\dagger; a_k^\dagger\rangle\rangle \\
=& -A_1^{(2)}\langle\langle a_{k_1} b_{k_2}^\dagger b_{k_4}; a_k^\dagger\rangle\rangle - A_1^{(2)}\langle\langle a_{k_1} b_{k_2}^\dagger b_{k_3}; a_k^\dagger\rangle\rangle - A_2^{(2)}\langle\langle a_{k_1}^\dagger a_{k_2} a_{k_3} b_{k_4}; a_k^\dagger\rangle\rangle \\
&- A_4^{(2)}\langle\langle a_{k_1}^\dagger b_{k_2}^\dagger b_{k_3}^\dagger; a_k^\dagger\rangle\rangle - A_5^{(2)}\langle\langle a_{k_1}^\dagger a_{k_2} b_{k_3}^\dagger; a_k^\dagger\rangle\rangle \\
=& -2A_1^{(2)}\langle b_k^\dagger b_k\rangle\langle\langle a_k; a_k^\dagger\rangle\rangle - 2A_2^{(2)}\langle a_k^\dagger a_k\rangle\langle\langle a_k; a_k^\dagger\rangle\rangle - A_5^{(2)}\langle a_k^\dagger a_k\rangle\langle\langle b_k^\dagger; a_k^\dagger\rangle\rangle \\
=& -2A_1^{(2)} m_k\langle\langle a_k; a_k^\dagger\rangle\rangle - 2A_2^{(2)} n_k\langle\langle a_k; a_k^\dagger\rangle\rangle - A_5^{(2)} n_k\langle\langle b_k^\dagger; a_k^\dagger\rangle\rangle \\
=& -2(A_1^{(2)} m_k + A_2^{(2)} n_k)\langle\langle a_k; a_k^\dagger\rangle\rangle - A_5^{(2)} n_k\langle\langle b_k^\dagger; a_k^\dagger\rangle\rangle \\
\langle\langle[b_k^\dagger, H^{(4)}]; a_k^\dagger\rangle\rangle =& -2A\Upsilon_k(m_k + n_k)\langle\langle a_k; a_k^\dagger\rangle\rangle - 4An_k\langle\langle b_k^\dagger; a_k^\dagger\rangle\rangle
\end{aligned} \tag{A.29}$$

3.

$$\begin{aligned}
\langle\langle[b_k^\dagger, H^{(6)}]; a_k^\dagger\rangle\rangle =& A_1^{(6)}\langle\langle[b_k^\dagger, a_{k_1}^\dagger a_{k_2} a_{k_3} b_{k_4}^\dagger b_{k_5} b_{k_6}]; a_k^\dagger\rangle\rangle + A_2^{(6)}\langle\langle[b_k^\dagger, a_{k_1}^\dagger a_{k_2}^\dagger a_{k_3} b_{k_4}^\dagger b_{k_5}^\dagger b_{k_6}]; a_k^\dagger\rangle\rangle \\
=& A_1^{(6)}\langle\langle[b_k^\dagger, b_{k_5}]a_{k_1}^\dagger a_{k_2} a_{k_3} b_{k_4}^\dagger b_{k_6}; a_k^\dagger\rangle\rangle + A_1^{(6)}\langle\langle[b_k^\dagger, b_{k_6}]a_{k_1}^\dagger a_{k_2} a_{k_3} b_{k_4}^\dagger b_{k_5}; a_k^\dagger\rangle\rangle \\
&+ A_2^{(6)}\langle\langle[b_k^\dagger, b_{k_6}]a_{k_1}^\dagger a_{k_2}^\dagger a_{k_3} b_{k_4}^\dagger b_{k_5}^\dagger b_{k_6}; a_k^\dagger\rangle\rangle \\
=& -2A_1^{(6)}\langle\langle a_{k_1}^\dagger a_{k_2} a_{k_3} b_{k_4}^\dagger b_k; a_k^\dagger\rangle\rangle - A_2^{(6)}\langle\langle a_{k_1}^\dagger a_{k_2}^\dagger a_{k_3} b_{k_4}^\dagger b_{k_5}^\dagger; a_k^\dagger\rangle\rangle \\
=& -2A_1^{(6)}\langle a_{k_1}^\dagger a_{k_2}\rangle\langle\langle a_{k_3} b_{k_4}^\dagger b_k; a_k^\dagger\rangle\rangle - 2A_1^{(6)}\langle a_{k_1}^\dagger a_{k_3}\rangle\langle\langle a_{k_2} b_{k_4}^\dagger b_k; a_k^\dagger\rangle\rangle \\
&- 2A_1^{(6)}\langle b_{k_4}^\dagger b_k\rangle\langle\langle a_{k_1}^\dagger a_{k_2} a_{k_3}; a_k^\dagger\rangle\rangle - A_2^{(6)}\langle a_{k_1}^\dagger a_{k_3}\rangle\langle\langle a_{k_2}^\dagger b_{k_4}^\dagger b_{k_5}^\dagger; a_k^\dagger\rangle\rangle \\
&- A_2^{(6)}\langle a_{k_2}^\dagger a_{k_3}\rangle\langle\langle a_{k_1}^\dagger b_{k_4}^\dagger b_{k_5}^\dagger; a_k^\dagger\rangle\rangle \\
=& -2A_1^{(6)} n_k m_k\langle\langle a_k; a_k^\dagger\rangle\rangle - 2A_1^{(6)} n_k m_k\langle\langle a_k; a_k^\dagger\rangle\rangle - 4A_1^{(6)} n_k m_k\langle\langle a_k; a_k^\dagger\rangle\rangle \\
\langle\langle[b_k^\dagger, H^{(6)}]; a_k^\dagger\rangle\rangle =& -8A_1^{(6)} n_k m_k\langle\langle a_k; a_k^\dagger\rangle\rangle
\end{aligned} \tag{A.30}$$

Substitute the results of (A.28), (A.29), (A.30) and (A.31) into (A.27) one gets

$$
\begin{aligned}
\omega_k\langle\langle b_k^\dagger; a_k^\dagger\rangle\rangle &= \langle\langle [b_k^\dagger, \hat{H}]; a_k^\dagger\rangle\rangle \\
&= \langle\langle [b_k^\dagger, H^{(2)}]; a_k^\dagger\rangle\rangle + \langle\langle [b_k^\dagger, H^{(4)}]; a_k^\dagger\rangle\rangle + \langle\langle [b_k^\dagger, H^{(6)}]; a_k^\dagger\rangle\rangle \\
&= -A_1^1\langle\langle a_k; a_k^\dagger\rangle\rangle - A_3^1\langle\langle b_k^\dagger; a_k^\dagger\rangle\rangle \\
&- 2A\Upsilon_k(m_k+n_k)\langle\langle a_k; a_k^\dagger\rangle\rangle - 4An_k\langle\langle b_k^\dagger; a_k^\dagger\rangle\rangle - 8A_1^{(6)}n_k m_k\langle\langle a_k; a_k^\dagger\rangle\rangle \\
&= -\left[A_1^1 + 2A\Upsilon_k(m_k+n_k+8A_1^{(6)}n_k m_k\right]\langle\langle a_k; a_k^\dagger\rangle\rangle - \left[A_3^1 + 4An_k\right]\langle\langle b_k^\dagger; a_k^\dagger\rangle\rangle \\
&= -B\Upsilon_k\langle\langle a_k; a_k^\dagger\rangle\rangle - R'\langle\langle b_k^\dagger; a_k^\dagger\rangle\rangle \\
\langle\langle b_k^\dagger; a_k^\dagger\rangle\rangle &= -\frac{B\Upsilon_k}{\varepsilon_k + R'}\langle\langle a_k; a_k^\dagger\rangle\rangle
\end{aligned}
\tag{A.31}
$$

where we use $R' = \omega_e(1 - \frac{n_k}{NS}) + \omega_A - \omega_0$.
Finally, substituting (A.31) into (A.26) yields

$$
\begin{aligned}
\omega_k\langle\langle a_k; a_k^\dagger\rangle\rangle &= \frac{1}{2\pi} + B\Upsilon_k\langle\langle b_k^\dagger; a_k^\dagger\rangle\rangle + R\langle\langle a_k; a_k^\dagger\rangle\rangle \\
&= \frac{1}{2\pi} - \frac{B^2\Upsilon_k^2}{\omega_k + R'}\langle\langle a_k; a_k^\dagger\rangle\rangle + R\langle\langle a_k; a_k^\dagger\rangle\rangle \\
&= \frac{1}{2\pi} + \frac{\omega_k R + RR' - B^2\Upsilon_k^2}{\omega_k + R'}\langle\langle a_k; a_k^\dagger\rangle\rangle
\end{aligned}
\tag{A.32}
$$

Eventually we get te required results

$$
\langle\langle a_k; a_k^\dagger\rangle\rangle = \frac{\omega_k + R'}{2\pi[\omega_k^2 + (R'-R)\omega_k - RR' + B^2\Upsilon_k^2]} \tag{A.33}
$$

A.3 Dispersion Relation

The zero in Green function of the form $\langle\langle a_k; a_k^\dagger\rangle\rangle$ may be evaluated where the denominator of (A.33) vanished, i.e

$$
\begin{aligned}
2\pi[\omega_k^2 + (R'-R)\omega_k - RR' + B^2\Upsilon_k^2] &= 0 \\
\omega_k^2 + (R'-R)\omega_k - RR' + B^2\Upsilon_k^2 &= 0
\end{aligned}
\tag{A.34}
$$

To solve (A.34), first let's simplify the following

$$\begin{aligned}
R' - R =& -2\omega_0 + \frac{\omega_e}{NS}(m_k - n_k) \\
R'R =& (\omega_e^2 + \omega_A)^2 - \omega_0^2 - \frac{\omega_A\omega_e}{NS}(m_k + n_k) - \frac{\omega_k^2}{NS}(m_k + n_k) \\
&+ \frac{\omega_e\omega_0}{NS}(m_k - n_k) + \omega_e^2\frac{n_k m_k}{N^2N^2} \\
B^2 =& (\omega_2\Upsilon_k)^2[1 - \frac{m_k + n_k}{NS} + \frac{n_k m_k}{N^2S^2} + \frac{(m_k + n_k)^2}{4N^2S^2} \\
&- \frac{(m_k + n_k)m_k n_k}{2N^3S^3} + \frac{(n_k m_k)^2}{4N^4S^4}
\end{aligned} \tag{A.35}$$

Now let assume approximately $\langle n_k\rangle = \langle m_k\rangle = \langle \hat{b}_k\rangle$, then (A.35) reduced to

$$\begin{aligned}
R' - R =& -2\omega_0 \\
RR' =& (\omega_e + \omega_A)^2 - (\omega_e^2 + \omega_A\omega_e)\frac{2\langle \hat{b}_k\rangle}{NS} - \omega_0^2 + \omega_e^2\frac{\langle \hat{b}_k\rangle^2}{N^2S^2} \\
B^2 =& \omega_e^2\Upsilon_k^2\Big[1 - \frac{2\langle b\rangle}{NS} + \frac{2\langle \hat{b}_k\rangle^2}{N^2S^2} - \frac{\langle \hat{b}_k\rangle^3}{N^3S^3} + \frac{\langle \hat{b}_k\rangle^4}{4N^4S^4}\Big]
\end{aligned} \tag{A.36}$$

Solving (A.34) by the method of completing the square gives

$$\Big(\omega_k + \frac{1}{2}(R' - R)\Big)^2 = \Big\{\frac{1}{4}(R' - R)^2 + RR' - B^2\Upsilon_k^2\Big\} \tag{A.37}$$

Substitution of (A.36) into (A.37), and letting $\frac{\langle b_k\rangle}{NS} = \frac{\langle n_k\rangle}{NS}$, yields

$$\begin{aligned}
(\omega_k - \omega_0)^2 =& \omega_0^2 + (\omega_e + \omega_A)^2 - 2(\omega_e^2 + \omega_e\omega_A)\frac{\langle b_k\rangle}{NS} - \omega_0^2 \\
&+ \omega_e^2\frac{\langle b_k\rangle^2}{N^2S^2} - (\omega_e\Upsilon k)^2\Big[1 - 2\frac{\langle b_k\rangle}{NS} + 2\frac{\langle b_k\rangle^2}{N^2S^2} - \frac{\langle b_k\rangle^3}{N^3S^3} + \frac{\langle b_k\rangle^4}{4N^4S^4}\Big] \\
(\omega_k - \omega_0)^2 =& \Big(\omega_A + \omega_e\Big)^2 - (\omega_e\Upsilon_k)^2 - 2\Big(\omega_e^2 + \omega_e\omega_A - (\omega_e\Upsilon_k)^2\Big)\frac{\langle b_k\rangle}{NS} \\
&+ \omega_e^2\Big(1 - 2\Upsilon_k^2\Big)\frac{\langle b_k\rangle^2}{N^2S^2} - 2\omega_e^2\Big(\frac{\langle b_k\rangle^3}{N^3S^3} + \frac{\langle b_k\rangle^4}{4N^4S^4}\Big)\Upsilon_k^2
\end{aligned} \tag{A.38}$$

At low temperatures ($k_BT \ll J$, where J is the exchange interactin energy) the number of excitation states are very small so that $\langle b_k\rangle = \langle n_k\rangle \ll S$. Thus we making an approximation of $\frac{\langle a_k^\dagger a_k\rangle}{NS} = \frac{\langle b_k\rangle}{NS} < 1$ and then we can neglect above quadratic power of $\langle b_k\rangle$ in (A.38), yields

$$\begin{aligned}
(\omega_k - \omega_0)^2 =& \Big(\omega_A + \omega_e\Big)^2 - (\omega_e\Upsilon_k)^2 - 2\Big(\omega_e^2 + \omega_e\omega_A - (\omega_e\Upsilon_k)^2\Big)\frac{\langle b_k\rangle}{NS} \\
&+ \omega_e^2\Big(1 - 2\Upsilon_k^2\Big)\frac{\langle b_k\rangle^2}{N^2S^2}
\end{aligned} \tag{A.39}$$

A simlified dispersion relation we obtain

$$(\omega_k-\omega_0)^2=\omega_A^2+2\omega_e\omega_A+\omega_e^2(1-\Upsilon_k^2)-(\omega_e\omega_A+\omega_e^2(1-\Upsilon_k^2))\frac{2\langle b_k\rangle}{NS}+\omega_e^2(1-2\Upsilon_k^2)\frac{\langle b_k\rangle^2}{N^2S^2} \tag{A.40}$$

The magnoic spin wave propagates with wave length $\lambda=4a$ in the first Brillouin zone, which correspnding wave vector $k=\frac{2\pi}{\lambda}=\frac{\pi}{2a}$ [101]. Threfore; we can approximate, the geometry of the space lattice factor defined by $\Upsilon_k=\frac{1}{z}\sum_\delta e^{i\vec{k}.\vec{\delta}}$, where $\vec{\delta}$ are the vectors connecting closest neighbors in the opposite sublattice and only connected intersublattice exchange field. The geometrical structural factor for the hypercubic spherical zone is $\Upsilon_k=\frac{1}{D}\sum_{i=1}^{D}\cos\left(\vec{k}_i.\vec{\delta}\right)$, where D is the dimensionality [56], assumes a spherical Brillouin zone and approximated as $\Upsilon_k=\cos\left(\frac{\pi k}{2k_m}\right)$, where $k_m=\frac{\pi}{2a}$, and a is an effective lattice parameter that can be modified for different situations [52]. Thus,(A.40) can reduced to

$$(\omega_k-\omega_0)^2=\omega_A^2+2\omega_e\omega_A+\omega_e^2\sin^2\left(\frac{\pi k}{2k_m}\right)-\left[\omega_e\omega_A+\omega_e^2\sin^2\left(\frac{\pi k}{2k_m}\right)\right]\frac{2\langle b_k\rangle}{NS}+\omega_e^2\left[\sin^2\left(\frac{\pi k}{2k_m}\right)-\cos^2\left(\frac{\pi k}{2k_m}\right)\right]\frac{\langle b_k\rangle^2}{N^2S^2} \tag{A.41}$$

In the limit of sufficiently small enough **k**, the energy of spin waves is vanishingly small, and it becomes $E_k=\hbar\omega_k\approx(cons.)\mathbf{k}$.

The integration on the excited mean magnon $\langle b_k\rangle=\frac{1}{e^{\beta E_k}-1}$ can be taken over the first Brillouin zone to all of the k-spaces; at low temperatures, a change in the integration variable is crucial [5, 4]. To convert the integration variable k into another dimensionless variable, we apply the substitutions $E_k\approx Ck$ and $q=\beta E_k$. Then, performs and gives:

$$\begin{aligned} q&=\beta E_k\\ q&=\beta Ck\\ \Rightarrow\quad k&=\frac{q}{\beta C}\\ k&=\frac{k_BT}{C}q \end{aligned} \tag{A.42}$$

By changing the variable $\mathbf{k}=(k_BT)\mathbf{q}$, where **q** represents the new converted vector, we get final expression as:

$$\langle \mathbf{n}_k \rangle = \int \frac{V}{(2\pi)^3} \frac{d^3k}{e^{E_k} - 1}$$
$$\langle \mathbf{n}_k \rangle = (k_B T)^3 \int \frac{V}{(2\pi)^3} \frac{d^3\mathbf{q}}{e^{E_q} - 1}$$
$$\langle \mathbf{n}_k \rangle = (k_B T)^3 \mathbf{F(q)} \tag{A.43}$$

where $\mathbf{F(q)} = \int \frac{V}{(2\pi)^3} \frac{d^3\mathbf{q}}{e^{E_q}-1}$, and therefore we can rewrite (A.41) in the form of

$$(\omega_k - \omega_0)^2 = \omega_A^2 + 2\omega_e\omega_A + \omega_e^2 \sin^2\left(\frac{\pi k}{2k_m}\right) - \left[\omega_e\omega_A + \omega_e^2 \sin^2\left(\frac{\pi k}{2k_m}\right)\right] \frac{2(k_B T)^3}{NS} \mathbf{F(q)}$$
$$+ \omega_e^2 \left[\sin^2\left(\frac{\pi k}{2k_m}\right) - \cos^2\left(\frac{\pi k}{2k_m}\right)\right] \frac{(k_B T)^6}{N^2 S^2} (\mathbf{F(q)})^2 \tag{A.44}$$

Again let's consider the geometeric structure factor; Υ_k, defined by $\frac{1}{z}\sum_\delta e^{i\tilde{k}\cdot\tilde{\delta}}$, where $\vec{\delta}$ is the vector connecting the nearest neighbour, $\vec{k}$ is the wave vector and z is number of nearest neighbour. For long wave length, we can approximate the crystal lattice structure factor as follow:

$$\Upsilon_k^2 = 1 - \frac{2}{z} a^2 k^2 \tag{A.45}$$

Substituting Eq.(A.45) in to Eq.(A.39) we obtain

$$(\omega_k - \omega_0)^2 = \Big(\omega_A + \omega_e\Big)^2 - \omega_e^2(1 - \frac{1}{z}a^2k^2) - 2\Big(\omega_e^2 + \omega_e\omega_A - \omega_e^2(1 - \frac{1}{z}a^2k^2)\Big)\frac{\langle b_k\rangle}{NS}$$
$$+ \omega_e^2\Big(1 - 2(1 - \frac{1}{z}a^2k^2)\Big)\frac{\langle b_k\rangle^2}{N^2S^2}$$
$$(\omega_k - \omega_0)^2 = \Big(\omega_A + \omega_e\Big)^2 - \omega_e^2 + \frac{\omega_e^2}{z}a^2k^2 - 2\Big(\omega_e^2 + \omega_e\omega_A - \omega_e^2 + \frac{\omega_e^2}{z}a^2k^2\Big)\frac{\langle b_k\rangle}{NS}$$
$$+ \omega_e^2\Big(-1 + \frac{\omega_e^2}{z}a^2k^2\Big)\frac{\langle b_k\rangle^2}{N^2S^2}$$
$$(\omega_k - \omega_0)^2 = \omega_A^2 + 2\omega_e\omega_A + \frac{\omega_e^2}{z}a^2k^2 - 2\Big(\omega_e\omega_A + \frac{\omega_e^2}{z}a^2k^2\Big)\frac{\langle b_k\rangle}{NS}$$
$$+ \omega_e^2\Big(-1 + \frac{\omega_e^2}{z}a^2k^2\Big)\frac{\langle b_k\rangle^2}{N^2S^2} \tag{A.46}$$

Eq.(A.46) can be rewrite in a simpler form as:

$$(\omega_k - \omega_0)^2 = \frac{\omega_e^2}{z}\Big\{z(\alpha^2 + 2\alpha) + a^2k^2 - 2\Big(z\alpha + a^2k^2\Big)\frac{\langle b_k\rangle}{NS}$$
$$- \Big(z - 2a^2k^2\Big)\frac{\langle b_k\rangle^2}{N^2S^2}\Big\} \tag{A.47}$$

By using the approximation provided in Eq.(A.43), we can rewrite Eq.(A.47) in a simple and straightforward form as:

$$(\omega_k - \omega_0)^2 = \frac{\omega_e^2}{z}\Big\{z(\alpha^2+2\alpha)+a^2k^2-2\Big(z\alpha+a^2k^2\Big)\frac{(k_BT)^3}{NS}\mathbf{F(q)} - \Big(z-2a^2k^2\Big)\frac{(k_BT)^6}{N^2S^2}(\mathbf{F(q)})^2\Big\} \tag{A.48}$$

At low temperature approximation we can estimate the $(k_BT)^3$ and $(k_BT)^6$ in Eq.(A.48) would be sufficiently small, and the ratio $\frac{\langle b_k\rangle}{NS}$ and $\frac{\langle b_k\rangle^2}{N^2S^2}$ in Eq.(A.47) also be sufficiently small, that is only a few number of spin excited with vanishingly small energy. As a result of this approximation the dispersion relation would reduced to

$$\omega_k - \omega_0 = \frac{\omega_e}{\sqrt{z}}\sqrt{\Big(z(\alpha^2+2\alpha)+a^2k^2\Big)} \tag{A.49}$$

Appendix B

B.1 Correlation Green Function

The correlation Green Function may be written as

$$\langle B(t')A(t)\rangle = \lim_{\varepsilon\to 0^+} i\int_{-\infty}^{\infty}\Big(\frac{\langle\langle A;B\rangle\rangle_{E+i\varepsilon} - \langle\langle A;B\rangle\rangle_{E-i\varepsilon}}{e^{\beta E}-1}\Big)e^{-iE(t-t')}dE \tag{B.1}$$

In this case we can express the magnon creation and annihilation operators by taking $a_k = A(t)$ and $a_k^\dagger = B(t')$ as follows

$$\begin{aligned}\langle a_k^\dagger a_k\rangle &= \lim_{\varepsilon\to 0^+} i\int_{-\infty}^{\infty}\Big(\frac{\langle\langle a_k;a_k^\dagger\rangle\rangle_{E+i\varepsilon} - \langle\langle a_k;a_k^\dagger\rangle\rangle_{E-i\varepsilon}}{e^{\beta E}-1}\Big)e^{-iE(t-t')}dE \\ \langle a_k^\dagger a_k\rangle &= \lim_{\varepsilon\to 0^+} i\int_{-\infty}^{\infty}\frac{dE}{e^{\beta E}-1}\Big(\langle\langle a_k;a_k^\dagger\rangle\rangle_{E+i\varepsilon} - \langle\langle a_k;a_k^\dagger\rangle\rangle_{E-i\varepsilon}\Big)e^{-iE(t-t')}\end{aligned} \tag{B.2}$$

where "E" is the actual energy of the Green function, whose pole is on the real axis, and "epsilon" is the imaginary portion of energy on the complex plane, according to [121]. In the presence of a magnetic field with the eigenfrequency ω_k, the energy of excited states of antiferromagnet magnon is

$$\mathrm{H}^{sw} = E_0 + \sum_k \hbar\omega_k a_k^\dagger a_k \tag{B.3}$$

with eigenfrequency $\omega_k = \omega_0 \pm \frac{\omega_e}{\sqrt{z}}\sqrt{(z\alpha^2 + 2z\alpha + a^2k^2)}$. The equation of motion for the operator is

$$i\frac{da_k}{dt} = [a_k, \mathrm{H}^{sw}] \tag{B.4}$$

where H is the magnon system Hamiltonian in units of $\hbar = 1$, then

$$\Big[a_k, \mathrm{H}^{sw}\Big] = \Big[a_k, \hbar\omega_k a_k^\dagger a_k\Big] = \hbar\omega_k a_k \tag{B.5}$$

Green Functions' equation of motion for operators at magnon energy E become

$$\begin{aligned} E\langle\langle a_k; a_k^\dagger\rangle\rangle &= \frac{1}{2\pi} + \langle\langle [a_k, \mathsf{H}^{sw}]; a_k^\dagger\rangle\rangle \\ E\langle\langle a_k; a_k^\dagger\rangle\rangle &= \frac{1}{2\pi} + \langle\langle \hbar\omega_k a_k; a_k^\dagger\rangle\rangle \\ E\langle\langle a_k; a_k^\dagger\rangle\rangle &= \frac{1}{2\pi} + \hbar\omega_k \langle\langle a_k; a_k^\dagger\rangle\rangle \\ (E-\hbar\omega_k)\langle\langle a_k; a_k^\dagger\rangle\rangle &= \frac{1}{2\pi} \\ \langle\langle a_k; a_k^\dagger\rangle\rangle &= \frac{1}{2\pi(E-\hbar\omega_k)} \end{aligned} \tag{B.6}$$

Now (B.2) can be rewrite using (B.6) one gets

$$\langle a_k^\dagger a_k\rangle = \lim_{\varepsilon\to 0^+} \frac{i}{2\pi}\int_{-\infty}^{\infty} \frac{e^{-iE(t-t')}dE}{e^{\beta E}-1}\left(\frac{1}{E-\hbar\omega_k+i\varepsilon} - \frac{1}{E-\hbar\omega_k-i\varepsilon}\right) \tag{B.7}$$

Using the symbolic Dirac identity the singular point on the real axis can write as

$$\frac{1}{x-x_0\pm i\varepsilon} = \mathcal{P}\frac{1}{x} \mp i\pi\delta(x-x_0) \tag{B.8}$$

where $\varepsilon\to 0$, $\varepsilon > 0$ and $\mathcal{P}$ denotes the **Cauchy** principal value of the integral. Thus

$$\begin{aligned} \langle\langle a_k; a_k^\dagger\rangle\rangle_{E+i\varepsilon} &= \mathcal{P}\frac{1}{E-\hbar\omega_k} - i\pi\delta(E-\hbar\omega_k) \\ \langle\langle a_k; a_k^\dagger\rangle\rangle_{E-i\varepsilon} &= \mathcal{P}\frac{1}{E-\hbar\omega_k} + i\pi\delta(E-\hbar\omega_k) \end{aligned} \tag{B.9}$$

where $\mathcal{P}$ is the principal part of the integral which exclude the poles. We remove the singularity on the real energy axis by shifting poles upward $(+i\varepsilon)$ and downward $(-i\varepsilon)$ and $\pm i\pi\delta(E-\hbar\omega_k)$ show the motion of the particle counterclockwise $(+)$ and clockwise $(-)$ directions. Therefore

$$\begin{aligned} \left(\frac{1}{E+i\varepsilon-\hbar\omega_k} - \frac{1}{E-i\varepsilon-\hbar\omega_k}\right) &= \mathcal{P}\frac{1}{E-\hbar\omega_k} - i\pi\delta(E-\hbar\omega_k) \\ &\quad - \mathcal{P}\frac{1}{E-\hbar\omega_k} + i\pi\delta(E-\hbar\omega_k) \\ &= -i2\pi\delta(E-\hbar\omega_k) \end{aligned} \tag{B.10}$$

By substituting (B.10) into (B.7) and evaluating at equal time correlation, i.e. $t = t'$ one gets

$$\begin{aligned} \langle a_k^\dagger a_k\rangle &= \frac{i}{2\pi}\int_{-\infty}^{\infty} \frac{-i2\pi\delta(E-\hbar\omega_k)}{e^{\beta E}-1}dE \\ &= \int_{-\infty}^{\infty} \frac{\delta(E-\hbar\omega_k)}{e^{\beta E}-1}dE \end{aligned} \tag{B.11}$$

At $E = \hbar\omega_k$, $\delta(E - \hbar\omega_k) = 1$, otherwise zero. Hence for single

$$\langle a_k^\dagger a_k \rangle = \frac{1}{e^{\beta\hbar\omega_k} - 1} \tag{B.12}$$

where $\beta = \frac{1}{k_B T}$ and $\langle a_k^\dagger a_k \rangle = \langle n_k \rangle$, Thus,

$$\langle n_k \rangle = \frac{1}{e^{\beta\hbar\omega_k} - 1} \tag{B.13}$$

B.2 Magnon number

The density state function can be used to approximate the mean number of excited magnons at temperature T by summing up all the states as a function of frequency ω_k

$$\rho(\omega_k)d\omega_k = \frac{4\pi k^2}{(2\pi)^3}\left(\frac{dk}{d\omega_k}\right)d\omega_k \tag{B.14}$$

and the weighted magnon density is calculated from

$$\sum_k \langle n_k \rangle = \int_V \langle n_k \rangle \rho(\omega_k) d\omega_k \tag{B.15}$$

The total number of magnons excited at temperature T is

$$\sum_k \langle n_k \rangle = \frac{V}{(2\pi)^3} \int_0^\infty \frac{4\pi k^2 dk}{e^{\beta\hbar\omega_k} - 1} \tag{B.16}$$

To calculate the number density it is necessary to change the integral variables from k to ω_k then, we differentiate both sides of Eq.(A.49) with respect to ω_k and yields

$$kdk = \frac{z}{a^2\omega_k^2}(\omega_k - \omega_0)d\omega_k \tag{B.17}$$

and we can solve for $k^2 dk$ using dispersion relation and (B.17) by letting $\omega = \omega_k - \omega_0$ and $\omega_c = \omega_A^2 + 2\omega_e\omega_A$

$$k^2 dk = \frac{\sqrt{z^3}}{a^3\omega_e^3}\omega\sqrt{\omega^2 - \omega_c}d\omega_k \tag{B.18}$$

Using Binomial approximation continuously and algebraic simplification we obtain

$$k^2 dk = \frac{\sqrt{z^3}}{a^3}\left\{A_1\frac{1}{\omega_e} - A_2\frac{\omega_k}{\omega_e^2} + A_3\frac{\omega_k^2}{\omega_e^3} - A_4\frac{\omega_k^3}{\omega_e^4}\right\}d\omega_k \tag{B.19}$$

Where the coefficient variable as a function of anostropy value (α) are represented by

$$\begin{aligned}
A_1 =& m^2 - \frac{1}{2}(\alpha^2+2\alpha) - \frac{1}{8}(\frac{\alpha^4+4\alpha^3+4\alpha^2}{m^2}) - \frac{1}{4}(\frac{\alpha^6+6\alpha^5+12\alpha^4+8\alpha^3}{m^4}) \\
A_2 =& 2m + \frac{3}{8}(\frac{\alpha^4+4\alpha^3+4\alpha^2}{m^3}) + \frac{1}{4}(\frac{\alpha^6+6\alpha^5+12\alpha^4+8\alpha^3}{m^5}) \\
A_3 =& 1 - \frac{3}{8}(\frac{\alpha^4+4\alpha^3+4\alpha^2}{m^4}) - \frac{1}{4}(\frac{\alpha^6+6\alpha^5+12\alpha^4+8\alpha^3}{m^6}) \\
A_4 =& -\frac{1}{4}(2\frac{\alpha^4+4\alpha^3+4\alpha^2}{m^5}) - \frac{1}{4}(5\frac{\alpha^6+6\alpha^5+12\alpha^4+8\alpha^3}{m^7})
\end{aligned} \tag{B.20}$$

We have used the following dimensionless parameters .

$$\begin{aligned}
\alpha =& \frac{H_A}{H_E} = \frac{\omega_A}{\omega_e} \\
m =& \frac{H_0}{H_E} = \frac{\omega_0}{\omega_e}
\end{aligned} \tag{B.21}$$

NB. we kept order of power of (α and m) up to 5 and above it neglected

The total number density in (B.16) can be rewrite using (B.19) as

$$\begin{aligned}
\sum_k \langle n_k \rangle =& \frac{V}{2\pi^2}\frac{\sqrt{z^3}}{a^3}\Big\{\frac{A_1}{\omega_e}\int_0^\infty \frac{d\omega_k}{e^{\beta\hbar\omega}-1} - \frac{A_2}{\omega_e^2}\int_0^\infty \frac{\omega_k}{e^{\beta\hbar\omega}-1}d\omega_k \\
&+ \frac{A_3}{\omega_e^3}\int_0^\infty \frac{\omega_k^2}{e^{\beta\hbar\omega}-1}d\omega_k - \frac{A_4}{\omega_e^4}\int_0^\infty \frac{\omega_k^3}{e^{\beta\hbar\omega}-1}d\omega_k\Big\}
\end{aligned} \tag{B.22}$$

Let $x = \frac{\hbar\omega_k}{k_B T}$ and the integration in (B.22) reduced to a simplest form

$$\begin{aligned}
\sum_k \langle n_k \rangle =& \frac{N\sqrt{z^3}}{2\pi^2}\Big\{A_1\frac{k_BT}{\hbar\omega_e}\int_0^\infty \frac{dx}{e^x-1} - A_2\Big(\frac{k_BT}{\hbar\omega_e}\Big)^2\int_0^\infty \frac{xdx}{e^x-1} + A_3\Big(\frac{k_BT}{\hbar\omega_e}\Big)^3\int_0^\infty \frac{x^2}{e^x-1}dx \\
&- A_4\Big(\frac{k_BT}{\hbar\omega_e}\Big)^4\int_0^\infty \frac{x^3}{e^x-1}dx\Big\}
\end{aligned} \tag{B.23}$$

Using the Riemann-Zeta integral function of the form $\int_0^\infty \frac{x^{s-1}}{e^x-1}dx = \zeta(s)\Gamma(s)$, where $s > 1$, Eq.(B.23) reduced to the form of

$$\begin{aligned}
\sum_k \langle n_k \rangle =& \frac{N\sqrt{z^3}}{2\pi^2}\Big\{A_1\zeta(1)\frac{k_BT}{\hbar\omega_e} - A_2\zeta(2)\Big(\frac{k_BT}{\hbar\omega_e}\Big)^2 + 2A_3\zeta(3)\Big(\frac{k_BT}{\hbar\omega_e}\Big)^3 \\
&- 6A_4\zeta(4)\Big(\frac{k_BT}{\hbar\omega_e}\Big)^4\Big\}
\end{aligned} \tag{B.24}$$

To simplify the notation in antiferromagnetic we can define the effective temperatures that characterized exchange temperature, $k_BT_E = \hbar\omega_e$, anisotropy-exchange or gap temperature $k_BT_{AE} = \hbar\sqrt{2\omega_e\omega_A + \omega_A^2}$ and critical spin flopping field $H_c = \sqrt{2H_EH_A + H_A^2}$; which, in low temperature approximation, is the magnetic field

equivalent of T_{AE} [41, 42]. Then, it is important for the calculation of a physical quantity to obtain an explicit relation for thermodynamical implication. let's again introduce another dimensionaless parameters as $\theta = \frac{T}{T_E} = \frac{k_B T}{\hbar\omega_e}$, the (B.24) rewrite as

$$\sum_k \langle n_k \rangle = \frac{N\sqrt{z^3}}{2\pi^2}\Big\{A_1\zeta(1)\theta - A_2\zeta(2)\theta^2 + 2A_3\zeta(3)\theta^3 - 6A_4\zeta(4)\theta^4\Big\} \tag{B.25}$$

Note:

*However, we note that zeta function diverges for $s = 1$, because it is a harmonic series. But its Cauchy principal value $\lim_{\varepsilon\to 0}\frac{\zeta(1+\varepsilon)+\zeta(1-\varepsilon)}{2}$ exists which is equal to the **Euler-Mascheroni** constant $\gamma = 0.5772$. This is employed in calculating the critical temperature for a **Bose-Einstein** condensate in a box with periodic boundary conditions, and for spin wave physics in magnetic systems.*

B.3 Magnetization

we calculate the magnetic system's sublattice magnetization.

$$M(T,H) = Ng\mu_B\Big(S - \frac{1}{N}\sum_k \langle n_k \rangle\Big) \tag{B.26}$$

We can simplify (B.26) as follows

$$\begin{aligned} M(T,H) &= Ng\mu_B S\Big(1 - \frac{1}{NS}\sum_k \langle n_k \rangle\Big) \\ M(T,H) &= M_s\Big(1 - \frac{1}{NS}\sum_k \langle n_k \rangle\Big) \end{aligned} \tag{B.27}$$

Where $M_s = Ng\mu_B S$ is the saturation magnetization. Since the mean magnon number $\langle n_k \rangle$ is the same as in (B.25), we can substitute into (B.27), it yilds

$$\begin{aligned} M(T,H) &= M_s\Big\{1 - \frac{\sqrt{z^3}}{2\pi^2 S}\Big\{A_1\zeta(1)\theta - A_2\zeta(2)\theta^2 + 2A_3\zeta(3)\theta^3 - 6A_4\zeta(4)\theta^4\Big\}\Big\} \\ M(T,H) &= M_s - \frac{M_s\sqrt{z^3}}{2\pi^2 S}\Big\{A_1\zeta(1)\theta - A_2\zeta(2)\theta^2 + 2A_3\zeta(3)\theta^3 - 6A_4\zeta(4)\theta^4\Big\} \end{aligned} \tag{B.28}$$

B.4 Susceptibility

Magnetic susceptibility is the degree to which a substance may become magnetized when subjected to an external magnetic field. It is a measure of the material's reaction to an applied field, indicating how much magnetization occurs when the field is applied.

When slight fluctuations in the magnetic field are considered, the magnetic susceptibility is computed to assess how the material will respond to these little changes. This calculation includes measuring the induced magnetization of the material while the external magnetic field is gradually changed. By examining these small variations, we may precisely calculate magnetic susceptibility and gain a thorough understanding of the material's magnetic characteristics.

$$\chi(T) = \frac{\partial M(T,H)}{\partial H_0}/H_0 = H \tag{B.29}$$

where H is small magnetic field variation. In Eq.(B.28) the quantity θ is independent H and the quantity A'a are functions of anisotropy and magnetic field. So that the derivative of Eq.(B.28) with respect to $H_0 = H$ becomes:

$$\begin{aligned}\chi &= -\frac{M_s\sqrt{z^3}}{\pi^2 S H_E}\left\{A_1'\zeta(1)\theta - A_2'\zeta(2)\theta^2 + 2A_3'\zeta(3)\theta^3\right\}\\ \chi &= -\frac{M_s\sqrt{z^3}}{S H_E}\left\{0.029A_1'\theta - 0.083A_2'\theta^2 + 0.122A_3'\theta^3\right\}\end{aligned} \tag{B.30}$$

where $A_1^{'}$, $A_2^{'}$ and $A_3^{'}$ are function of anisotropic parameter and magnetic field.

B.5 Heat capacity

The heat capacity of magnetism calculated by

$$\begin{aligned}U(T,\omega) &= 2\sum_k \hbar\omega_k\langle n_k\rangle\\ U(T,\omega) &= 2\frac{4\pi V}{(2\pi)^3}\int_0^\infty \frac{\hbar\omega_k}{e^{\beta\hbar\omega_k}-1}k^2dk\end{aligned} \tag{B.31}$$

We can substitute for k^2dk from (B.19) into (B.31)

$$\begin{aligned}U(T,\omega) &= \frac{V}{\pi^2}\int_0^\infty \frac{\hbar\omega_k}{e^{\beta\hbar\omega_k}-1}\left\{\frac{\sqrt{z^3}}{2a^3}\left\{\frac{1}{\omega_e}A_1 - A_2\frac{\omega_k}{\omega_e^2} + A_3\frac{\omega_k^2}{\omega_e^3} - A_4\frac{\omega_k^3}{\omega_e^4}\right\}d\omega_k\right\}\\ &= \frac{N\sqrt{z^3}}{2\pi^2}\int_0^\infty \frac{\hbar\omega_k}{e^{\beta\hbar\omega_k}-1}\left\{A_1\frac{\omega_k}{\omega_e} - A_2\frac{\omega_k^2}{\omega_e^2} + A_3\frac{\omega_k^3}{\omega_e^3} - A_4\frac{\omega_k^4}{\omega_e^4}\right\}d\omega_k\end{aligned} \tag{B.32}$$

Using $x = \frac{\hbar\omega_k}{k_B T}$ and evaluating $C(T) = \frac{\partial U(T,\omega)}{\partial T}$ for heat capacity Eq.(B.32) yields

$$\begin{aligned}C(T) = \frac{Nk_B}{2\pi^2}\sqrt{z^3}\Big\{&2A_1\theta\int_0^\infty \frac{x}{e^x-1}dx - 3A_2\theta^2\int_0^\infty \frac{x^2}{e^x-1}dx\\ &+ 4A_3\theta^3\int_0^\infty \frac{x^3}{e^x-1}dx - 5A_4\theta^4\int_0^\infty \frac{x^4}{e^x-1}dx\Big\}\end{aligned} \tag{B.33}$$

Again, using the Riemann-zeta integral function (B.33) reduced to

$$C(T) = \frac{Nk_B}{2\pi^2}\sqrt{z^3}\left\{2A_1\zeta(2)\theta - 6A_2\zeta(3)\theta^2 + 24A_3\zeta(4)\theta^3 - 120A_4\zeta(5)\theta^4\right\} \tag{B.34}$$